Morning aerosol vertical profiles in the Planetary Boundary Layer: Observations on a Zeppelin NT Airship and comparison with a Regional Model

INAUGURAL-DISSERTATION

zur

Erlangung des Doktorgrades

der Mathematisch-Naturwissenchaftlichen Fakultät

der Universität zu Köln

vorgelegt von

Konstantinos Kazanas

aus Athen, Griechenland

Köln 2017

Berichterstatter:	Prof. Dr. Andreas Wahner
	PD Dr. Thomas F. Mentel
Tag der letzten mündlichen Prüfung:	27.06.2017

Abstract

In order to study atmospheric air quality and pollutant exchanges, most field campaigns use ground based observations, which usually probe the surface layer. In the frame work of the PEGASOS project a Zeppelin-NT airship was equipped with measurement instruments for both gas and aerosol phase constituents. For the time periods of the PEGASOS campaigns in 2012: 19/05-27/05 at Cabauw (Netherlands) and 18/06-13/07 at Po-Valley (Italy), a chemical weather forecast system based on the EURAD-IM chemical transport model has been set up, first, to provide online support for the flight planning, and second, to interpret the observations in conjuction with the model results. First, the model results are compared with observations, over the whole campaign period and statistical parameters are calculated in order to evaluate the overall model performance. One measurement day with extensive early morning gas-phase vertical profiles (12/07/2012) is selected for detailed study of the model performance with respect to meteorology and gas-phase composition. It is found that the model performs qualitatively well and agreements between model prediction and observation are overall satisfying. Second, one measurement day with gas-phase and, at the same time, aerosol-phase vertical profiles (06/20/2012) is selected in order to study the model performance concerning aerosols. The regionality of ammonium-nitrate is discussed. For the 06/20/2012, at the location of San Pietro Capofiume, the model indicates a large fraction of sulfate and nitrate as transported. In addition, the local production rates of H_2SO_4 and HNO_3 cannot be accounted for such a high sulfate concentration over nitrate concentration. The latter two support the hypothesis of a regionally formed and transported ammonium-sulfate and a locally formed ammonium-nitrate.

Zusammenfassung

Um die atmosphärische Luftqualität und den Schadstoffaustausch zu studieren, werden häufig Beobachtungen aus bodengestützen Feldkampagnen verwendet, die die bodennahe Luftschicht ('surface layer') beproben. Im Rahmen des PEGASOS-Projektes wurde ein Zeppelin-NT Luftschiff mit Meßinstrumenten sowohl zur Beobachtung der Gasphase, als auch zur Messung Aerosolphase ausgestattet. Für die Zeitabschnitte der Pegasos-Kampagnen in 2012: 19/05-27/05 in Cabauw (Niederlande) und 18/06-13/07 im Po-Valley (Italien), wurde ein chemisches Wettervorhersagemodell aufgesetzt, das auf dem EURAD-IM chemischen Transportmodell beruht. Eine online Version wurde zur Unterstützung der Flugplanung zu Verfügung gestellt und eine zweite Version zur modellgestützten Interpretation der Messergebnisse genutzt. In einem ersten Schritt wurden Beobachtung und Modellergebnis für den gesamten Kampagnenzeitraum verglichen und die Modellperformance anhand statistischer Parameter bewertet. Ein Messtag mit umfassenden Vertikalprofilen am Morgen (07/12/2012) wurde für eine detaillierte Studie der Modellperformance im Bereich meteorologische Parameter und Gasphase ausgewählt. Bezüglich der Vorhersage von Gasphasenzusammensetzung liefert das Modell qualitative gute Voraussagen und insgesamt war die Modellperformance befriedend. Ein zweiter Messtag (20/06/2012) mit ähnlichen Vertikalprofilen wurde ausgewählt um die Modellperformance bezüglich Aerosole zu charakterisieren. Dieser Tag (20/06/2012) wurde auch verwendet um die Beobachtungen im Hinblick auf die Regionalität der Aerosolquellen mit Schwerpunkt auf Ammoniumnitrat zu interpretieren. Am 20/06/2012 zeigt die Höhenabhängigkeit der Modellergebnisse, dass am Ort der Messung, San Pietro Capofiume, große Anteile des Sulfataerosols aber auch des Nitrataerosols durch Transport bedingt sind. Der Vergleich der lokalen Produktionsraten von H_2SO_4 and HNO_3 kann jedoch nicht den Überschuss an Sulfataerosolen im Vergleich zu den Nitrataerosolen erklären. Beide Beobachtungen zusammen sprechen für ein antransportiertes Aerosol aus Ammoniumsulfat und Ammoniumnitrat, mit einer zusätzlichen lokalen Komponente des Nitrataerosols.

Contents

List of Figures

List of Tables

Chapter 1

Introduction

The lowest layer of the atmosphere, and the most important for life on Earth, is called the troposphere. Its importance lies on two facts. On one hand, within the troposphere almost everything classified as weather takes place, which has an impact on the human activities. On the other, whatever composes the tropospheric air is what all the living creatures breathe.

The troposphere ranges in thickness from 8 km at the poles to 16 km over the equator and is bounded above by the tropopause. The vertical profiles of pressure and density are approximated by considering the atmosphere in an hydrostatic equilibrium. The hydrostatic law that results, causes air pressure and density to decrease approximately exponentially with increasing altitude, as described in Bohren and Albrecht [1998], so that the largest fraction of the total atmospheric mass (the latter being 5.14×10^{18} kg, as determined by Trenberth and Guillemot [1994]), is located in the troposphere. Below the tropopause, the altitude of which depends on latitude and season, temperature increases strongly moving down through the troposphere, to the surface.

Throughout most of the atmosphere, the air acts as a carrier for a large number of trace gases and a mixture of solid and liquid materials in the form of finely dispersed particles. These assemblies of particles suspended in the air are called aerosols. In atmospheric science, aerosols are defined as minute particles suspended in the atmosphere. Their presence is noticed directly, as they scatter and absorb sunlight. Their scattering of sunlight gives the red-yellow colors in sunrises and sunsets, and reduces visibility (Figure 1.1). This visibility, is determined by the mass and size distribution of aerosols in the air (Lee et al. [2005]). While, the horizontal visibility is important for the road traffic, the vertical visibility plays a significant role as well, especially in aviation and astronomy. As an indirect effect, aerosols in the lower atmosphere can modify the size of cloud particles,

FIGURE 1.1: Effects of aerosols in the atmosphere.

changing how the clouds reflect and absorb sunlight, thereby affecting the Earth's energy budget (Ball and Robinson [1982]).

Aerosols are divided in two categories according to their origin: primary and secondary. Primary aerosols are those directly emitted and appear in the atmosphere as already shaped particles. They result from fragmentation processes in the Earth's surface, or from high temperature processes. Secondary aerosol particles appear in the atmosphere from "nothing" as a result of gas-to-particle conversion. Because of that, these secondary aerosols are present in the sub-micron size fraction. This process, is accomplished either by condensation, which adds mass onto pre-existing aerosols, or by direct nucleation from gaseous precursors.

As far as inorganic secondary aerosol formation is conserned, ammonia (NH_3), a predominant alkaline component in the atmosphere, reacts with acid gases and forms ammonium (NH_4^+) aerosol salts. Sulfuric acid (H_2SO_4), as the product of the sulfur dioxide (SO_2) oxidation, is the main gaseous precursor for sulfate aerosol. Its reaction with NH_3 forms ammonium-bisulfate ($(NH_4)HSO_4$) and subsequently ammonium-sulphate ($(NH_4)_2SO_4$). Nitric acid (HNO_3), as the product of nitrogen dioxide (NO_2) reaction with hydroxyl radicals (OH) during the day, or as the product of dinitrogen pentoxide (N_2O_5) reaction with water during the night is the main gaseous precursor for nitrate aerosols (NO_3^-). The reaction of HNO_3 with NH_3 forms ammonium-nitrate (NH_4NO_3). The partioning between gas (g) and aerosol (s) phase for sulfate and nitrate is described by the reactions 1.1 and 1.2.

$$H_2SO_4(g) + NH_3(g) \rightleftharpoons (NH_4)HSO_4(s) \tag{1.1}$$

$$HNO_3(g) + NH_3(g) \rightleftharpoons (NH_4)NO_3(s) \tag{1.2}$$

Organics, in gaseous form, are also present in the atmosphere. Volatile organic compounds (VOCs), are emitted from plants and trees (like isoprene, monoterpenes and sesquiterpenes), but also from vehicles and industry (aromatics), or other airborne activities. When entering the atmosphere, oxidation of VOCs from hydroxyl (OH), O_3,

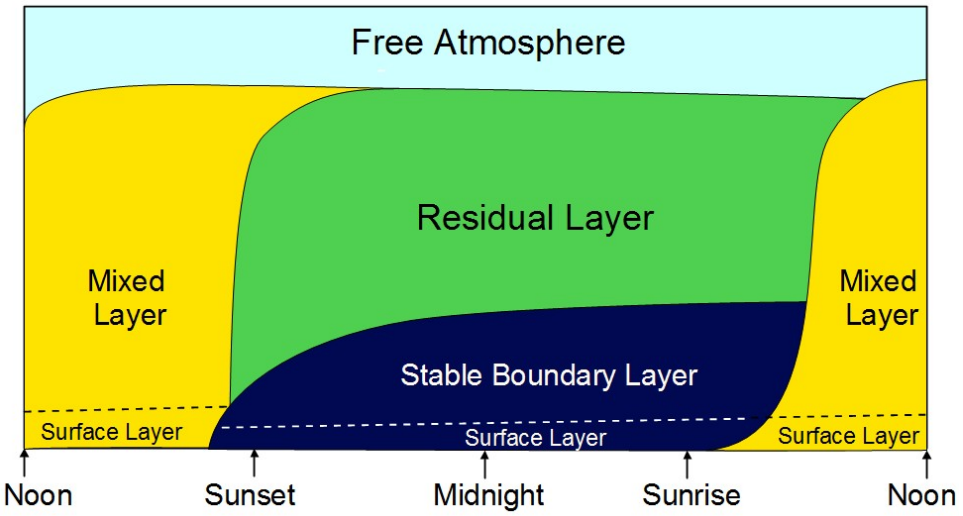

FIGURE 1.2: Idealized planetary boundary layer evolution, adapted by Stull [2012].

or HNO_3, takes place (Griffin et al. [1999]). The oxidation products, are less volatile than the reactants. When the supersaturation of a product is high enough to overcome the nucleation barrier given by the Kelvin effect, it will condense and form particles. This process is called homogeneous nucleation. When pre-existing aerosols are available, the oxidation products can condense on these without supersaturation, if the saturation vapour pressure, determined by the mixture is reached. Secondary organic aerosols, since they have a large number of different components, are in general difficult to be studied.

As a result of these mechanisms, the composition of aerosols in a local area is largely influenced by the concentrations of NH_3, H_2SO_4, HNO_3, organics, and water vapour in the atmosphere. The chemical transformations that occur in the troposphere, so between different gas compounds, as between gas and aerosol compounds, are more prominent and important in the planetary boundary layer (PBL).

The PBL is defined as the lowest part of the atmosphere, in contact with the planetary surface. The thickness of the PBL is variable and evolves as a function of daytime, as shown in Figure 1.2, since the heat transfer from the surface depends on the diurnal heating of the surface from the sun. In the morning, the earth's surface is warmed up by solar radiation so the lower layers are heated up, while cooler layers lie above, leading to the development (rise) of a convectively mixed layer (ML). In the evening, radiative heating from the ground is absent. The temperatures of layers closer to the ground are lowered, while still warmer air lies in higher layers, above. The mixing with air parcels from above is prevented and a stable layer is formed at the earth's surface, called stable nocturnal boundary layer (NBL). Because the NBL develops from the ground, the air above it separates the ML from the ground and preserves the properties of the previous

day's ML, without direct contact to the surface. Reflecting the residual of the previous day's ML, the layer above the NBL is defined as the residual layer (RL). In the next morning, radiative heating starts again and a new ML develops by attenuating first the NBL and then the RL. The thin layer where stable air from above enters (entrains) the convective ML is defined as the entrainment zone. In order to study the diurnal evolution of the PBL and its effect on the chemical constituent concentrations, it appears necessary to perform measurements, on one hand with a time extend from the early morning hours to noon, and on the other, with a vertical extend from the surface up to an altitude comparable with the maximum PBL height.

During the most of the previous field campaigns, the observations that have been used were ground based. Those include measurements at stable points in space which are usually in the low surface layer, whether studying gas phase (Rohrer et al. [1998], Han et al. [2011]), or aerosol phase (Spracklen et al. [2011], Crippa et al. [2014], Aan de Brugh et al. [2012]). The variability in the concentrations close to the surface due to an evolving PBL has been captured, but little information can be derived about the variability in the higher altitudes. Airborne studies have also been done in the past (Shon et al. [2008], Menut et al. [2000], Reddington et al. [2011]), where fast moving aircrafts have been used. However, those aircrafts were not proven to be suitable for the study of processes in the PBL for the following reasons. First, the aircraft velocity was relatively high as compared to the slow PBL evolution. Second, the distance covered in only some minutes was long to study the local PBL evolution. Finally, the high flight altitude was too high as compared with the PBL height. Using the Zeppelin NT as a platform of gas and aerosol measurement instruments in the PBL, overcomes the above limitations. The ability to perform flights at low velocities in altitudes lower than 1000 m above the surface, makes it the ideal platform for characterizing the processes within the PBL.

In addition, nitrate, as an aerosol component, has received comparatively little attention. It is not as easily predicted as sulfate, since it is partly transported and partly locally produced, making the distinction between the 'transported' component and the 'local' component not straightforward. However, in studies including nitrate, it is shown that it is an important aerosol species both today and over the 21st Century and important in areas where large urban and agricultural emissions coincide (Walker et al. [2012]). In addition, as noted in Schmidt et al. [2014], nitrate was only included in two of the models that contributed to the Coupled Model Intercomparison Project (CMIP5) and this inclusion brought models closer to the observed surface temperature trend.

Linking the above, it is apparent that the dataset compiled by on board the Zeppelin NT observations, is unique and promising. It can provide a new insight to processes in

terms of high resolution vertical profiles, dynamics, and chemistry, both gas and aerosol phase.

A significant part of this work was focused on the set up of an operational forecast system running on a 1 km spatial resolution grid as a means of online support during the course of a measurement campaign. This included the meteorological initialization on a 1 km gridded topology, allowing consequently the extension of the chemistry transport model to a 1 km horizontal resolution, by using aggregated emission fields in the same resolution.

The main target of this work was to enable the comparison of the measurements by instruments on board on the Zeppelin NT with the output of a regional chemistry transport model. Chemical constituents treated, include both gas-phase and aerosol species. The model is evaluated over the course of a seven week period, covering two campaigns in 2012, in two European countries. A better understanding of the success and/or failure of the model to capture observations is aimed by studying specific campaign days. Finally, a discussion aims to investigate the regional character of sulfate, ammonium, and nitrate aerosol components.

Chapter 2

Methodology

2.1 The PEGASOS project

2.1.1 Project description

The Pan-European Gas-AeroSOls-climate interaction Study (PEGASOS), as a European large scale integrating project, had the target to study in which degree do the regional atmospheric processes affect global processes and vice versa, as concerns both chemistry and changing climate. The ultimate aim is the reduction of the uncertainty of those feedbacks. In addition, mitigation strategies and policies will be proposed, in order to improve air quality while limiting their impact on climate change. In order to optimize the methodologies and the understanding of air quality and climate interactions, the project was organized into separate scientific themes. The first theme was the anthropogenic and biogenic emissions and their response to climate and socio-economy. The second theme was the atmospheric interactions among chemical and physical processes. The third theme was the regional and global links between atmospheric chemistry and climate change. Finally, the last theme was the air quality in a changing climate and the integration with policy.

Local pollutant exchanges from surface to air and vice versa, air quality, and weather are undoubtedly connected with global atmospheric chemistry and climate. However, the aforementioned operate in different temporal and spatial scales. The PEGASOS project aims to provide understanding about the connection between those scales by studying the area of Europe considering changing pollutant emissions with a time horizon of 50 years. In order to quantify the feedbacks between air quality and a changing climate our understanding of several atmospheric processes needs to be improved. Within the project, the dynamically changing emissions and deposition will be analysed and linked

FIGURE 2.1: The Zeppelin NT airship during landing.

to tropospheric chemical reactions and interactions with climate. The emerging connections between chemistry-climate and surface processes will be presented. Scales of study include local, regional and global phenomena. Because of the complexity of the processes under study the need of a unique measurement platform, the Zeppelin NT, has risen.

In 2012 and 2013, airship based measurements of gas phase and aerosol phase were performed in several European regions. The Zeppelin NT, equipped with measurement instruments, was transferred to the Cabauw region in the Netherlands, from 19 May to 27 May 2012, to the Po-Valley region in Northern italy, from 18 June to 13 July 2012, and the following year, 2013, to the Hyytiälä and Jämijärvi regions in Finland.

2.1.2 The Zeppelin NT as a measurement platform

The Zeppelin NT is a semi-rigid airship that has a total length of 75 m and a maximum hull diameter of 14m (Figure 2.1). Its skeletal carbon structure is covered by multilayer laminate. The hull is inflated with helium (He) which is used as a lifting gas. Together with the attached propellers, the Zeppelin NT achieves the required uplift with a maximum payload of 1900 kg. The three propeller configuration (one at the back and two at the sides) allows for take-off and landing without horizontal velocity. Depending on the weather conditions, the Zeppelin NT has a maximum flight endurance of 24 h. It has a maximum cruising speed of 115 km/h, a maximum range of 900 km, and a maximum flight altitude of 2600 m.

However, the actual maximum altitude is limited by the following factors. First, the expansion of He in the hull, because of reduced outside pressure when in altitude, has

a limit for the sake of the Zeppelin integrity, setting a pressure limit. While altitude increases, the He expansion is assisted by Ballonets (additions inside the hull inflated with ambient air), which at the same time lose air. At the point where the maximum pressure of He has been reached and the Ballonets have lost all their air, the maximum altitude has been reached. However, the heavier the payload, more He has to be inflated in the hull, allowing less inflated Ballonets at ground level which consequently limits the allowable He expansion. Second, when the ambient temperature increases, the ambient air density decreases, so the difference in density between ambient air and He decreases and so does the lifting capacity. Opposing, when the temperature of the hull increases due to solar radiation, the He density decreases, so the difference in density between ambient air and He increases (superheat effect) and so does the lifting capacity. Taking into account all the above, with full scientific payload, the maximum altitude, during the campaign, varied between 400 m and 750 m.

2.1.3 Instruments on board

For the PEGASOS campaigns a variety of instruments were developed and adapted to fulfil the Zeppelin requirements. These requirements include the minimum possible weight, so that altitude and flight endurance are affected as little as possible, and the mounting onto fixed points, in agreement with airship security regulations. Light racks, mountable to the seat rail inside the Zeppelin cabin, were developed for the purpose of hosting the electronics and parts of the instruments. However, space and payload limitations did not allow simultaneous installation of all. Three combinations of instruments, named cabin layouts (CL), were decided in advance in such a way that each combination corresponded to a different scientific task.

Several instrument racks were present in every cabin layout. These were the COD, CPN, NOX and Top-Platform. The COD instrument measured the CO concentration. The CPN rack included instruments to measure particle size distribution and particle number concentration. The NOX rack included instruments measuring concentrations of NO, NO_2, and O_3 and upwelling spectral actinic flux. Photolysis frequencies were calculated from the upwelling and the downwelling spectral flux measured at the Top-Platform. In the Top-Platform instruments that measured the concentrations of the radicals OH and HO_2 as well as the total OH reactivity. The always present instrument group is completed with the addition of the meteorological boom which measured temperature, relative humidity, and three dimensional wind.

The cabin layout CL8 aimed to a detailed photochemistry characterization. In addition to the always present instruments it contained the LOP, FFL, and HGC racks. The

LOP rack contained an instrument detecting HONO. The FFL rack contained an instrument measuring HCHO. The HGC rack included instruments that determined VOC concentrations.

The cabin layout CL9 was compiled in order to investigate the process of nucleation. Together with the always present, the API and the NAS were added. The first one can determine the composition of naturally charged ions and clusters while the second one measures the distribution of ions over a range of electrical mobilities, and the distribution of particles between 2nm and 40nm.

Finally, the cabin layout CL5 was used to study secondary organic aerosols (SOA). The PSI rack and the AMS instrument, were added to the constant configuration. The PSI included instruments that measured black carbon mass concentration, number size distribution of particles with diameters larger than 200nm as well as hygroscopicity (a factor that characterizes particle growth). The AMS instrument is described in the following paragraph.

The development and installation of the AMS instrument under the Zeppelin requirements is described in detail in Rubach [2013]. The particles are sampled through an inlet followed by an aerodynamic lens that focuses particles with size between 0.1 μm and 0.7 μm on a beam. Entering a vacuum chamber, particles are accelerated to velocities inverse proportional to their size, before entering the particle sizing chamber, in which packages of particles are created with common starting point and starting time (by a chopper) but different velocities. They are directed into the particle detection chamber where they are impacted on a heated surface and vaporized. The resulting ions then are accelerated by electrostatic fields into a mass spectrometer which detects ion rates on a mass to charge ratios spectrum. These ion rates are interpreted as mass concentrations of the different aerosol species.

2.2 The model system

The EURAD-IM (EURopean Air pollution and Dispersion) model system is a numerical model system able to simulate the physical and chemical evolution of trace gases and aerosols in the troposphere and lower stratosphere. The suffix IM (Inverse Model) indicates that the system has been expanded by an inverse part. The forward part of the model system - the standard forecast system that is used in this work - consists of two major models: First, the meteorological model WRF (Weather Research and Forecast) acts as the meteorological driver for the chemistry transport model. It calculates

and delivers the meteorological fields that are necessary like wind, temperature and relative humidity. Second, the EURAD-IM chemistry transport model (EURAD-CTM) is a mesoscale model that simulates the processes of horizontal and vertical diffusion, horizontal and vertical advection, chemical transformation, and wet/dry deposition, for tropospheric gases and aerosols.

2.2.1 The meteorological model

The WRF model is a numerical weather prediction model designed for both research and operational applications. The non-hydrostatic fully compressible Euler equations are solved to calculate the prognostic variables:

- horizontal velocity components u and v (in Cartesian coordinate),
- vertical velocity w,
- perturbation potential temperature,
- perturbation geopotential,
- perturbation surface pressure of dry air,
- and a number of optional variables as turbulent kinetic energy and water vapor mixing ratio.

The horizontal grid follows the Arakawa C-grid staggering. The vertical grid follows the terrain (sigma levels), with vertical stretching permitted, so the vertical levels are defined as:

$$\sigma_k = \frac{p_k - p_{top}}{p_{bot} - p_{top}} \tag{2.1}$$

where:

- k the layer number
- p_k the pressure at layer k
- p_{bot} the pressure at the surface
- p_{top} the pressure at the top of the model domain, which is kept constant (1000 Hp)

The time integration is done using a 2nd- or 3rd- order Runge-Kutta scheme with variable time step capability.

2.2.2 The chemistry transport model

2.2.2.1 Functional principles

The EURAD-IM chemical transport model (CTM) is an Eulerian meso-scale model involving advection, diffusion, chemical transformation, wet and dry deposition and sedimentation of tropospheric trace gases and aerosols (Jakobs et al. [1995],Memmesheimer et al. [2004]). It solves the following equation:

$$\frac{\partial c_i}{\partial t} = -\nabla(uc_i) + \nabla(K\nabla c_i) + E_i + F_i + \frac{\partial c_i}{\partial t}|_{chem} + \frac{\partial c_i}{\partial t}|_{cloud} + \frac{\partial c_i}{\partial t}|_{aerosol} \tag{2.2}$$

and with c_i indicating the mean concentration of the species i, the terms on the right hand side of the Equation 2.2 represent changes of concentration due to the following processes:

- $\nabla(uc_i)$: advection meaning transport by wind, where u is the wind velocity vector
- $\nabla(K\nabla c_i)$: turbulent diffusion
- E_i: emission rates
- F_i: fluxes
- $\frac{\partial c_i}{\partial t}|_{chem}$: gas phase chemical conversion
- $\frac{\partial c_i}{\partial t}|_{cloud}$: transport in clouds, aqueous chemistry and wet deposition
- $\frac{\partial c_i}{\partial t}|_{aerosol}$: aerosol chemistry (processed in MADE)

The operator splitting technique is applied in a way that advection and diffusion are applied symmetrically around the solver modules for gas and aerosol phase processes. The model state is updated in time as follows:

$$x_i(t + \Delta t) = T_h T_u D_u C M D_u T_u T_h x_i(t) \tag{2.3}$$

where:

- $x_i(t + \Delta t)$ the model state, that is concentration/mixing ratio of species i
- t the time step
- Δt the length of a time step
- T_h the advection module in horizontal direction

- T_u the advection module in vertical direction
- D_u the vertical diffusion
- C the gas-phase chemistry solver
- M the aerosol dynamics solver

The T and D operators are applied at one half of the model's timestep before and one half after the C and M operators.

2.2.2.2 Treatment of aerosols

Within the CTM, aerosols are treated by the Modal Aerosol Dynamics module for Europe (MADE). Based on gas-phase concentrations calculated during the CTM run, meteorological values provided by the WRF, and emissions, the MADE simulates the bidirectional transfer between gas and aerosol phase, in a way that aerosol and gas phase are directly coupled.

As concerns size, MADE is trimodal, that is, the particles are separated into three modes. The coarse particles, making the coarse mode, namely marine sea salt, mineral dust, and coarse particles of anthropogenic origin, are primary aerosols with no exception, meaning they are emitted as they are. The minimum median diameter of this mode is 1.0 μm. The fine particles are separated into two modes. The Aitken mode, representing freshly emerged, very small aerosols, has a minimum median diameter of 0.01 μm. The accumulation mode, representing aged aerosols, has a minimum median diameter of 0.07 μm. Particles in the Aitken mode have high number concentration, especially near their source, and through the process of coagulation (the collision of two particles into one), end up relatively fast in the accumulation mode. However, particles in the accumulation mode coagulate slowly to reach the coarse mode. Sulfate, ammonium, nitrate and organics masses are assigned to the fine particle category, with median diameter less than 1.0 μm but with most of the mass in less than 0.75 μm. So the modeled sum of Aitken and Accumulation mode for the three prementioned aerosol species is comparable to the AMS measurements. Table 2.1, lists aerosol species treated in MADE with their modal assignment.

For fine particles, the most important mechanism is the solution of the equilibrium of the system H^+—NH_4^+—SO_4^{2+}—NO_3^-—H_2O. The solution, based on the Pitzer-Simonson-Clegg model from Clegg et al. [1992] and the Analytical Predictor for Condensation described in Jacobson [1997], namely PSC/APC, is implemented and developed using an iterative approach with temperature dependant activity coefficients (factor used in

	Aitken	Accumulation	Coarse
Primary Aerosols			
elemental carbon	■	■	
primary organic	■	■	
primary anthropogenic	■		■
marine (sea salt)		■	■
soil derived mineral dust			■
Secondary Inorganic Aerosols			
sulfate	■	■	
ammonium	■	■	
nitrate	■	■	
aerosol liquid water	■	■	
Secondary Organic Aerosols			
anthropogenic from aromatic	■	■	
anthropogenic from alkenes	■	■	
anthropogenic from olefines	■	■	
biogenic from α-pinene	■	■	
biogenic from limonene	■	■	

TABLE 2.1: Aerosol species processed in MADE and their modal assignment.

thermodynamics to account for deviations from ideal behaviour), by Friese and Ebel [2010]. Even though this solution is accurate, it is also computationally demanding due to its iterative nature. For operational purposes, a High Dimensional Model Representation (HDMR) from PSC/APC was built and implemented by Nieradzik [2005], which significantly reduces computing time and allows for three dimensional chemistry transport calculations.

2.2.3 The forecast sequence

The daily chemical weather forecast that was used in this project is shown in Figure 2.2, and the following description refers to the same figure. First, the meteorology part is initiated (light blue). After the area of interest has been chosen and projected in the model domain the terrestrial data is downloaded, which includes topography information like surface height above sea level as well as soil type and vegetation. This data, in addition to meteorological initial (meteorological state at 24:00 UTC of previous day) and boundary (meteorological state at line enclosing area of interest, taken from a global meteorological model) is needed for the meteorology calculation of the 'current' day of interest. This calculation, as described in 2.2.1 provides the meteorological fields of the projected area. Secondly, as a preparation for the chemistry transport model the emissions fields should be processed to fit the area of interest and the 'current'

day (yellow). The TNO 2012 emission inventories are used as a primary source. From these inventories the area of interest is cut to fit our area of interest and the model resolution. This process includes the calculation of the hourly emission rates from the yearly rates taking into account the day of year, meteorology as well as mean human hourly activity. In addition, since a comparison with the Zeppelin observations is desired, the raw observations data is processed, so that each measurement is given a time/location in the model timeframe/domain (red).

The above mentioned, together with chemical initial (chemical state at 24:00 UTC of previous day, taken from the previous day chemical forecast) and boundary (chemical state at line enclosing area of interest, taken from a global model for the coarse grid or from the mother domain for a nest grid) conditions, make the input for the chemical transport model. This calculation provides the chemistry fields, for gas and aerosol phase for the the initially chosen area, as well as the one to one (measurement-model value) comparison.

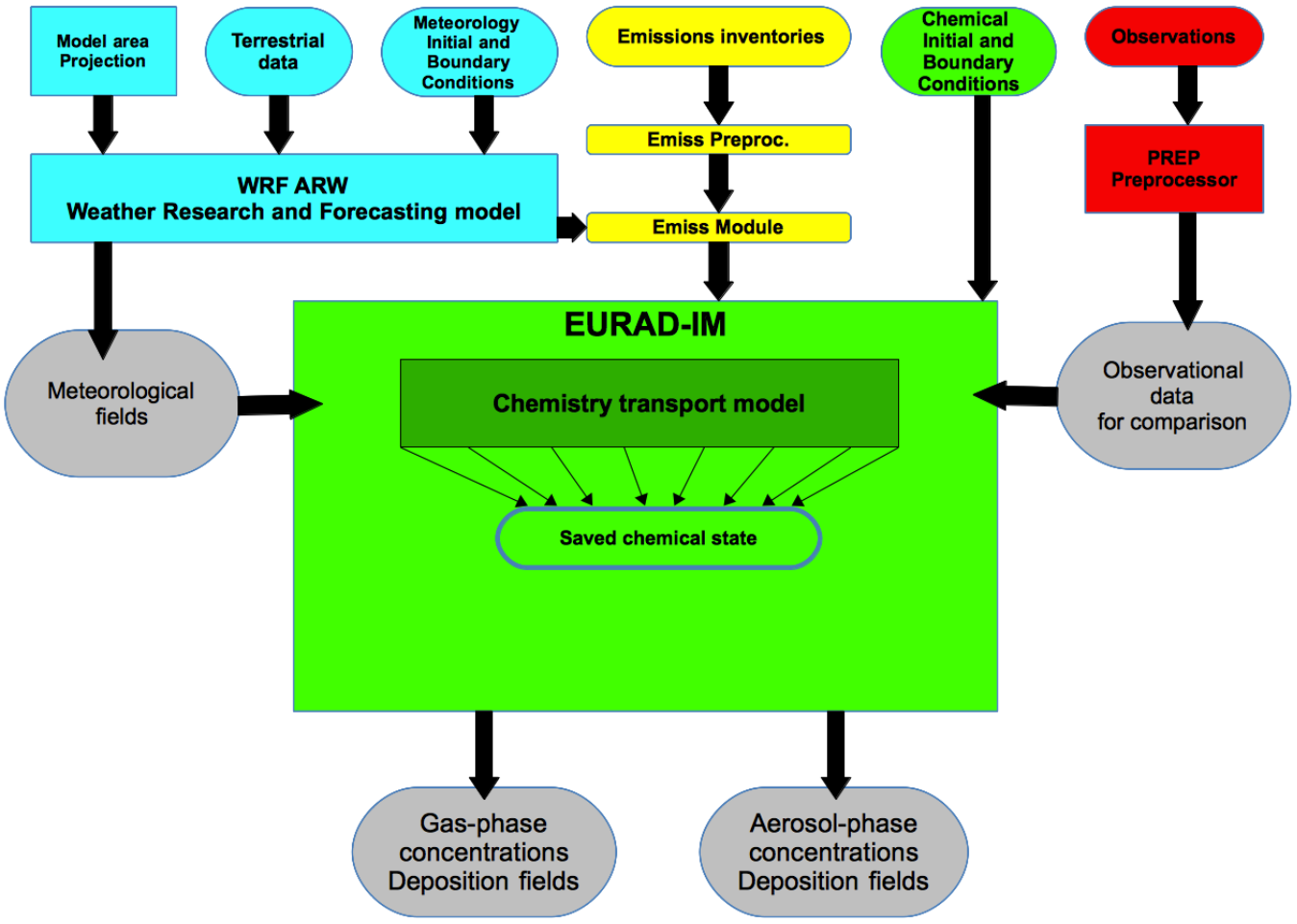

FIGURE 2.2: The scheme of the forward part of the EURAD-IM forecast system.

2.3 Tool developments

2.3.1 Online campaign support activities

As part of support activities, a special chemical and meteorological forecast tool for flight missions has been developed. Operated at the Rhenish Institute of Environmental Research at the University of Cologne (RIU), the EURAD-IM model has been extended to versatile high resolution (1km) model domains for operational mission planning. This system was operated on a dedicated computing platform, which allows for daily forecasts with fixed schedule, and was applied to both PEGASOS campaigns of spring 2012 and spring 2013.

Within the operational forecast chain two fixed grids are being computed for the areas of greater Europe (p15, with a resolution of 15km) and Central Europe (p05, 5km). During a campaign, the measurement area and consequently the calculation area can change by day. To account for this, a sequence of "jumping" grids (jc1, with a resolution of 1km) was set up, covering both the transfer flights from the airport of Friedrichshafen to the main measurement areas, and the daily flight patterns (transects or vertical profiles). In addition, an alternative or "follow-up" grid has been simulated to provide a forecast for the most probable (next day) region to succeed the current location of the Zeppelin NT. In order to operate the jumping grids, the input files of EURAD-IM should be prepared or "cut" beforehand to the respective grid parameters and that is meteorology - which is provided by the WRF model, and emissions which are cut beforehand by a "mother" emission grid (GIS aggregated TNO data) to meet the position and size of the 1km grid. The 1km grids, as support to the PEGASOS 2012 campaigns to the Netherlands and to northern Italy, together with the Zeppelin transfer track are shown in 2.3.

The forecast results have been presented on an online "forecast browser" (e.g. for the PEGASOS campaign: http://www.riu.uni-koeln.de/PEGASOS/) for selected species at a selected number of model layers. The "forecast browser" (that is an online image-viewer), has been created to provide an easy-to-use tool to browse the forecast products in time, height, species, and domain. Different types of visualizations were available like horizontal 2d plots, time-height plots, vertical cross-sections and time-series. A snapshot of the "forecast browser" displaying a horizontal 2d plot is shown in Figure 2.4.

2.3.2 Post campaign developments

After the campaigns, and when the measurement data was made available, additional processing was done to enable the measurement-model comparison and interpretation.

(A)

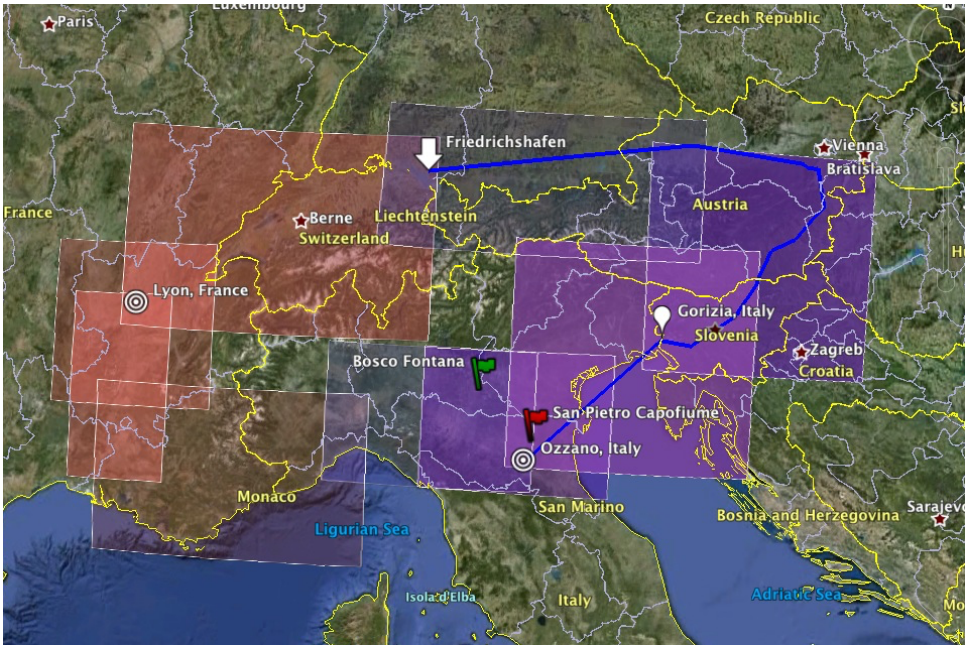

(B)

FIGURE 2.3: Transfer and main measurement area 1km grid boundaries and the Zeppelin NT transfer track (red), for the PEGASOS 2012 campains: (A) in the Netherlands, where the CESAR tower is located, and (B) in Italy, where the San Pietro Capofiume site is located.

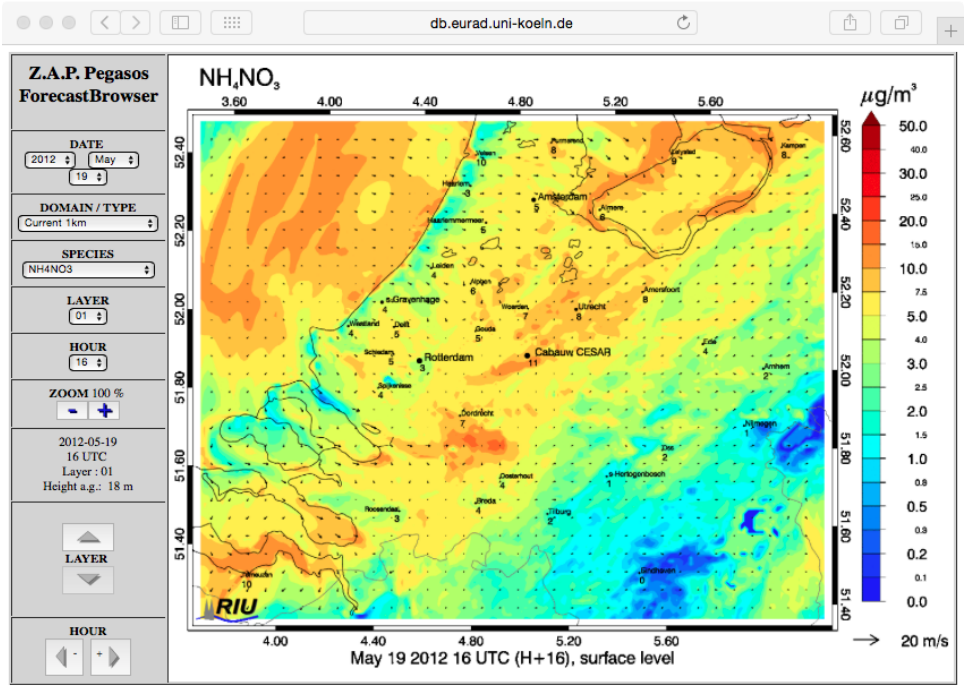

FIGURE 2.4: Snapshot of the Forecast browser.

First, in the pre-processor of EURAD-IM for observations, a part was added to account for the PEGASOS observations for all the measured species and parameters. By mapping the Zeppelin track in the three-dimensional model domain at the correct time, each observed value corresponds to a predicted value.

In addition, since the study was focused on vertical profiles, a type of time-height plot (Hovmöller) was developed, that displays the diurnal vertical profile evolution. During the model calculation, which has a time resolution with respect to the horizontal resolution of the configured grid (60-300 sec), the concentrations and parameters are updated for output with a time resolution of 10 min (higher than the default output time resolution of 1 h), for the Zeppelin location, for all the model levels (from the surface to a selected maximum height). For this location then, the vertical profile is color coded and plotted from 00:00 to 24:00 as a background. Then the measurements along the Zeppelin track can be overlayed with the same color coding to enable comparison. An example for predicted O_3 on 2012-07-12 together with the Zeppelin track at that day, is shown in Figure 2.5.

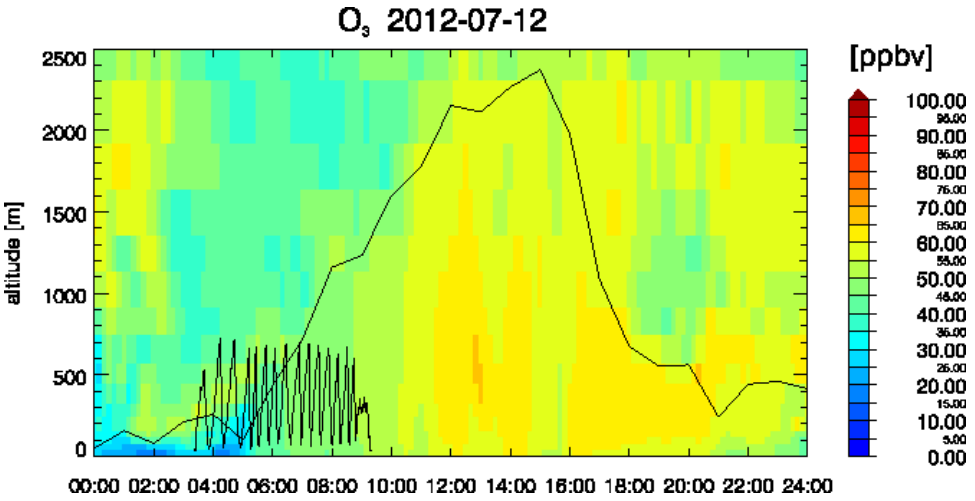

FIGURE 2.5: Time-height plot example with the Zeppelin track overplotted.

2.4 Expected challenges

The aim of this thesis is to compare results from a regional model with observations along the Zeppelin NT track. Expected difficulties that are related to the spatial and temporal resolution of the model as compared with the Zeppelin track and time resolution of measurements are mentioned as follows:

First, the comparison is done 'point to point', without taking mean values. Each measurement is compared with the respective value in the model, without interpolation. Taking this into account, it is known from the beginning that the observations will not be captured in detail. Even though the general dynamics and chemistry features will appear in the model, that doesnt mean that they will appear in the exact same time and location as in the measurements.

Second, unlike ground measurements that are able to measure through 24 hours of a day, the Zeppelin NT has a short measuring time span. So, instead of studying the diurnal evolution for constituents, which would have been easier as concerns the comparison with a model, observations span only several hours (the vertical profile with the longest duration is about 6 hours on 2012-07-12). It would have been interesting to have measurement time frames that start in the evening and finish in the morning of the next day. Since these kind of flights were not performed, there are no observations during the evening breaking up of the PBL, and this process will not be treated in this thesis.

The horizontal resolution of the model is 1 km. However, the Zeppelin perfomed vertical profiles by circling a location with a radius of about 500 meters as shown in Figure 2.6. As a result, the horizontal movement could span maximum 4 grid boxes in the model

domain. That could give unwanted, but explained concentration fluctuations due to the space discretization. The vertical resolution of the model is variable with height with denser levels close to the surface. The vertical profiles were performed with a maximum height of 800-1000 meters which spans 7 to 9 layers in the model domain. For one ascending of the Zeppelin only 7-9 model points are given for comparison. As an example, for the vertical profile at 4:00 of 2012-07-12, shown in Figure 2.6, the measurements can be compared with 8 model values. In the diurnal boundary layer cycle the dynamics that occur are expected to be somewhat resolved but in a coarse way in comparison with the measurement resolution.

In general, the exact mixed layer height is difficult to be predicted as it is difficult to have a very good representation of the meteorological and dynamical conditions. Studies have shown (as an example Viterbo et al. [1999]) that even with the same forcing conditions but with (slightly) different stability treatment in the mixing scheme, big differences in the mixed layer height are produced. The prediction efficiency depends on how much of the micrometeorology is captured by the model as well as how exact are the calculated values for the heat, latent and sensible (latent is related to changes in phase between liquids, gases, and solids while sensible is related to changes in temperature with no change in phase), and relative humidity. The knowledge of the correct soil heat capacity also plays a sygnificant role as it determines the soil response to heating from the sun. Today, the mixed layer height can be predicted within an uncertainty of approximately 100 meters. Since the mixing conditions are those who determine the vertical transport of chemical constituents, it is known from the beginning that differences between the predicted and observed mixed layer height will have undoubtely an big effect on the prediction quality of all chemical species.

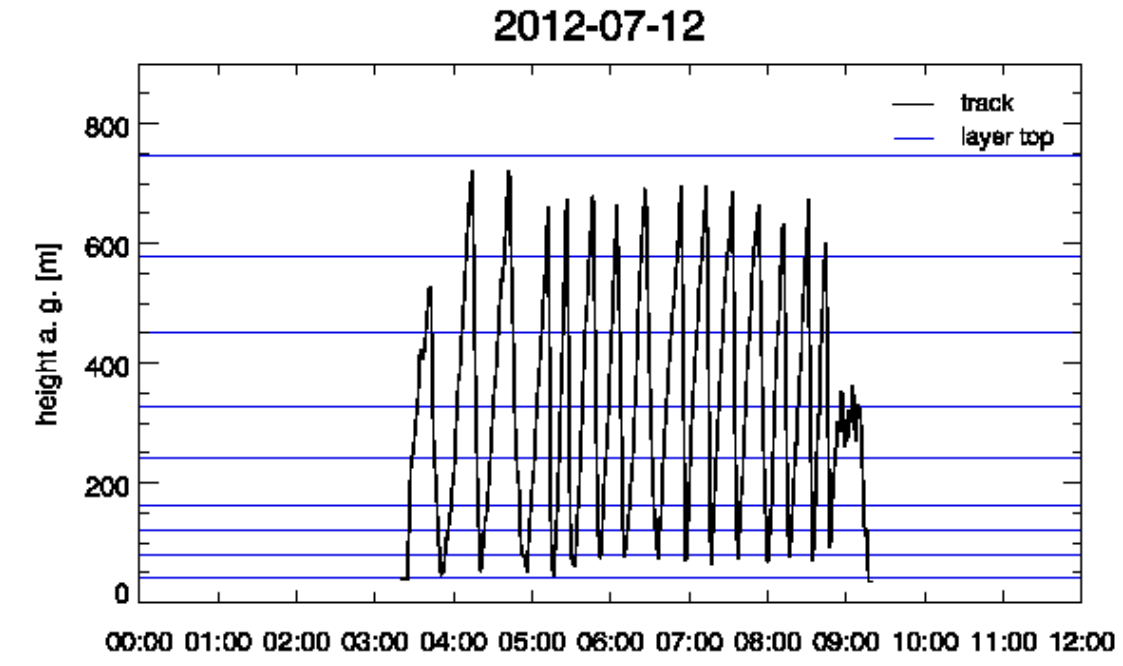

(A)

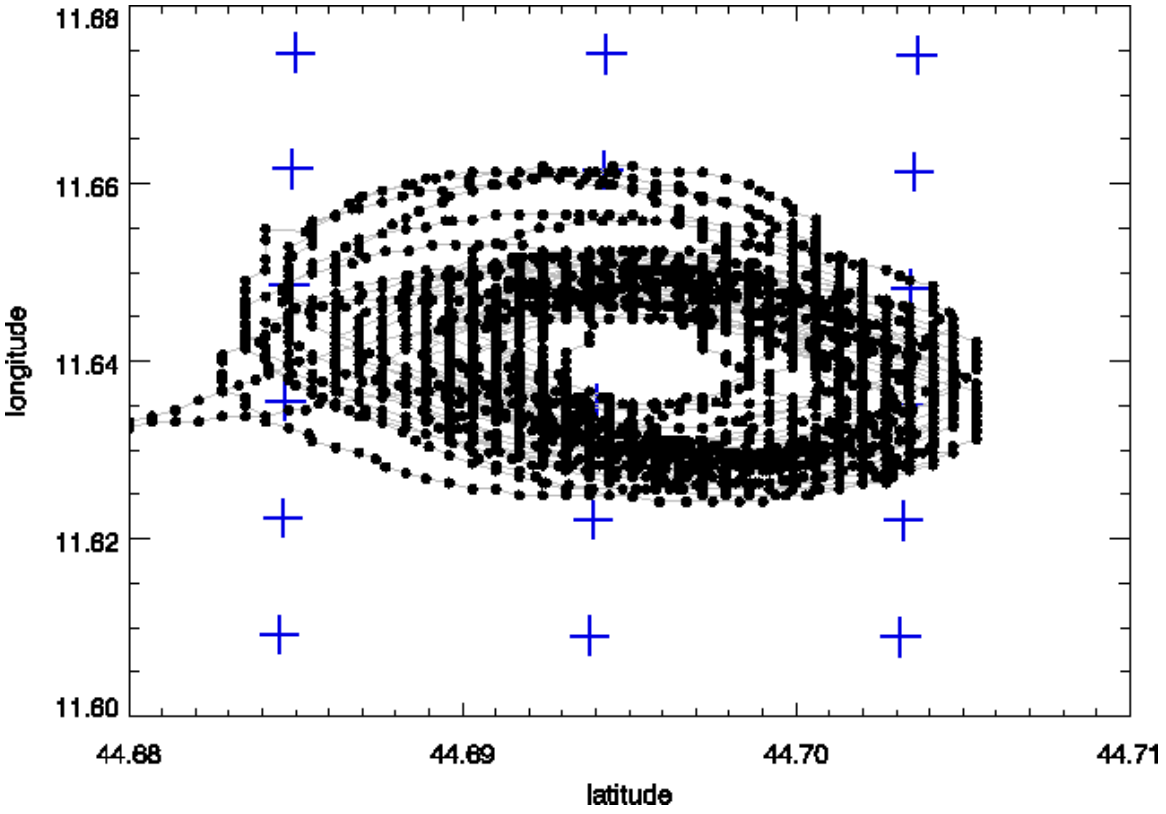

(B)

FIGURE 2.6: Zeppelin track at 2012-07-12 (vertical profiles) plotted with: (A) vertical model grid - blue lines and (B) horizontal model grid (cell centers) - blue crosses

2.5 Evaluation metrics

In order to evaluate a model against observations, one can select among a variety of statistical metrics. The large number and the diversity of the existing metrics makes the selection for the judjement of the overall model performance difficult. In addition, several of these metrics are not efficient, since they are subject to assymetry and/or bias. In this project, as a first measure of the model performance, the mean value of observations ($\bar{O}$), and the mean value of respective predictions ($\bar{M}$) is calculated. These mean values are combined graphically yielding the center of gravity (COG) in a scatterplot where all observations are plotted in the y axis and the respective predictions in the x axis. In this case, the center of gravity has coordinates:

$$[cog_x, cog_y] = [\bar{M}, \bar{O}] \tag{2.4}$$

A new set of metrics is proposed in Yu et al. [2006], based on the concept of factors, that is both unbiased and symmetric. This means, first that the undue influence of small numbers in denominator is avoided, and second that overprediction and underprediction are treated proportionately. In this project, the normalized mean bias factor (NMBF) will be used. The NMBF comes as a result of the sum of the individual factor bias with observations (or model) conceived as a weighting function. It ranges from $-\infty$ to $+\infty$ and the calculation is done as follows:

$$NMBF = \begin{cases} (\frac{\bar{M}}{\bar{O}} - 1) & \text{if } \bar{M} \geq \bar{O} \quad \text{(overprediction)} \\ (1 - \frac{\bar{O}}{\bar{M}}) & \text{if } \bar{M} < \bar{O} \quad \text{(underprediction)} \end{cases} \tag{2.5}$$

The interpretation of the NMBF is done as follows: if NMBF is positive, the model overestimates the observations by a factor of NMBF+1. If NMBF is negative, the model underestimates the observations by a factor of 1-NMBF. Although the widely used Pearson correlation coefficient (r) can be near unity despite systematic model underprediction or overprediction, it is calculated in this project as a measure of the strength and direction of the linear relationship between predicted and observed concentrations. The calculation is based on the formula:

$$r = \frac{\sum_{i=1}^{N}(M_i - \bar{M})(O_i - \bar{O})}{\sqrt{\sum_{i=1}^{N}(M_i - \bar{M})^2}\sqrt{\sum_{i=1}^{N}(O_i - \bar{O})^2}} \tag{2.6}$$

To sum up, in this thesis, the model is evaluated against the observations using the COG, the NMBF, and the r. However, widely known metrics as the normalized mean bias (NMB), the normalized mean error (NME) and the root mean square error (RMSE), are also calculated and illustrated in extended tables in Appendix A

Chapter 3

Description of the data set

3.1 Measurement data

3.1.1 Observations availability

The flights during the 2012 PEGASOS campaings are categorized into transfer flights, transect flights, vertical profiling flights and lagrangian transects. Transfer flights refer to the long flights that brought the Zeppelin from the airport in Friedrichshafen in Germany, with intermediate pre-planned stops, to the airports close to the main measurement areas and back. The airports close to the main measurement areas that were used were in Rotterdam, Netherlands and Ozzano, Italy. The transfer flights are not treated in this work. In the main measurement areas, transect flights and vertical profiling flights were performed, to explore the horizontal and vertical variability respectively. Transect flights were performed in a nearly constant altitude detecting the spatial distribution, temporal evolution and gradients in trace species concentration. In contrast, vertical profiling flights were performed by flying the Zeppelin in circles over a constant geographical location at different altitudes. The lagrangian transects refer to a special type of flight were the Zeppelin is left to follow the wind, exploring the time evolution of air masses. Excluding the transfers, data available for the different flights and their availability are listed in Table 3.1.

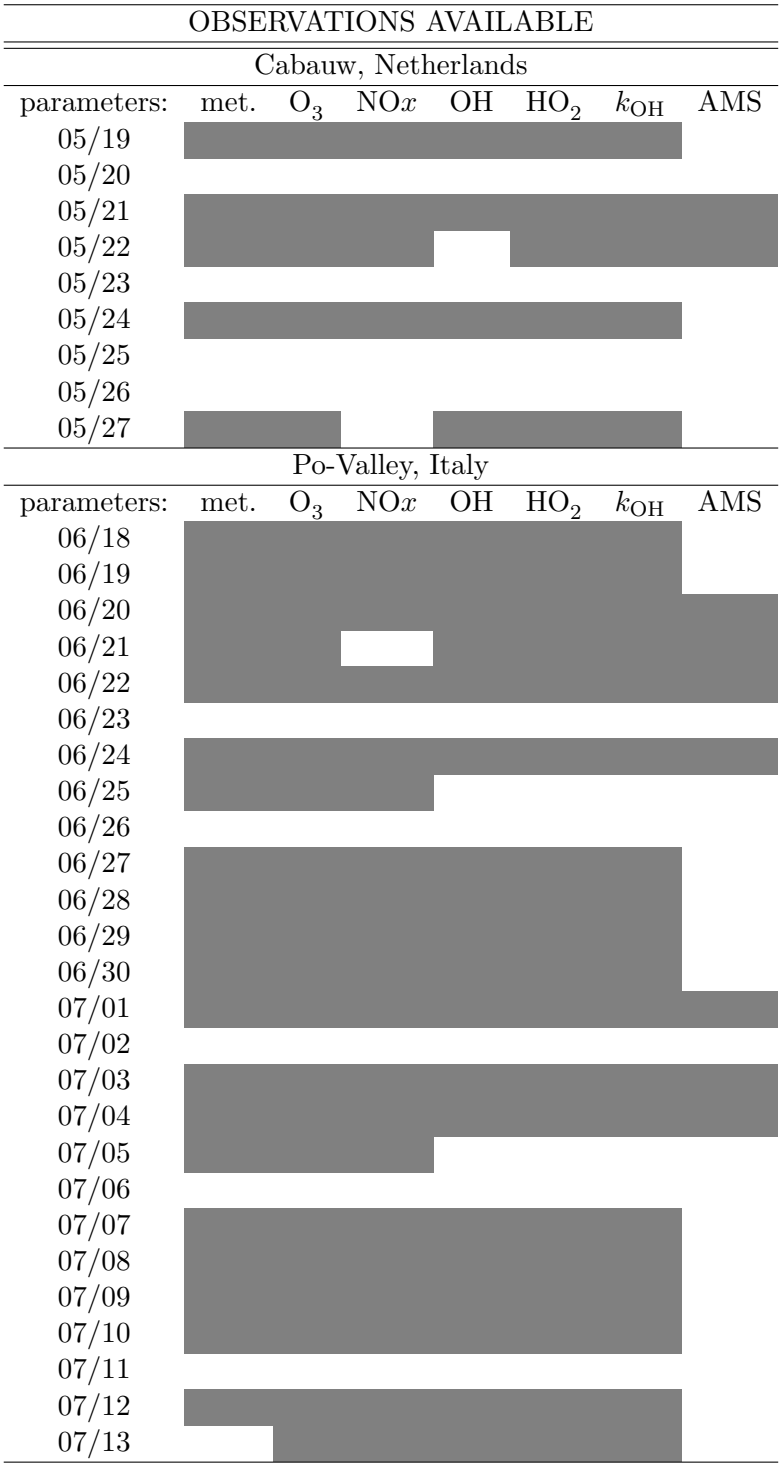

TABLE 3.1: Observations availability for the two 2012 PEGASOS campaigns. The column 'met.' stand for the meteorological variables, and the column AMS stands for the Aerosol Mass Spectometer measurements.

3.2 Model data

3.2.1 Grid setup

The EURAD-IM chemical weather forecast system operates using the nesting technique. This means that there is a grid sequence starting from the coarse "mother" of all domains, which is followed by a finer "nest" domain, which is followed by the finest "nest" domain. While the "mother" of all domains uses boundary conditions from a global model, the finer and finest domains use boundary conditions created by their "mother's" domains respectively. During the PEGASOS campaign, and for this project, the "mother" of all domains - Europe, had a spatial resolution of 15 km and its "nest" - Central Europe, had a resolution of 5 km. For the support of the PEGASOS measurement areas various finest "nests" were used, with a spatial resolution of 1 km. The main 1 km grids used in this work are: the "Cabauw" area grid including Rotterdam (airport location) and the CESAR measurement tower (CT), and the "Po-Valley" area grid including Ozzano (airport location) and the San-Pietro-Capofiume (SPC) measurement site. The grid parameters for the above mentioned computational domains are noted in Table 3.2.

GRID PARAMETERS				
	Europe	Central Europe	Cabauw	Po-Valley
short name	p15	p05	pc1	pv1
boundaries from	global	p15	p05	p05
horiz. resolution	15 km	5 km	1 km	1 km
nr of cells (east-west)	349	316	176	231
nr of cells (north-south)	287	388	141	171
nr of cells (bottom-top)	23	23	23	23
time-step	300 sec	120 sec	60 sec	60 sec

TABLE 3.2: Parameters of the coarse (15 km), fine (5 km), and finest (1 km) computational domains.

3.2.2 Emissions

The EURAD-IM chemical weather forecast system treats both anthropogenic and biogenic emissions as described in Elbern et al. [2007], Nieradzik and Elbern [2006]. An emission module within the system converts the annual emission rates, received by the inventories, to hourly emission rates, with the use of temporal and spatial allocation factors. Moreover, a vertical distribution of the emission rates of each emitted species takes places, based on the source of the emissions and the type of the point sources. For anthropogenic emissions, the TNO-MACC-II emission inventory of the year 2009 is used, with 7×7 km horizontal resolution, described in Kuenen et al. [2014]. The biogenic

emissions, are calculated by the Model of Emissions of Gases and Aerosols from Nature (MEGAN), which is described in Guenther et al. [2012].

The raw emission data from the inventories are available as emission rates in an annual cycle, measuring the average amount of specific pollutants released into the atmosphere by a specific process (fuel/equipment/source), in Mg/year for every country. As far as anthropogenic emissions are concerned, the emission rates of NOx, SOx, CO, NH_3, particular matter (coarse and PM2.5), and non-methane volatile organic compound (NMVOC) are provided for the European emission domain in $0.125^o \times 0.0625^o$ longitude-latitude resolution. Those are subdivided into 10 anthropogenic source/sectors (codes), namely energy industries, non-industrial combustion, industry (combustion and other processes), fossil fuel distribution, product use, road transport, non-road transport and other mobile sources, waste treatment and agriculture. Those datasets are disaggregated based on the emission origin using the Corine Land Cover dataset (Stjernholm [2009]) and the OpenStreetMap dataset (Haklay and Weber [2008]). Eventually, this aggregated information is converted to a suitable format, using a geographic information system (ArcGIS), in order to adjust the projection and the resolution in the needed set up. Moreover, in order to estimate accurately the hourly emission rates, the country code and the time-zone of each cell of the grid is provided, as well as the point sources.

In this work, emission data were cut beforehand to fit the 1km domains. Especially during the online campaign support period this procedure was implemented in the operational routine, to account for the daily possible domain change. As an example, a snapshot of the calculated hourly emission rates at 12:00 UTC, for NOx and NH_3, for the Cabauw and the Po-Valley domains respectively, is shown in Figures 3.1 and 3.2. While NH_3 rates appear relatively smooth, NOx rates appear with sharp gradients beacause of the road network emerging in both areas while denser in the Cabauw domain.

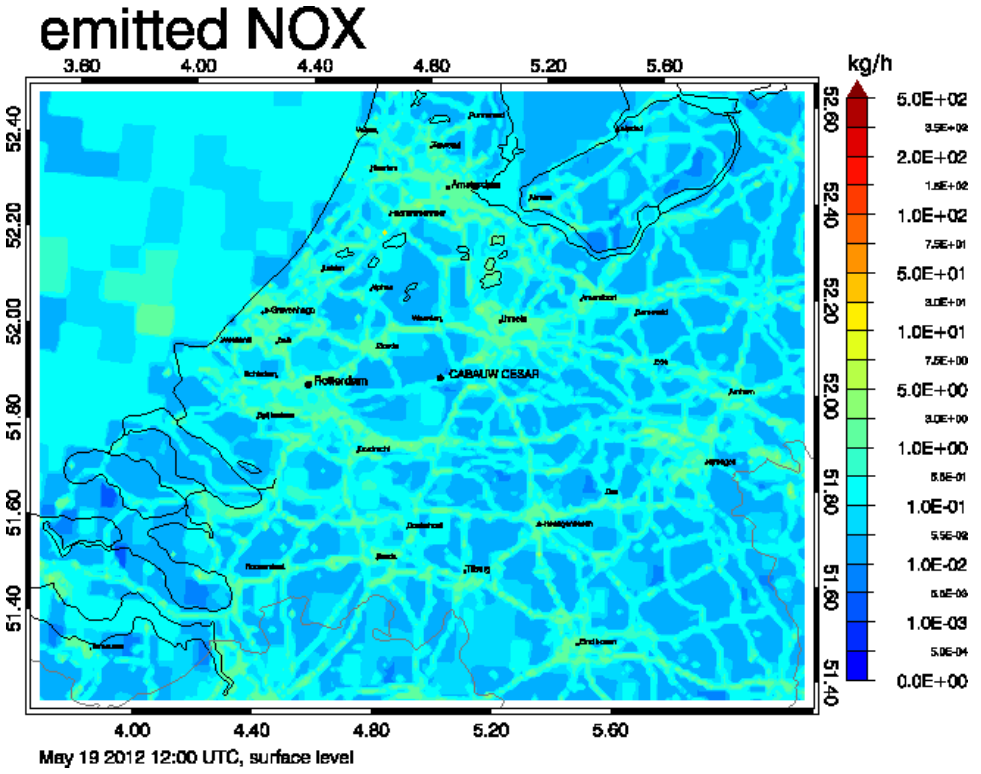

(A)

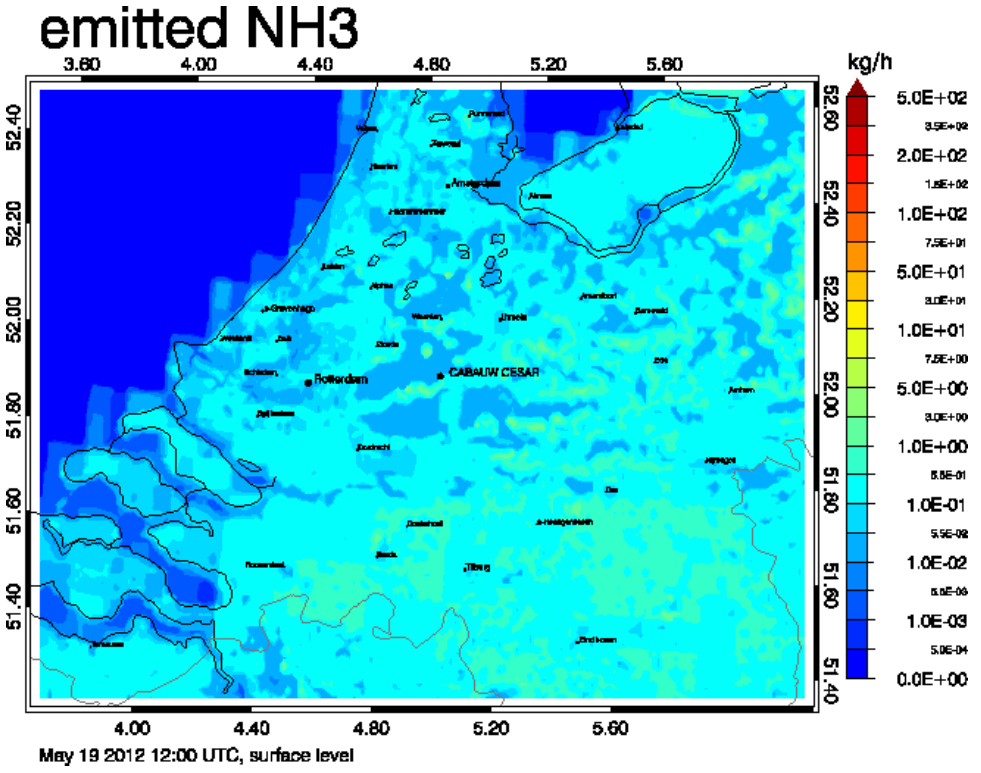

(B)

FIGURE 3.1: Predicted emissions of NOx (A) and NH_3 (B), for the Cabauw area.

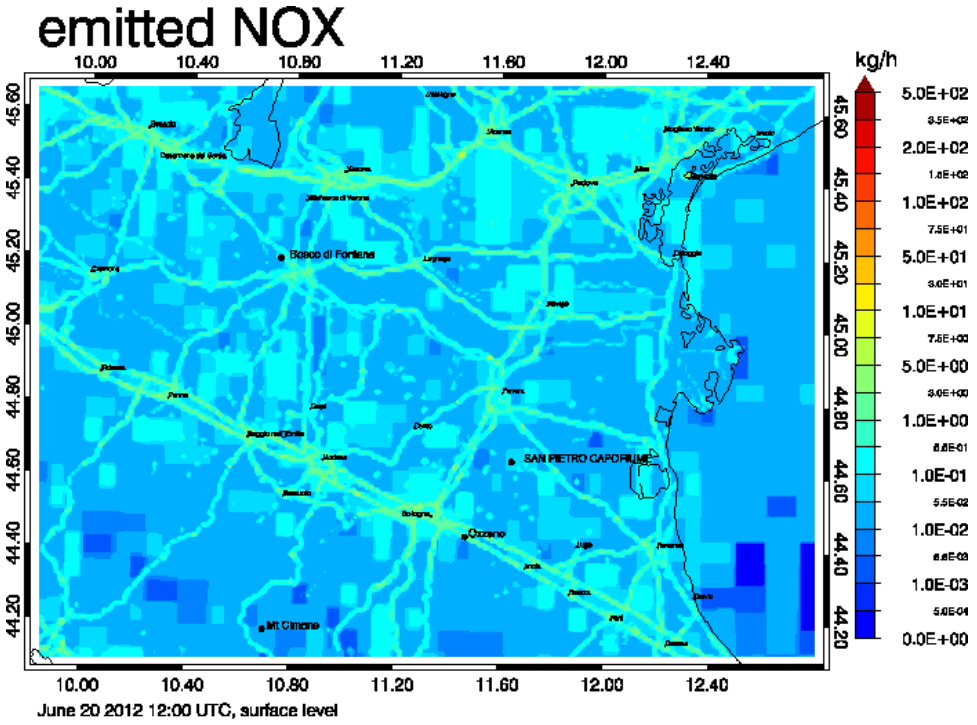

(A)

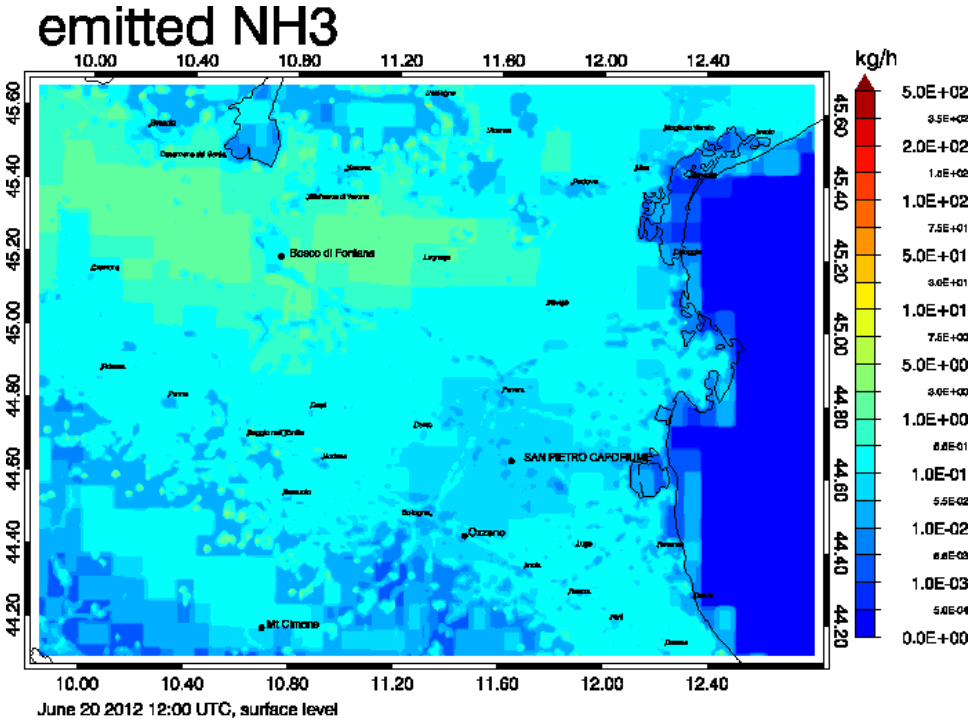

(B)

FIGURE 3.2: Predicted emissions of NOx (A) and NH_3 (B), for the Po-Valley area.

3.3 Illustration of dataset on the example of OH

By using the aforementioned model set up, using the available measurement data, a dataset is obtained that includes separately each observation and the corresponding predicted value at the relevant time, location, and altitude, along the Zeppelin track. The complete dataset collected is presented in Appendix A.

An example of the collected dataset for the OH radical for the 12/07/2012 is presented in Figure 3.3. At that day the Zeppelin performed a vertical profiling flight between 100 m and 700 m which started at 03:27 and ended at 09:09 UTC. The altitude during the flight is noted with a blue line, while observed and predicted values are noted with red and black respectively. Although the daily variability is captured by the prediction, the predicted values show a lower vertical variability and underestimate the observations with a NMBF of -0.54 that translates to a factor of 1.54. The maximum discrepancies between predicted and observed concentrations appear after 08:00 UTC.

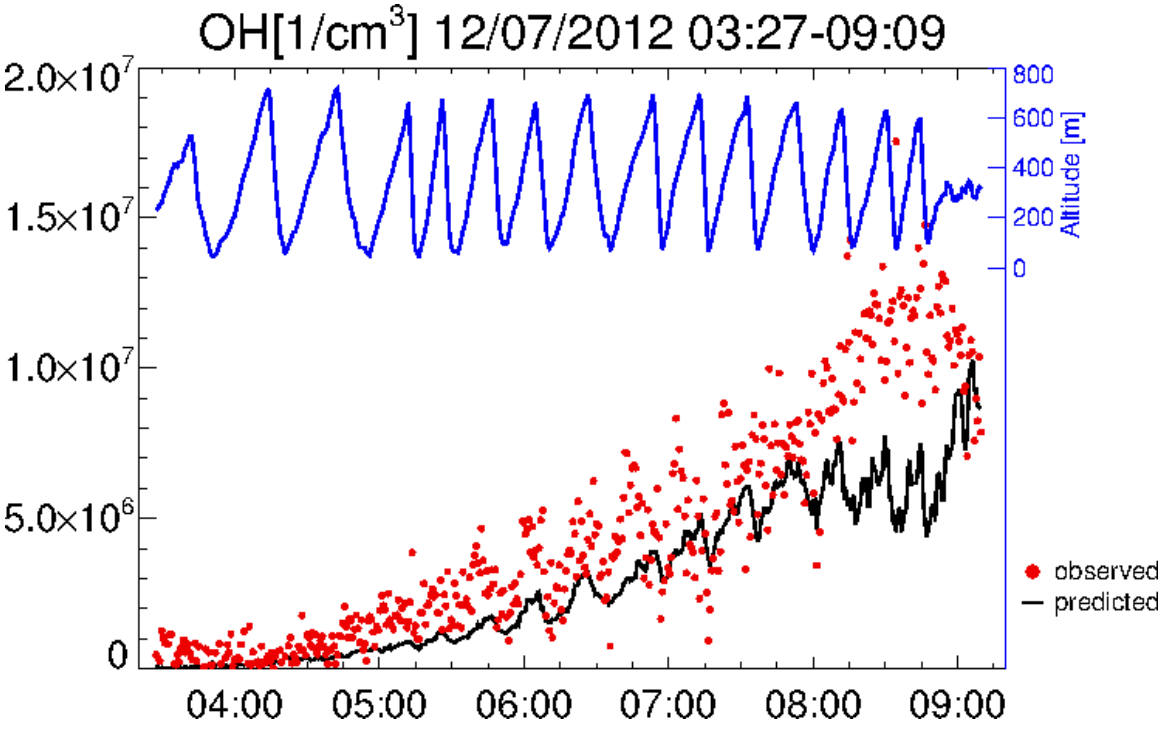

FIGURE 3.3: Example of predicted and observed OH radical along the Zeppelin track.

Chapter 4

Results and Discussion

4.1 Campaign overall comparison

Before selected days will be analyzed in detail, the model results are evaluated against observations over the whole campaign. Inspecting, first, the model behavior over a relatively long period of time, will assist, when later analyzing selected days, to characterize the model discrepancies as 'expected' or 'extremes'. The time span will extend along the two spring/summer 2012 campaign periods, at Cabauw, in the Netherlands, from 19-05-2012 to 27-05-2012 , and at Po-Valley, in Italy, from 18-06-2012 to 13-07-2012. These time spans include both vertical profiling flights and horizontal transects. Excluding the transfer flights, in total, we count 26 measurement days, of which 5 were perfomed in the Cabauw area in the Netherlands, and 21 in the Po-Valley area in Northern Italy. The observations availability over the two campaign periods has been presented in Table 3.1.

4.1.1 Meteorological parameters

The prediction quality of both gas-phase and aerosol-phase constituents in the atmosphere is strongly connected with the prediction quality of temperature, vertical temperature profiles, clouds, and the relative humidity. These meteorological parameters are influenced by large- and small-scale weather systems. While large-scale weather systems are controlled by regions of high and low pressure, small-scale weather systems are controlled by ground temperatures, soil moisture, and small-scale variations in pressure (Jacobson [2012]). In this section the predicted temperature and relative humidity, both

related to aerosol growth, are compared with observations, over the two campaign periods. In addition, the predicted PBL height is examined and compared to the retrieved PBL height.

Starting with the absolute temperature, the scatterplots of model results against observations, are displayed in Figure 4.1, color coded with altitude, for the Cabauw campaign (top panel), and the Po-Valley campaign (bottom panel). In both campaigns all points are close to the 1:1 axis. An exception is noted for the flight of 22/05 in which the temperature above the North Sea in the Netherlands is overestimated. In the Cabauw area, lower temperatures are noted with a mean predicted value of 16.40°C and a mean observed value of 19.206°C giving a NMBF of -0.04 (factor of 1.04) and a high correlation coefficient of 0.89. In the Po-Valley, relatively higher temperatures are noted, with a mean predicted value of 24.07°C and a mean observed of 24.74°C giving a NMBF of -0.03 (factor of 1.03) and a high correlation coefficient of 0.90. In both areas the temperature appears only slighly underestimated with this being more distinct in Cabauw. In the bottom panel of Figure 4.1 the altitude dependance of temperature in the Po-Valley area is indicated by the color code. As expected, temperature has lower values in high altitudes and higher values in low altitudes in both predicted and observed values. The model captures the temperature gradient sufficiently well, for the period of study, and considering the small spatial extend of the area under study, the bias could be addressed to the surface temperature, which drives the temperature layering in the vertical extend.

The relative humidity, however, shows more dispersion along the 1:1 axis in Figure 4.2. In general, higher relative humidity is found in Cabauw in both observations and predictions, as compared to the Po-Valley. In Cabauw, the mean predicted value (63%) overestimates the mean observed value (57%) with a NMBF of +0.10. In Po-Valley, a wider range of both observed and predicted values is noted with the mean predicted value (55%) overestimating the mean observed value (52%). A tendency appears for underestimation in the lower altitudes of the flight, and for overestimation in the higher altitudes of the flight.

Temperature and relative humidity have a counteracting role on aerosol growth. With an increase on temperature, evaporation increases, so more substance moves from aerosol to gas phase. With an increase on relative humidity, particles swell, containing more water, so more water is available for gas substance to dissolve into aerosol phase. E.g. dissolution of gas-phase HNO_3 to particle-phase NO_3^- is favored in a higher relative humidity environment. How much of the H_2O mass is available for aerosol phase is shown by the absolute water content (awc). The awc is calculated by the temperature

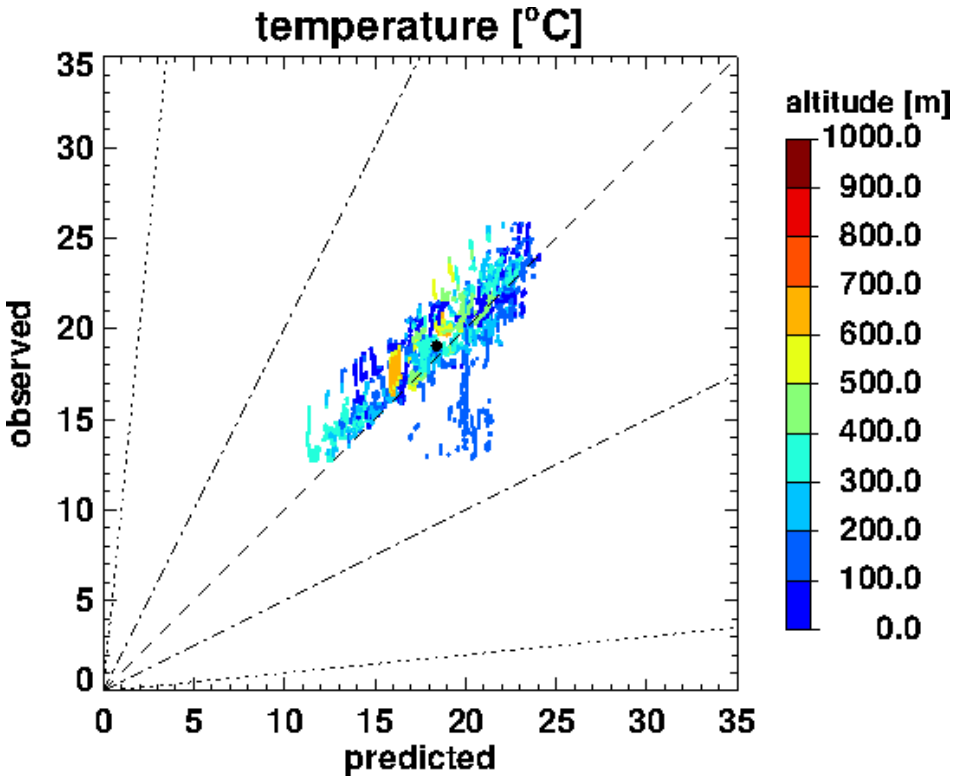

(A) CABAUW

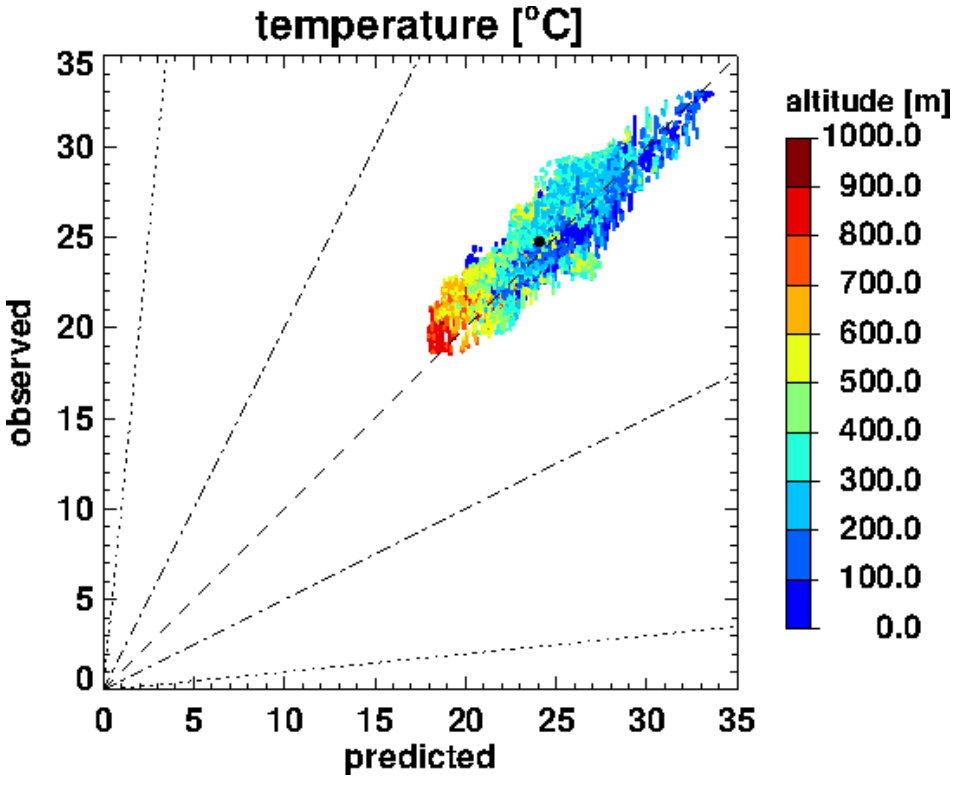

(B) PO-VALLEY

FIGURE 4.1: Scatterplots of predicted versus observed absolute temperature, for the Cabauw PEGASOS campaign (A) and the Po-Valley PEGASOS campaign (B). Included days are noted in column 'met.' of Table 3.1. Points are colored with altitude. 1:1 (dashed), 2:1 (dashed-dotted), 10:1 (dotted) lines are indicated. Statistics are shown in Table 4.1.

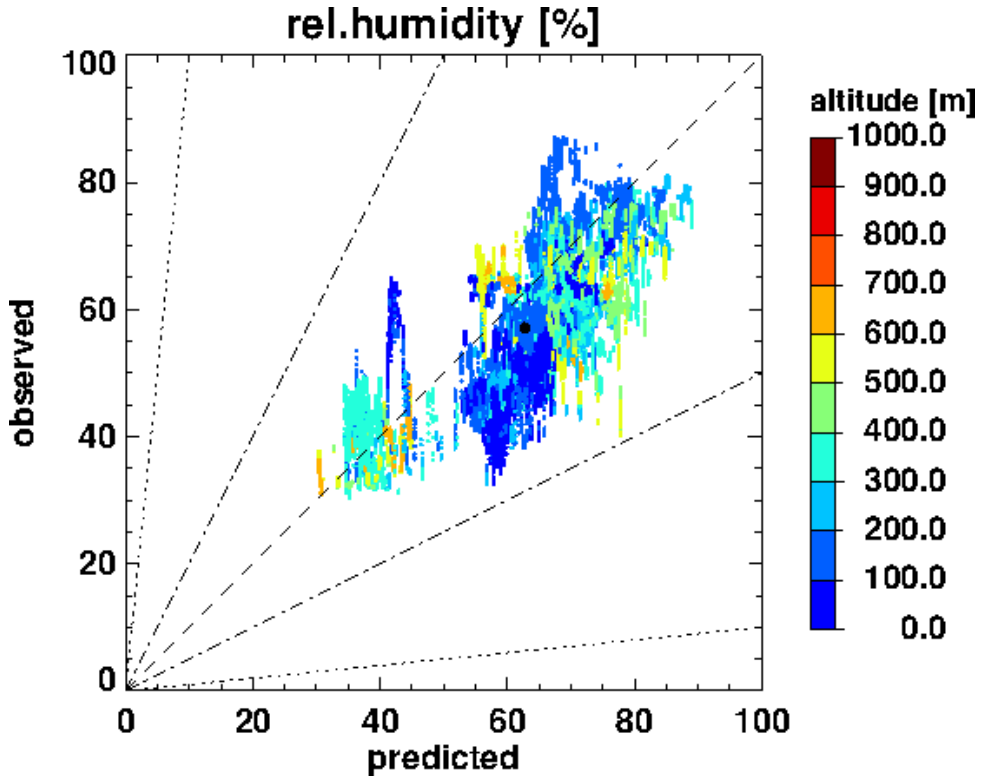

(A) CABAUW

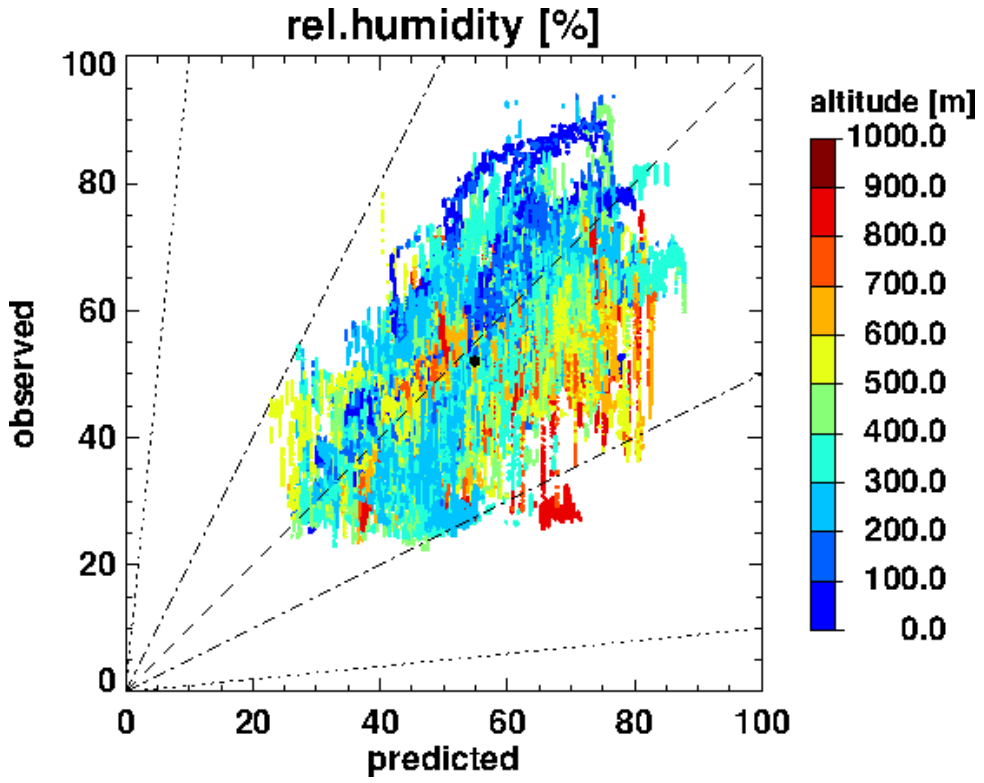

(B) PO-VALLEY

FIGURE 4.2: Scatterplots of predicted versus observed relative humidity, for the Cabauw PEGASOS campaign (A) and the Po-Valley PEGASOS campaign (B). Included days are noted in column 'met.' of Table 3.1. Points are colored with altitude. 1:1 (dashed), 2:1 (dashed-dotted), 10:1 (dotted) lines are indicated. Statistics are shown in Table 4.1.

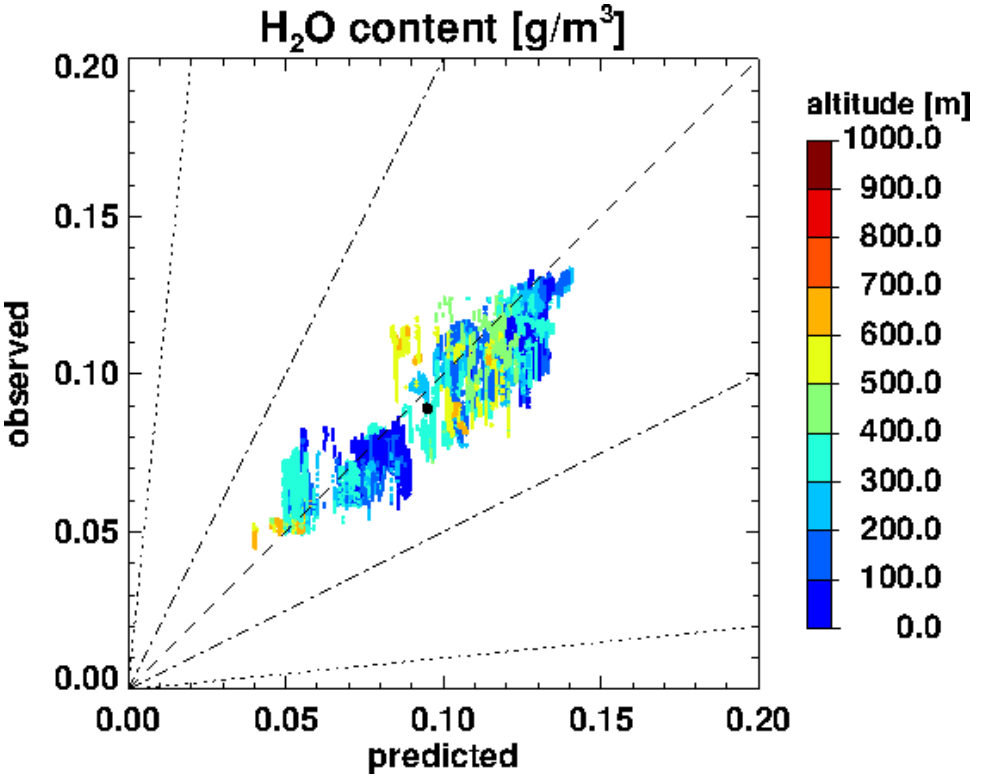

(A) CABAUW

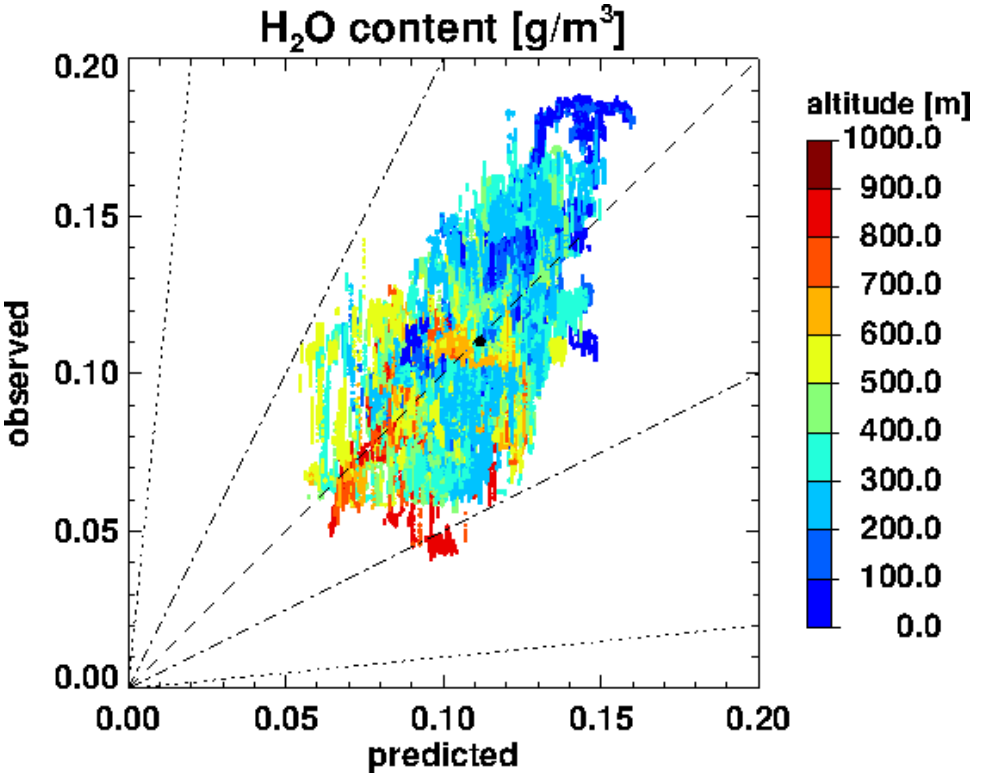

(B) PO-VALLEY

FIGURE 4.3: Scatterplots of predicted versus observed water content, for the Cabauw PEGASOS campaign (A) and the Po-Valley PEGASOS campaign (B). Included days are noted in column 'met.' of Table 3.1. Points are colored with altitude. 1:1 (dashed), 2:1 (dashed-dotted), 10:1 (dotted) lines are indicated. Statistics are shown in Table 4.1.

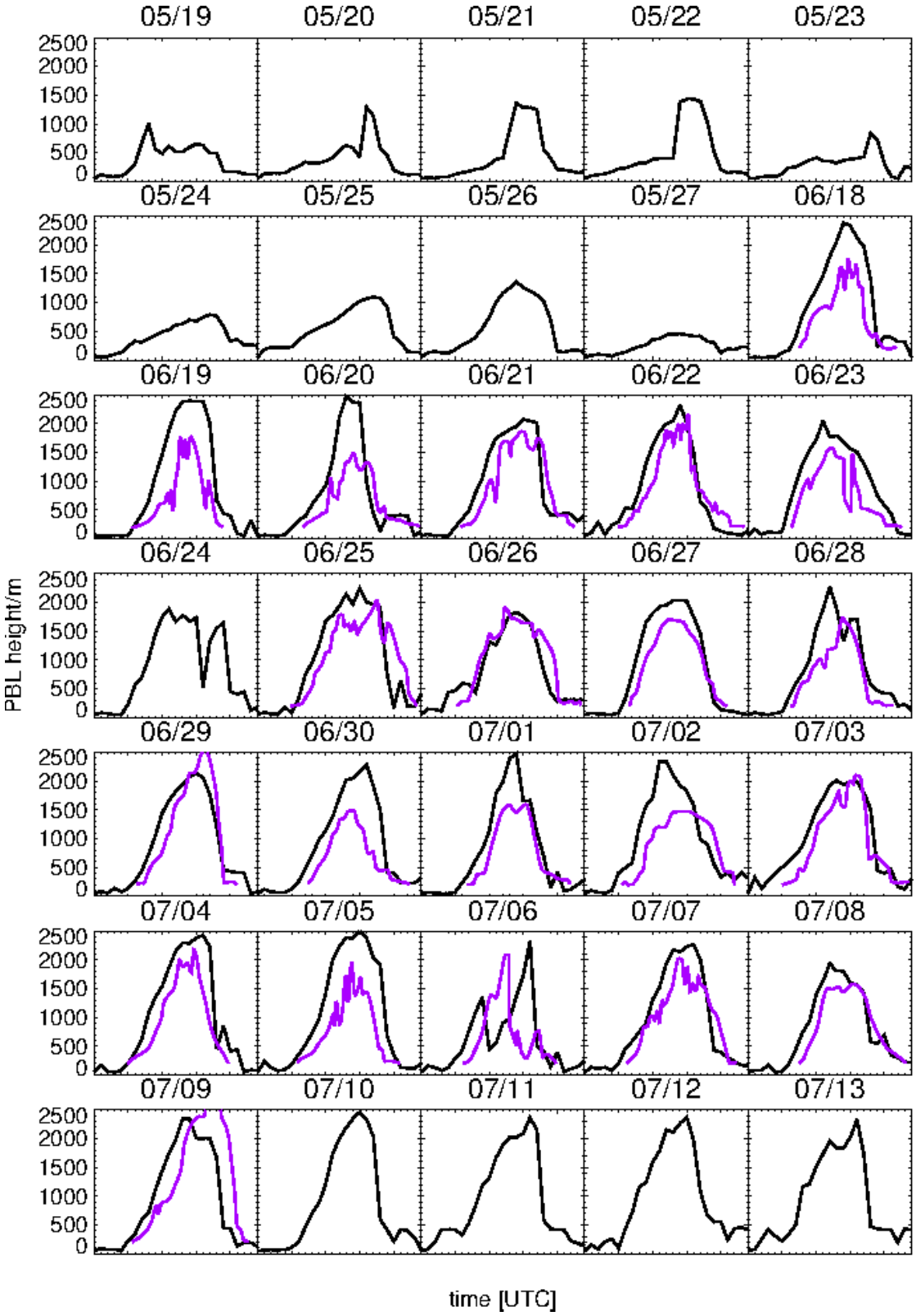

FIGURE 4.4: Predicted PBL height (black) for the main measurement days at the locations of: CESAR tower, Cabauw (19/05/2012-27/05/2012), and San Pietro Capofiume, Po-Valley (18/06/2012-13/07/2012). Lidar retrieved PBL height (violet) at San Pietro Capofiume.

and the relative humidity according to the formula:

$$awc = C\frac{P_w}{T} \tag{4.1}$$

where:

awc absolute water content

C constant

P_w absolute water vapor pressure (Wexler and Hyland [1980])

T absolute temperature

In Figure 4.3 the observed awc is plotted against the predicted for both campaign periods, as calculated by the above equation. As with relative humidity, a wider range of values in noted in Po-Valley than in Cabauw. In addition, in Po-Valley, observations have larger variability than predictions. The mean predicted values, very close to the mean observed values yield 0.06 gr/m^3 and 0.11 gr/m^3 for Cabauw and Po-Valley respectively. Again, as with the relative humidity, in Po-Valley, a tendency appears for underestimation of the awc in the lower altitudes and for overestimation of the awc in the higher altitudes of the flight.

In order to demonstrate how the model handles the dynamics, the calculated PBL height for the two campaign periods is displayed in Figure 4.4. The predicted PBL heights is somewhat lower with a mean maximum PBL height of 1070 m for the Cabauw area at the location of the CESAR tower (19/05-27/05), and relatively higher, to a mean maximum PBL height of 2254 m for the Po-Valley area at the location of San Pietro Capofiume (18/06-13/07). This is the case for the following reasons. First, Po-Valley is located on lower latitude than Cabauw. Second, the Po-Valley campaign extended in the early summer period while the Cabauw campaign extended in late spring. Because of both, higher ground temperatures in Po-Valley forced a higher PBL than in Cabauw.

It can be noted that in certain cases the ending value of the PBL height at 24:00 UTC does not coincide with the starting value at 00:00 UTC of the next day. Here, the analysis meteorological data from the Meteorological Archival and Retrieval System (MARS), the main repository of meteorological data at ECMWF have been used to initialize meteorology calculations. This data contains the global analyses for the four main synoptic hours 00, 06, 12 and 18 UTC, representing the best gridded estimate of the state of the atmosphere, meaning, the best fit to observations for each day (Persson [2001]). The afternoon/evening weakly forced PBL, is poorly characterized in meteorological models. As a consequence, the PBL height values at the end of the day (24:00 UTC) in

most cases are biased and that could transfer the error to the next day. The analysis data used here reflect the optimization applied (which is apparent in 00:00 UTC of each day) in order to have the best fit with the meteorological observations (that was used to produce the analysis data). For the period 18/06-09/07, the calculated PBL is compared to the lidar retrieved PBL (provided by G.P.Gobbi, ISAC-CNR). For the days that retrievals were available the predicted mean maximum PBL height (2247 m) overestimated the retrieved mean maximum PBL height (1891 m).

4.1.2 Gas phase comparison

Starting the gas-phase evaluation with ozone (O_3), the scatterplots of model results against observations, color coded by flight altitude, are displayed in Figure 4.5. Although the picture appears complicated due to the large number of observations gathered, it is noted that in both campaigns the majority of points are distributed in the factor 2 area with more points in the underestimation area in Po-Valley flights. In Cabauw, the mean predicted value (57.55 ppbv) is very close to the mean observed value (56.03 ppbv) giving a NMBF of +0.03. The correlation coefficient is +0.55, meaning that predicted concentration varies together with observed concentration. In Po-Valley, the mean observed value (65.33 ppbv) is underestimated by the mean predicted value (54.11 ppbv) giving a NMBF of -0.21. However, the correlation coefficient is higher (+0.69), meaning that predicted and observed concentrations vary together, and more than in Cabauw. It can be seen that in certain cases, in lower altitudes, prediction did not capture the variability in observations, and vice-versa, variability was predicted that did not show in the observations.

The scatterplots of nitrogen oxides (NO_x) are displayed in Figure 4.6, again color coded by flight altitude. In both campaigns points are scattered around the center of gravity in the factor 10 over- and underestimation area. The strong underestimation in the lowest altitudes indicates a 'difficulty' with the emission rates of NO_x. Since they are emitted from the surface, higher concentration values are both observed and predicted in lower altitudes, which decrease with altitude. In the Po-Valley it becomes apparent that the observed values show larger variability than the predicted values. In Cabauw, the mean predicted value (2.70 ppbv) underestimates the mean observed value (6.39 ppbv) with an NMBF of -1.37, meaning an underestimation with a factor of 2.37. The correlation coefficient is low (+0.41). In Po-Valley, the mean observed value (2.41 ppbv), is underestimated by the mean predicted value (1.36 ppbv) giving a NMBF of -0.78, meaning an underestimation with a factor of 1.78 with a low correlation coefficient (+0.32), and it is found to be lower than what observed in Cabauw. The lower predicted

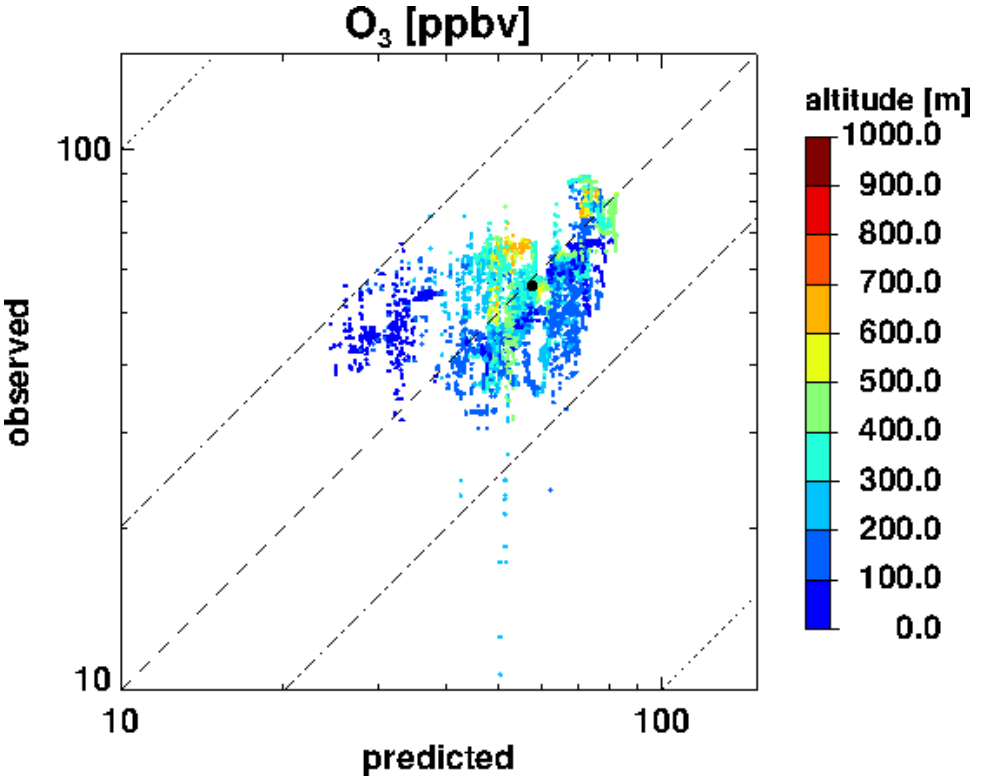

(A) CABAUW

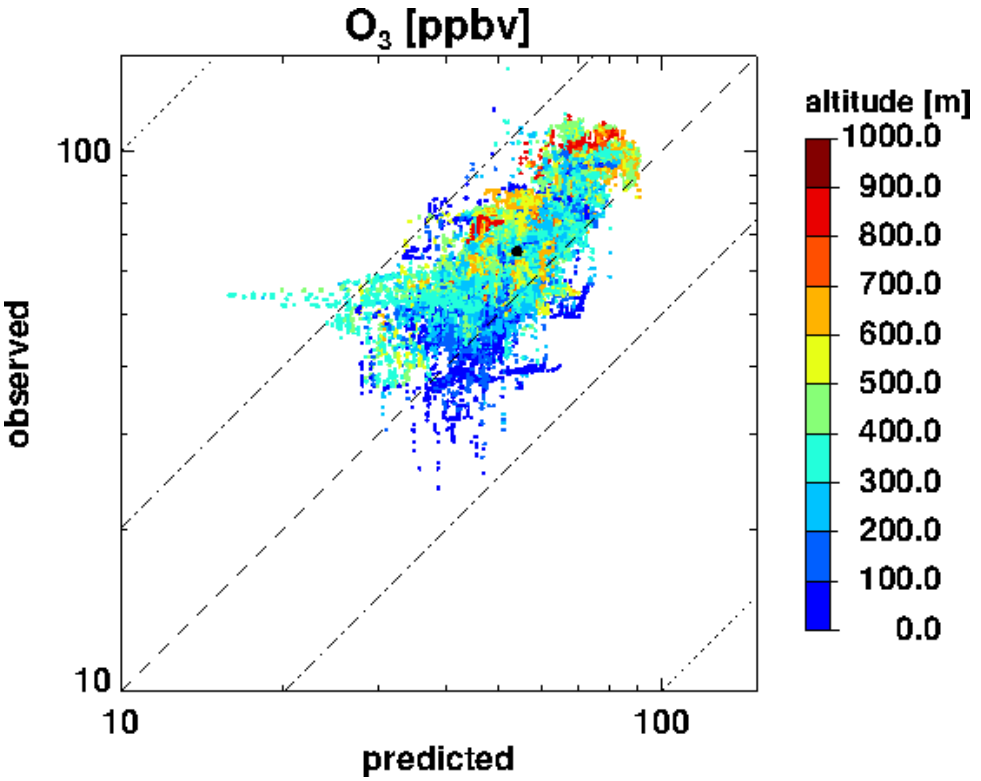

(B) PO-VALLEY

FIGURE 4.5: Scatterplots of predicted versus observed ozone, for the Cabauw PEGASOS campaign (A) and the Po-Valley PEGASOS campaign (B). Included days are noted in Table 3.1. Points are colored with altitude. 1:1 (dashed), 2:1 (dashed-dotted), 10:1 (dotted) lines are indicated. Statistics are shown in Table 4.1.

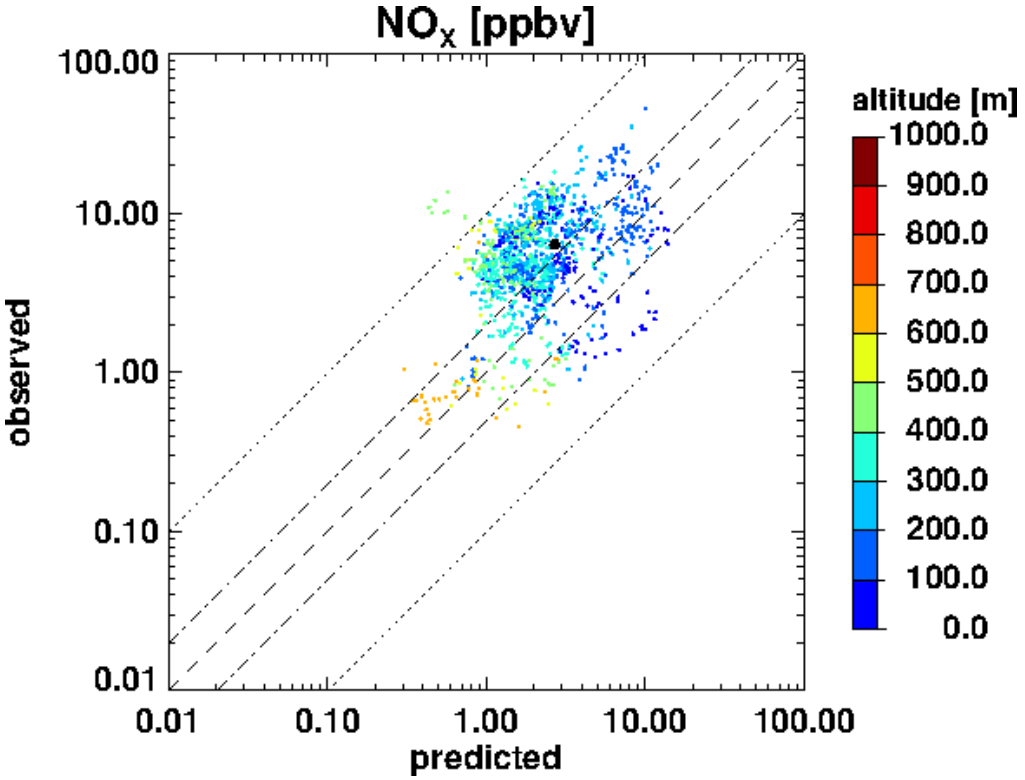

(A) CABAUW

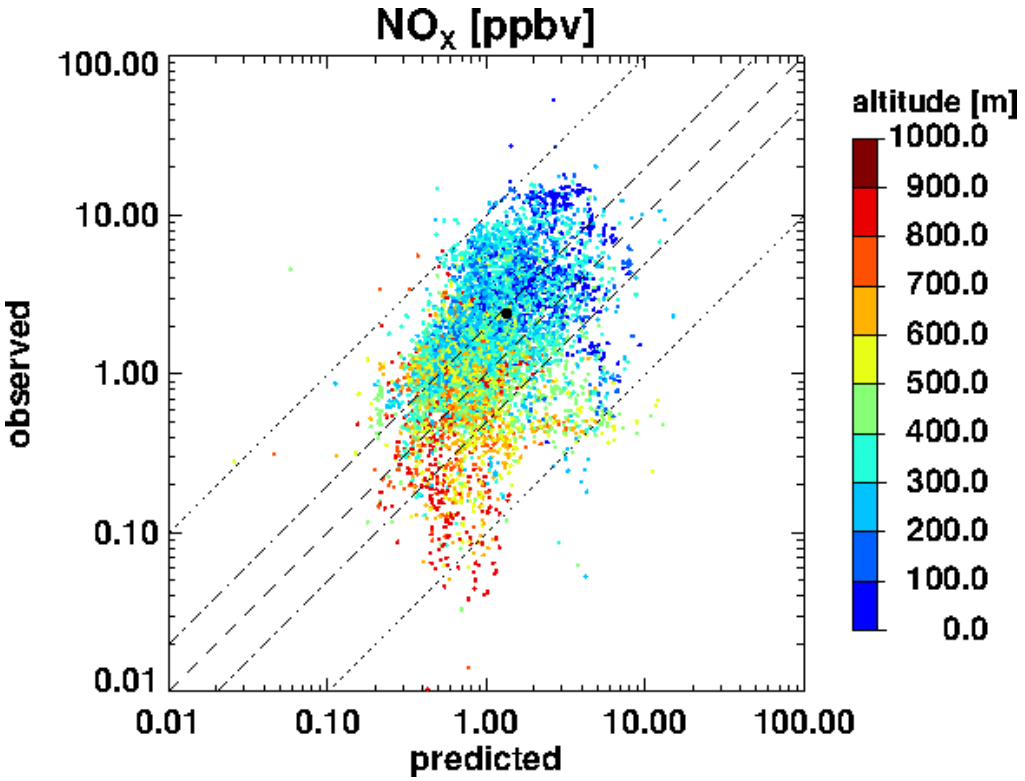

(B) PO-VALLEY

FIGURE 4.6: Scatterplots of predicted versus observed nitric oxides, for the Cabauw PEGASOS campaign (A) and the Po-Valley PEGASOS campaign (B). Included days are noted in Table 3.1. Points are colored with altitude. 1:1 (dashed), 2:1 (dashed-dotted), 10:1 (dotted) lines are indicated. Statistics are shown in Table 4.1.

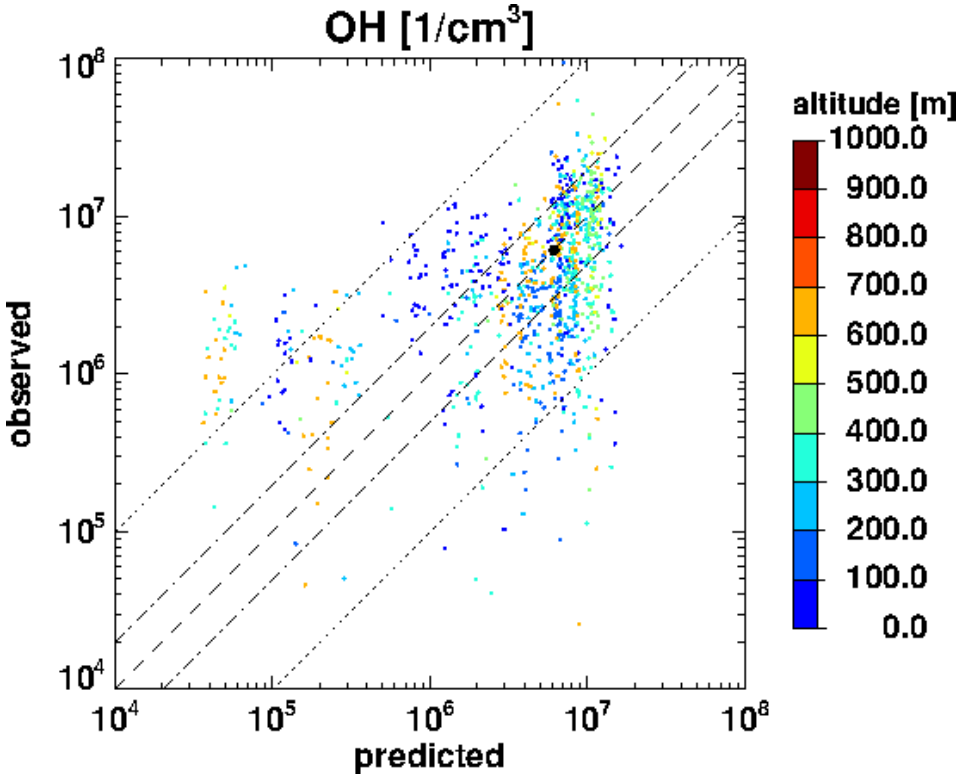

(A) CABAUW

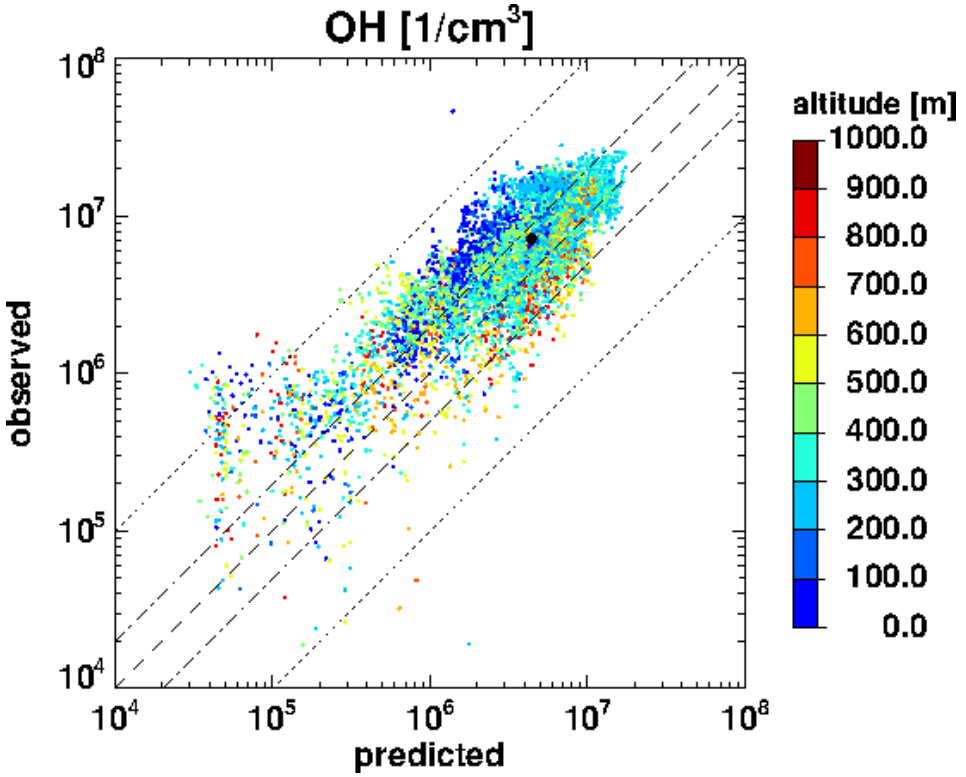

(B) PO-VALLEY

FIGURE 4.7: Scatterplots of predicted versus observed hydroxyl radical, for the Cabauw PEGASOS campaign (A) and the Po-Valley PEGASOS campaign (B). Included days are noted in Table 3.1. Points are colored with altitude. 1:1 (dashed), 2:1 (dashed-dotted), 10:1 (dotted) lines are indicated. Statistics are shown in Table 4.1.

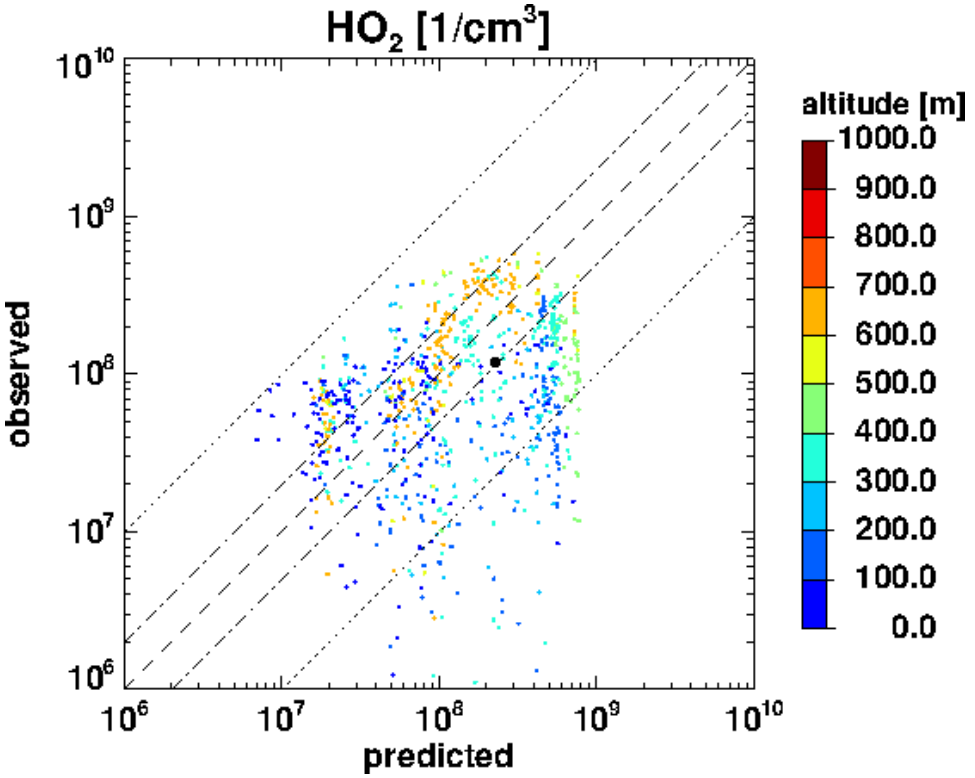

(A) CABAUW

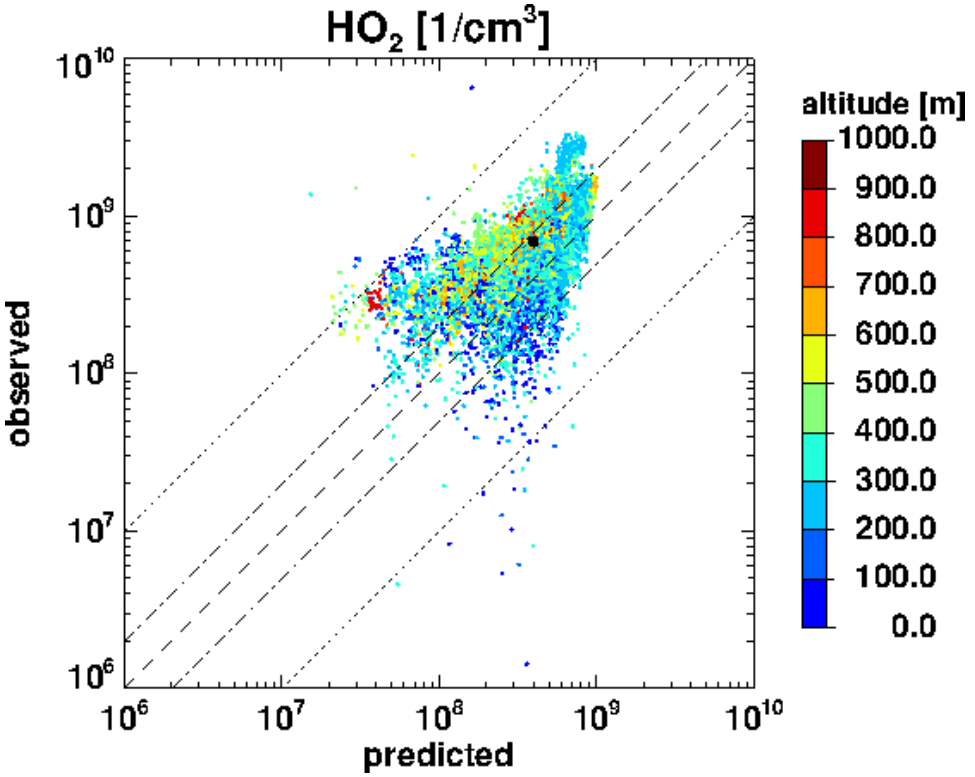

(B) PO-VALLEY

FIGURE 4.8: Scatterplots of predicted versus observed hydroperoxyl radical, for the Cabauw PEGASOS campaign (A) and the Po-Valley PEGASOS campaign (B). Included days are noted in Table 3.1. Points are colored with altitude. 1:1 (dashed), 2:1 (dashed-dotted), 10:1 (dotted) lines are indicated. Statistics are shown in Table 4.1.

and observed concentrations noted in Po-Valley reflect a more agricultural nature of the area as compared with the industrial area of Cabauw.

In most cases, the removal of trace gases from the troposphere, is initialized by reactions with hydroxyl radicals, namely the hydroxyl (OH). The OH radical is formed by e.g. photolysis of O_3 and HONO (nitrous acid) and recycled from the hydroperoxyl radical (HO_2). The products of these reactions are eventually deposited on the Earth's surface. The concentration of these hydroxyl radicals is considered as a measure of self-cleansing of the atmosphere, as discussed in Rohrer et al. [2014].

The OH radical observations are plotted against predictions, colored with altitude, in Figure 4.7. In Cabauw campaign the majority of points are scattered in the factor 10 over- and underestimation area while in the Po-Valley campaign the majority of points lie between the factor 2 overestimation and the factor 10 underestimation lines. In both campaigns, groups of observations appear strongly underestimated with a factor larger than 10. In Cabauw, the mean predicted value ($6.14\times10^6 cm^{-1}$) is very close to the mean observed value ($6.09\times10^6 cm^{-1}$). The correlation coefficient is low (+0.39). In Po-Valley, the mean observed value ($7.18\times10^6 cm^{-1}$), is higher than what observed in Cabauw, due to more sunny weather, which enhances hydroxyl formation. It is underestimated by the mean predicted value ($4.44\times10^6 cm^{-1}$) giving a NMBF of +0.62. The correlation coefficient is high (+0.73). The HO_2 radical observations are plotted against predictions in Figure 4.8. The number density of HO_2 is about 10^2 times the number density of OH. In both campaigns the majority of points are scattered in the factor 10 over- and underestimation area. In Cabauw, the mean predicted value ($2.27\times10^8 cm^{-1}$) overestimates the mean observed value ($1.19\times10^8 cm^{-1}$) with an NMBF of +0.91. The correlation coefficient is low (+0.23). In Po-Valley, the mean observed value ($6.86\times10^8 cm^{-1}$), higher than what observed in Cabauw, is underestimated by the mean predicted value ($3.99\times10^8 cm^{-1}$) giving a NMBF of +0.72. The correlation coefficient is high (+0.63).

In order to fully comprehend the OH concentration, its sources and sinks should be quantified. However, OH reacts with a large number of compounds making the quantification for every individual difficult. Instead, the term total OH reactivity k_{OH}, which is the inverse lifetime:

$$k_{OH} = \frac{1}{\tau_{OH}} \tag{4.2}$$

is used to directly describe the total OH loss as an approach to calculate its budget (Wegener et al. [2014]). Evaluating an atmospheric model in terms of OH reactivity appears to be crucial for two reasons. First, it could reveal how complete the atmospheric model is, as concerns the included reactions. In addition, it could give an insight on

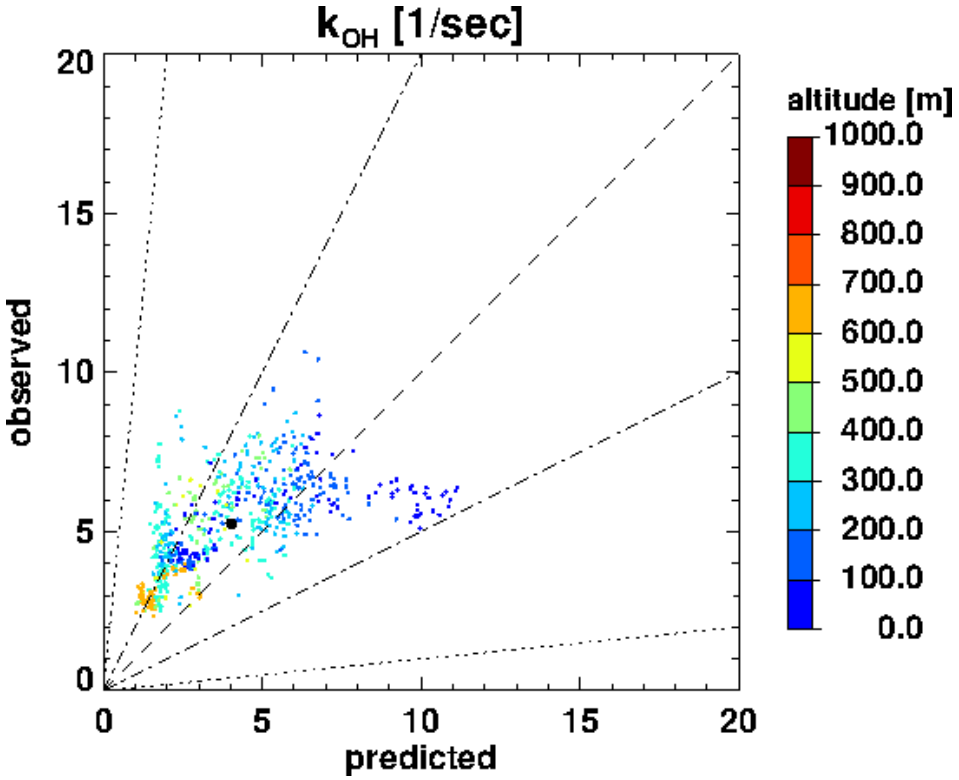

(A) CABAUW

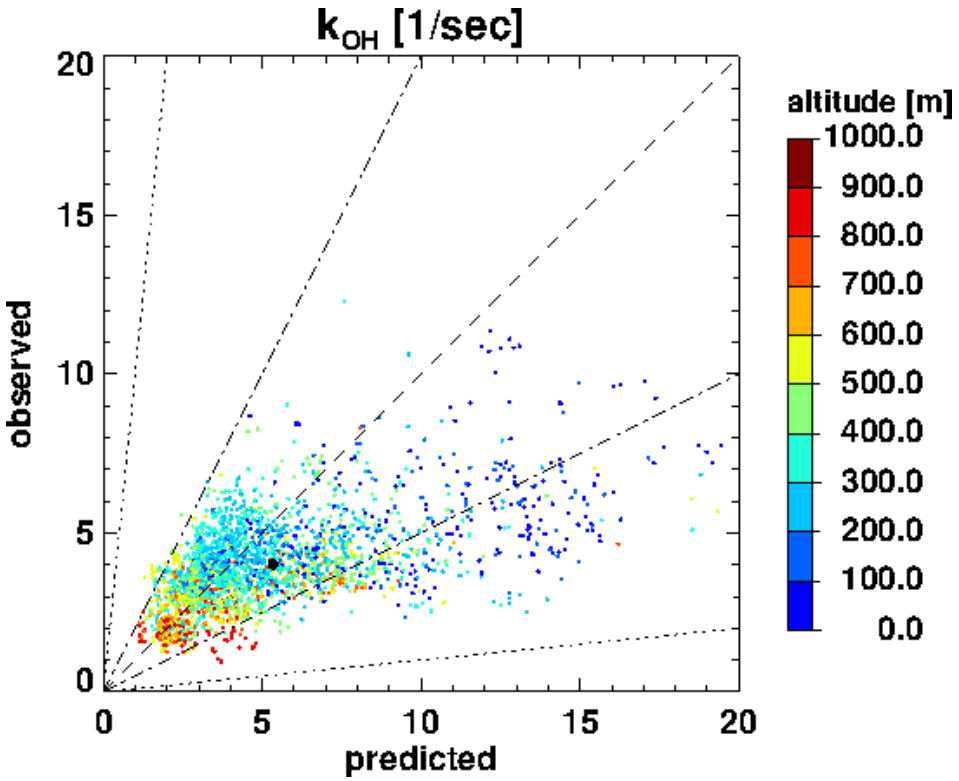

(B) PO-VALLEY

FIGURE 4.9: Scatterplots of predicted versus observed OH reactivity, for the Cabauw PEGASOS campaign (A) and the Po-Valley PEGASOS campaign (B) respectively, colored with altitude. Included days are noted in Table 3.1. 1:1 (dashed), 2:1 (dashed-dotted), 10:1 (dotted) lines are indicated. Statistics are shown in Table 4.1.

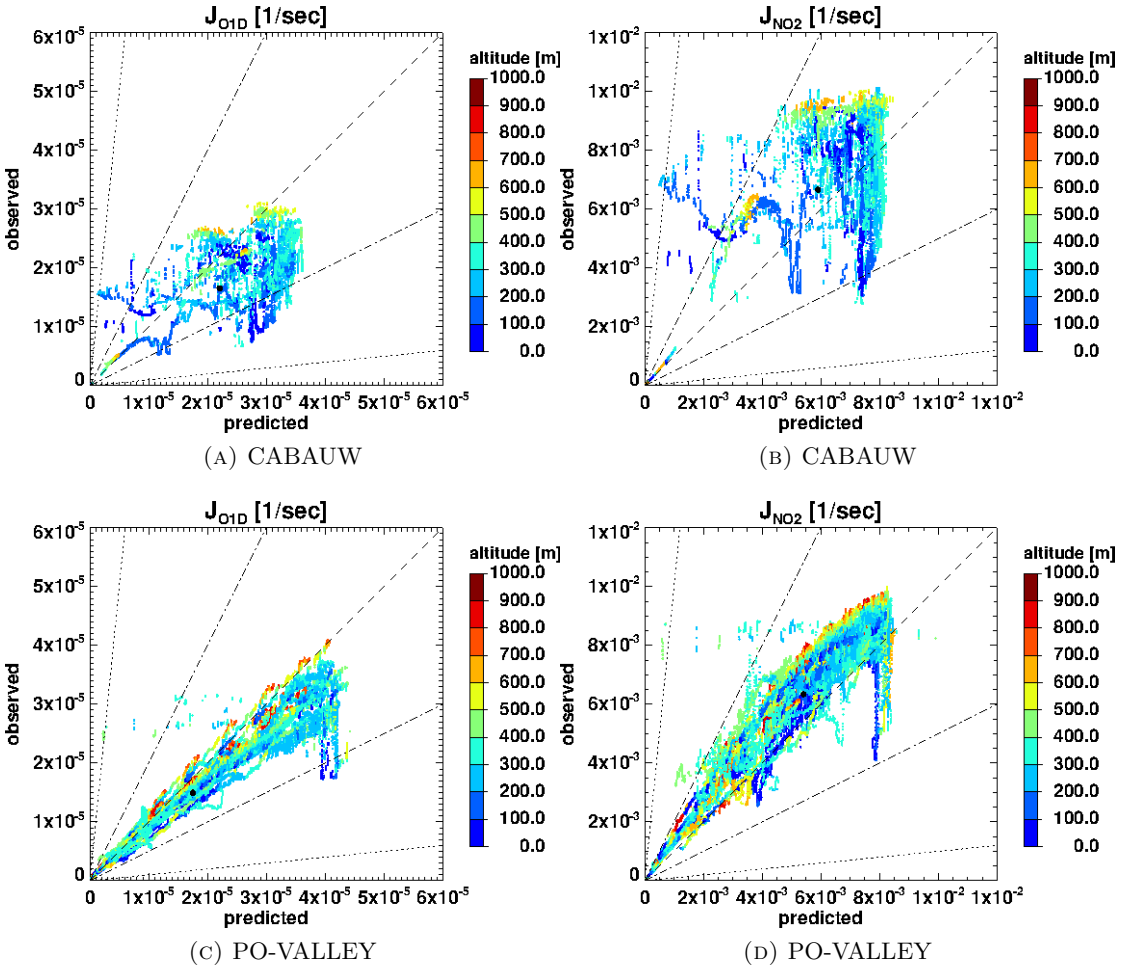

(A) CABAUW (B) CABAUW

(C) PO-VALLEY (D) PO-VALLEY

FIGURE 4.10: Scatterplots of predicted versus observed J_{O^1D} (left) and J_{NO_2} (right), for the Cabauw PEGASOS campaign (top) and the Po-Valley PEGASOS campaign (bottom), colored with altitude. Statistics are shown in Table 4.1.

reactivity that cannot be addressed to known reactions of compounds with OH, what is termed as 'missing reactivity' (Hofzumahaus et al. [2009]).

Here, the predicted OH reactivity with VOCs and CO is plotted against the corresponding observations, color coded with altitude, in Figure 4.9. In both campaigns one can notice high values in low altitudes and low values in high altitudes. This makes sense since VOCs and other trace gases (CO,NOx) are emitted from the surface so their concentration is higher close to surface, causing higher loss to OH, thus higher reactivity. In both campaigns, but especially in Po-Valley, a tendency for overestimation in lower altitudes is noted. In Cabauw, the observed mean value (5.25 sec^{-1}) is underestimated by the predicted mean value (4.02 sec^{-1}) with a NMBF of -0.31. In Po-Valley, the observed mean value (4.01 sec^{-1}) is overestimated by the predicted mean value (5.34 sec^{-1}) with a NMBF of +0.33.

Chemistry in the atmosphere depends sensitively on photodissociation processes, like

the decomposing of O_3 to the state $O(^1D)$ which reacts with H_2O giving OH, and the decomposing of NO_2 to NO and O, an important step in the photochemical production of O_3 (Kraus and Hofzumahaus). The photolysis frequencies of these processes, j_{O^1D} and j_{NO_2}, predicted and observed, for both campaigns, color coded with altitude, are plotted in Figure 4.10. For both photolysis frequencies we note more dispersed values around the 1:1 axis in Cabauw than in Po-Valley. A reason for this could be the cloud influence which is stronger in Cabauw. In both campaigns, j_{O^1D} is overestimated while j_{NO_2} is underestimated. The "shadowing" by cloud coverage is in general wavelength dependent and stronger for j_{NO_2} than for j_{O^1D}. With O_3, and consequently the O_3 column being underestimated in Po-Valley, a higher j_{O^1D} results, thus the overestimation (Lohse [2015]).

4.1.3 Aerosol phase comparison

In this section the model results for aerosol phase constituents are evaluated against observations over the two spring/summer 2012 campaign periods. It must be said that the Cabauw campaign includes less aerosol measurement days than the Po-Valley campaign, and consequently smaller number of observation-model pairs. The statistical indices mentioned are listed in Table 4.1. The scatterplots of predicted against observed concentrations for sulfate, ammonium, nitrate, and organics, for the two campaign periods, are presented in Figures 4.11, 4.12, 4.13, and 4.14, respectively.

On first sight, it is noted that sulfate, as compared to the other inorganic aerosol components, ammonium and nitrate, shows the smallest variability. The two sulfate scatterplots (Figure 4.11) note the following. In the Cabauw area, the mean predicted value (3.89 $\mu g/m^3$) overestimates the mean observed value (1.99 $\mu g/m^3$), with a NMBF yielding +0.95. The correlation coefficient is high (+0.76). In the Po-Valley area, the mean predicted value (3.59 $\mu g/m^3$) overestimates the mean observed value (1.95 $\mu g/m^3$), with a NMBF of +0.84. The correlation coefficient is low (+0.33).

Inspecting the ammonium-nitrate scatterplots, a similar structure can be noted in both, with a larger range of predicted and observed values apparent in nitrate. The two ammonium scatterplots (Figure 4.12) note the following. More homogeneous observations and predictions are noted in the Cabauw area, while a larger variability is noted in observations as compared to the variability in predictions in the Po-Valley area. In the Cabauw area, all points are dispersed in the factor 2 over- and underestimation area. The mean predicted value (2.35 $\mu g/m^3$) is very close to the mean observed value (2.33 $\mu g/m^3$), with an NMBF of +0.01. The correlation coefficient is low (+0.21). In the Po-Valley area, the majority of points lie between the factor 2 underestimation and

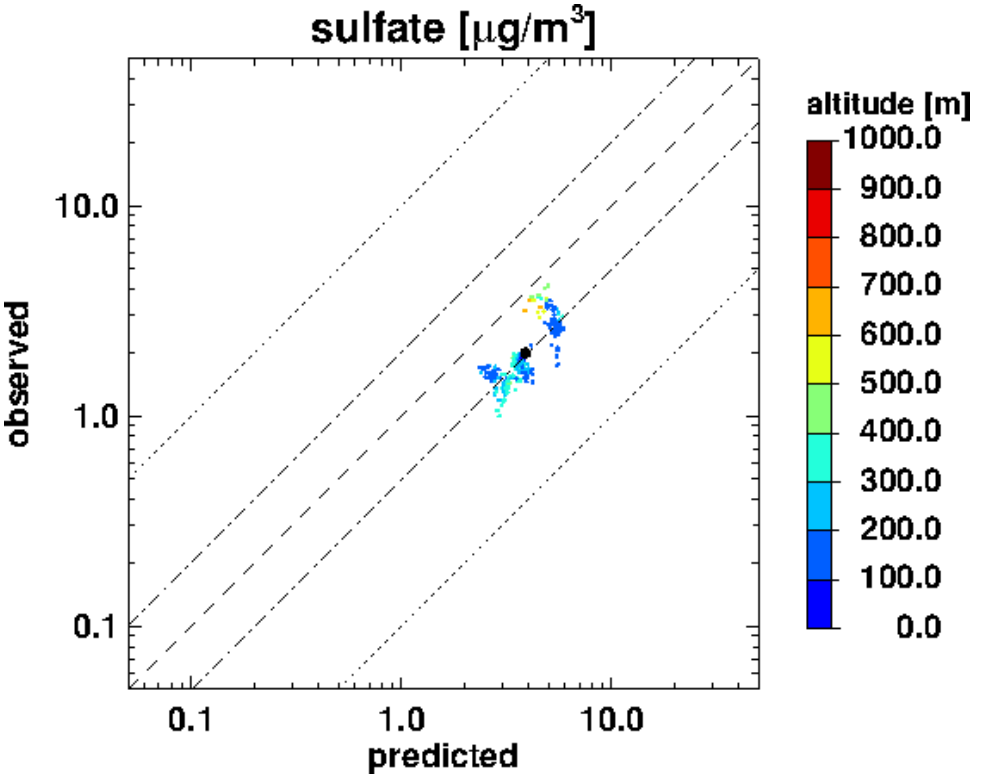

(A) CABAUW

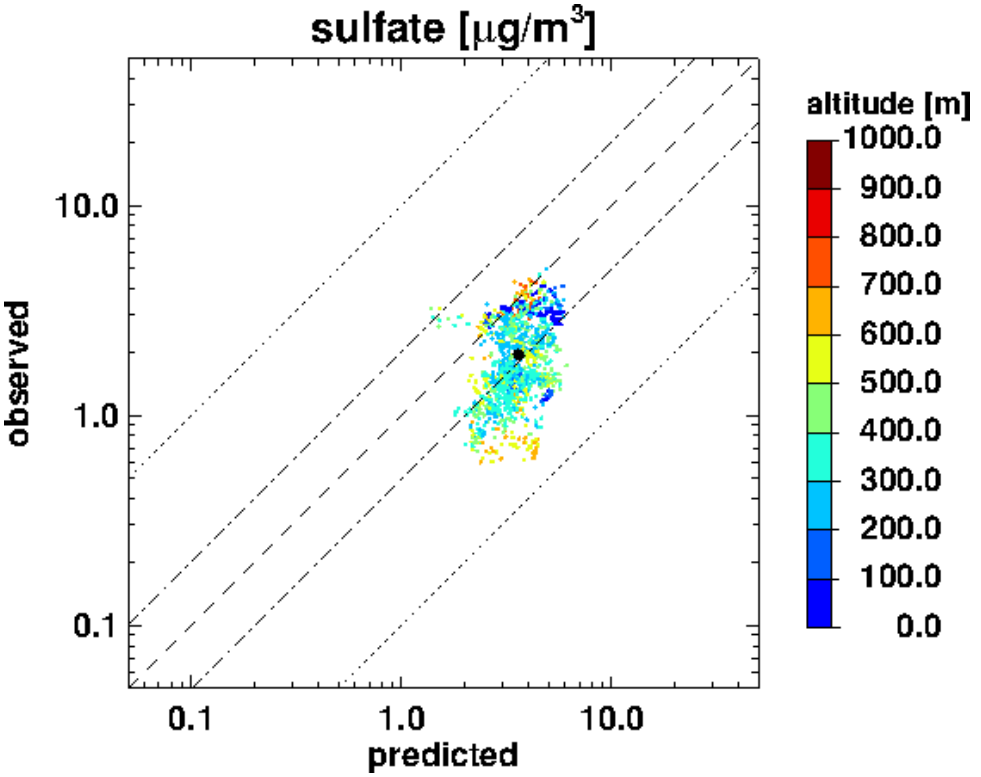

(B) PO-VALLEY

FIGURE 4.11: Scatterplots of predicted versus observed sulfate, for the Cabauw PEGASOS campaign (A) and the Po-Valley PEGASOS campaign (B). Included days are noted in column 'AMS' of Table 3.1. Points are colored with altitude. Statistics are shown in Table 4.1. Statistics are shown in Table 4.1.

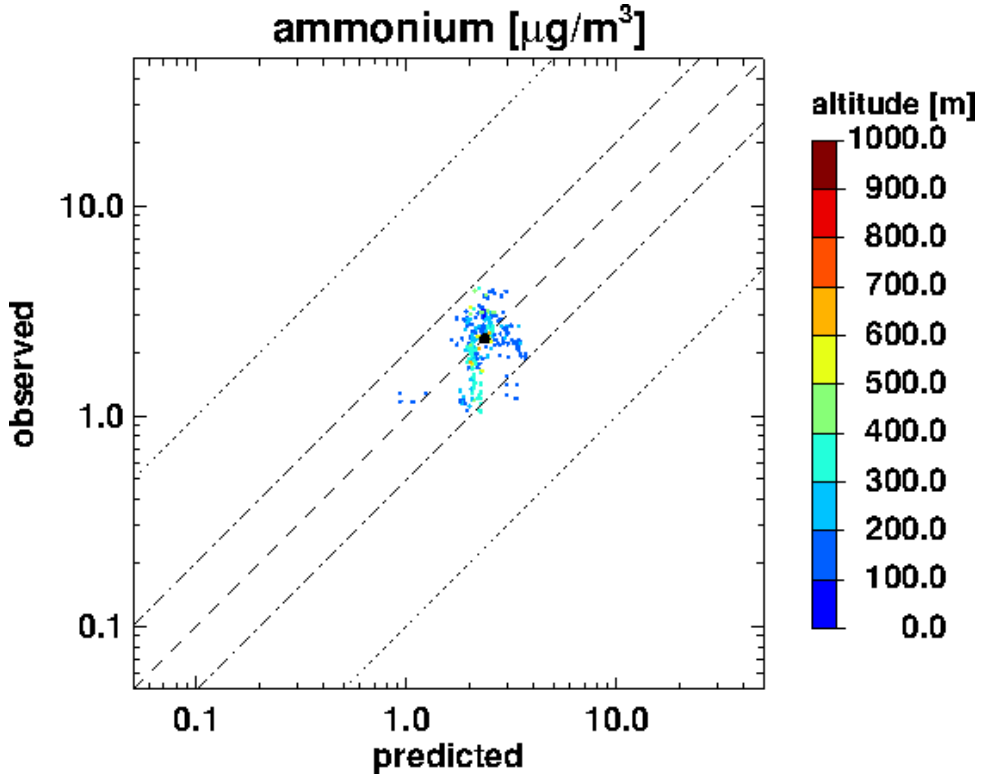

(A) CABAUW

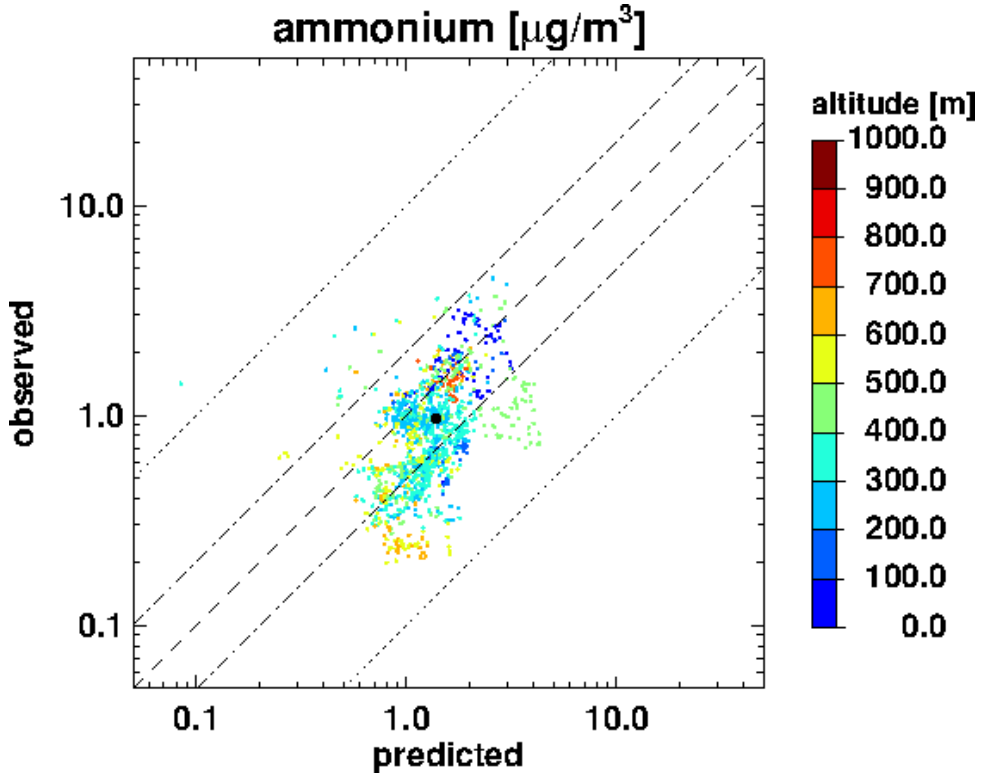

(B) PO-VALLEY

FIGURE 4.12: Scatterplots of predicted versus observed ammonium, for the Cabauw PEGASOS campaign (A) and the Po-Valley PEGASOS campaign (B). Included days are noted in column 'AMS' of Table 3.1. Points are colored with altitude. Statistics are shown in Table 4.1. Statistics are shown in Table 4.1.

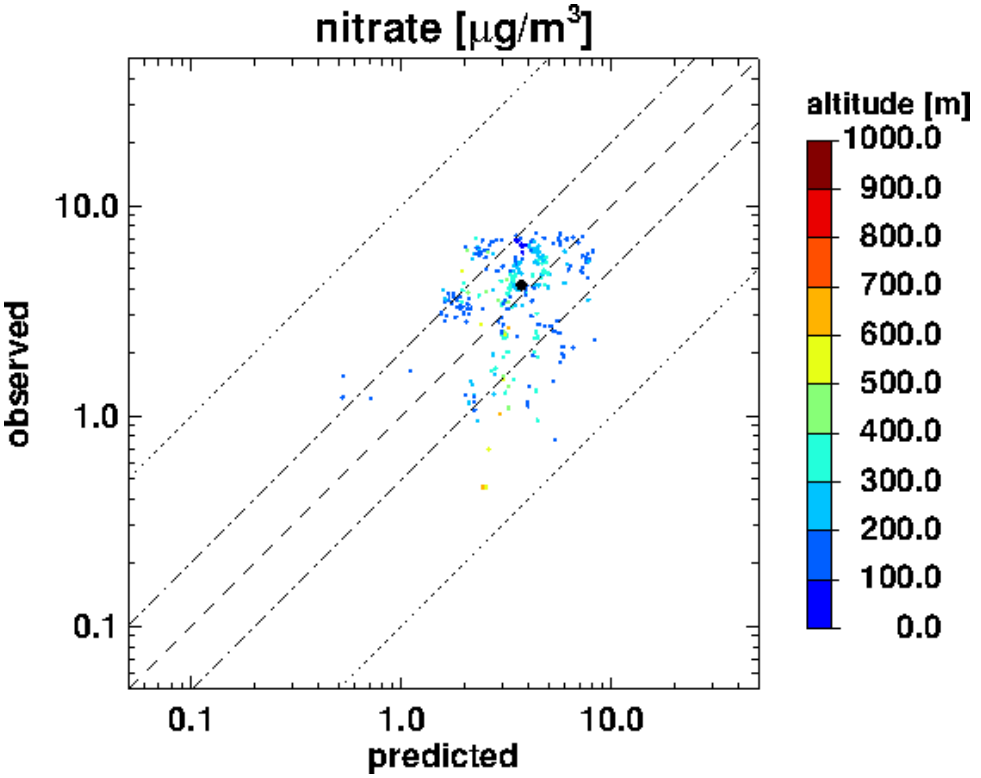

(A) CABAUW

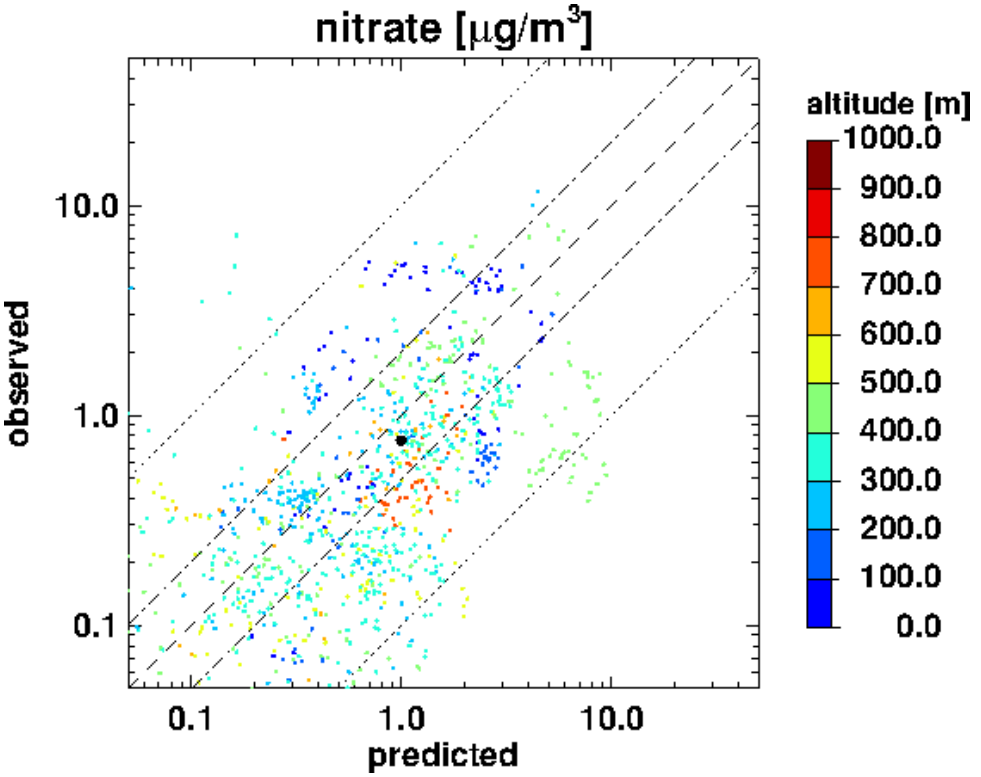

(B) PO-VALLEY

FIGURE 4.13: Scatterplots of predicted versus observed nitrate, for the Cabauw PEGASOS campaign (A) and the Po-Valley PEGASOS campaign (B). Included days are noted in column 'AMS' of Table 3.1. Points are colored with altitude. Statistics are shown in Table 4.1. Statistics are shown in Table 4.1.

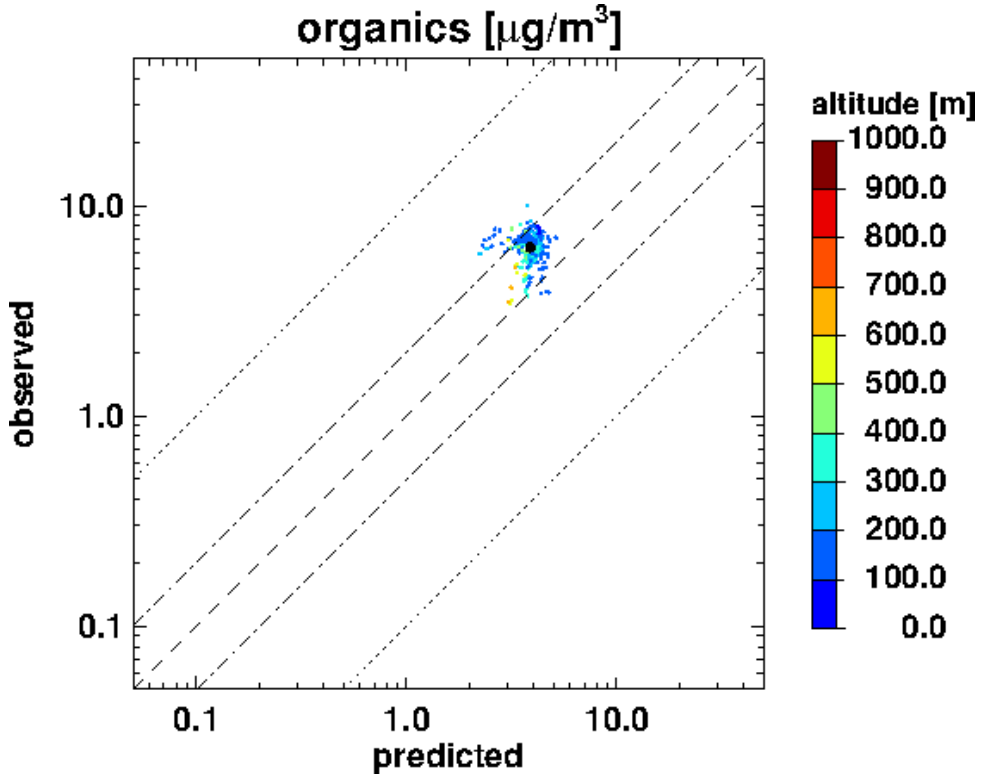

(A) CABAUW

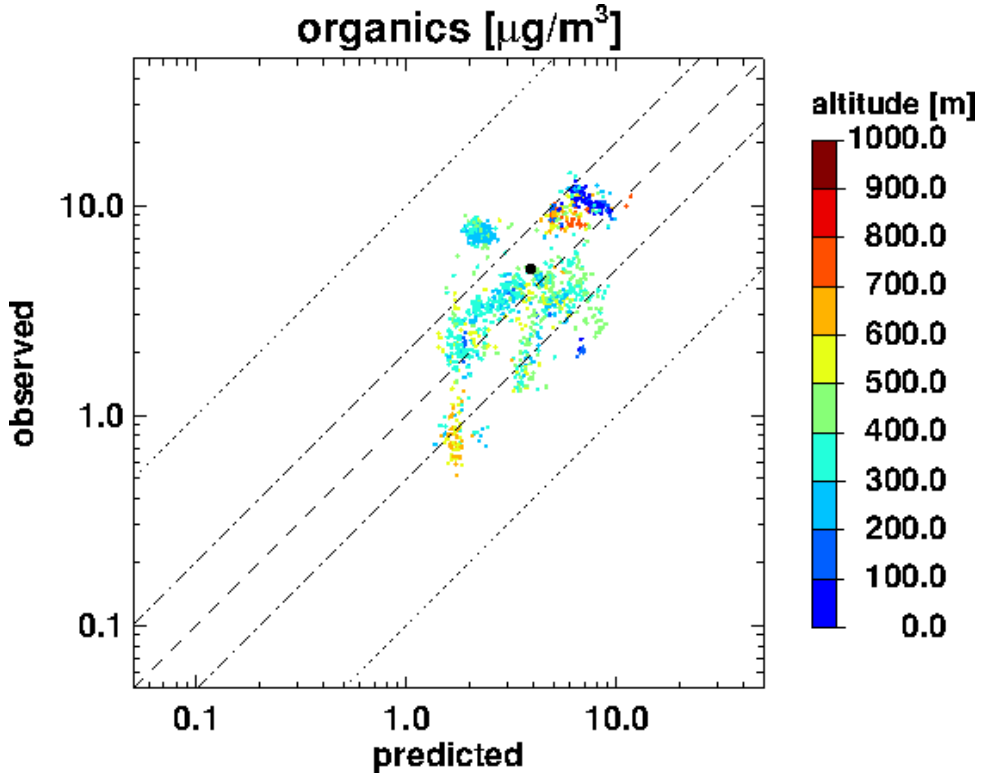

(B) PO-VALLEY

FIGURE 4.14: Scatterplots of predicted versus observed organic aerosol, for the Cabauw PEGASOS campaign (A) and the Po-Valley PEGASOS campaign (B). Included days are noted in column 'AMS' of Table 3.1. Points are colored with altitude. Statistics are shown in Table 4.1. Statistics are shown in Table 4.1.

the factor 10 overestimation area. The mean predicted value is lower than in Cabauw (1.38 $\mu g/m^3$) and overestimates the mean observed value (0.96 $\mu g/m^3$), with a NMBF of +0.43. The correlation coefficient is higher than in Cabauw (+0.42). The two nitrate scatterplots (Figure 4.13) note the following. In the Cabauw area, the majority of points are dispersed in the factor 2 over- and underestimation area with a significant number of points that lie in the factor 10 overestimation area especially in Po-Valley. In addition, in the Po-Valley area a larger variability in both predicted and observed values is noted, symmetrically along the 1:1 axis. In Cabauw, the mean predicted value (3.72 $\mu g/m^3$) underestimates the mean observed value (4.18 $\mu g/m^3$) with a NMBF of -0.12 (a factor of 1.12). The correlation coefficient is low (+0.29). In Po-Valley, the mean observed value (0.76 $\mu g/m^3$), much lower than what observed in Cabauw, is overestimated by the mean predicted value (0.99 $\mu g/m^3$) with a NMBF of +0.31 (a factor of 1.31). The correlation coefficient is low but higher than in Cabauw (+0.34).

As far as organic aerosols are concerned, the two respective scatterplots (Figure 4.14) note the following. Homogeneity is noted in the Cabauw area while a more irregular pattern with different regimes appears in the Po-Valley area. In the Cabauw area, the mean predicted value (3.88 $\mu g/m^3$) underestimates the mean observed value (6.33 $\mu g/m^3$) with a NMBF of -0.63. The correlation coefficient is very low (+0.02). In the Po-Valley area, the mean predicted value (3.91 $\mu g/m^3$) underestimates the mean observed value (4.99 $\mu g/m^3$) with a NMBF of -0.28. The correlation coefficient is higher than in Cabauw (+0.45).

4.1.4 Summary

In this chapter, predicted gas-phase concentrations, namely of trace gases and radicals, predicted parameters like reactivity and photolysis frequencies, and predicted aerosol concentrations, namely sulfate, ammonium, nitrate, and organics, were evaluated against observations over the two periods of the 2012 PEGASOS campaigns. The statistical indices mentioned are listed in Table 4.1. In overall, all correlations between predicted and observed concentrations were found positive, with coefficients ranging between +0.23 and +0.73 for the gas-phase and between +0.02 and +0.76 for the aerosol-phase. As far as gas-phase is concerned, better scores with respect to NMBF, between predicted and observed values, are noted for O_3 and OH. The fact that ozone is overall underpredicted in Po-Valley is probably related to the fact that photochemical ozone production is underestimated in the model. The largest discrepancies are noted for NO_x and especially for NO yielding the largest NMBF (-2.0 for Cabauw and -1.09 for Po-Valley). As far as aerosol-phase is concerned, better scores with respect to NMBF, are noted for ammonium at Cabauw and for organics at Po-Valley. In overall, the discrepancies between

predictions and observations are comparable with similar works (Walker et al. [2012], Aan de Brugh et al. [2012], Crippa et al. [2014], Spracklen et al. [2011], Pye et al. [2010], Fountoukis et al. [2014]).

Commenting on the comparisons of sulfate and nitrate the following can be stated. In general, the low vapor pressure of sulfuric acid (H_2SO_4) allows it to condense easily on particle and to dissolve into droplets. Because the rate of condensation is independent of the amount of water in the particles, thus of water vapor in the atmosphere, sulfuric acid is always found in the particles and can hardly be found in the gas phase. However nitric acid (HNO_3) is much more volatile than H_2SO_4 and has a smaller tendency to form particles by homogeneous or condensation onto pre-existing particles. Therefore, due to its volatility, particulate nitrate often appears in lower concentrations than sulfate (Seinfeld and Pandis [1998]). In Po-Valley predicted and observed nitrate is indeed lower in concentration that sulfate. However, the same is not noted in Cabauw, where the mean observed sulfate concentration is lower than the mean observed nitrate concentration as displayed in Figure 4.15. The latter is caused by the higher source strength of NOx and HNO_3 in Cabauw. Such a high source strength for the Cabauw area is not reflected in the model results where the mean nitrate concentration is somewhat lower from the mean sulfate concentration.

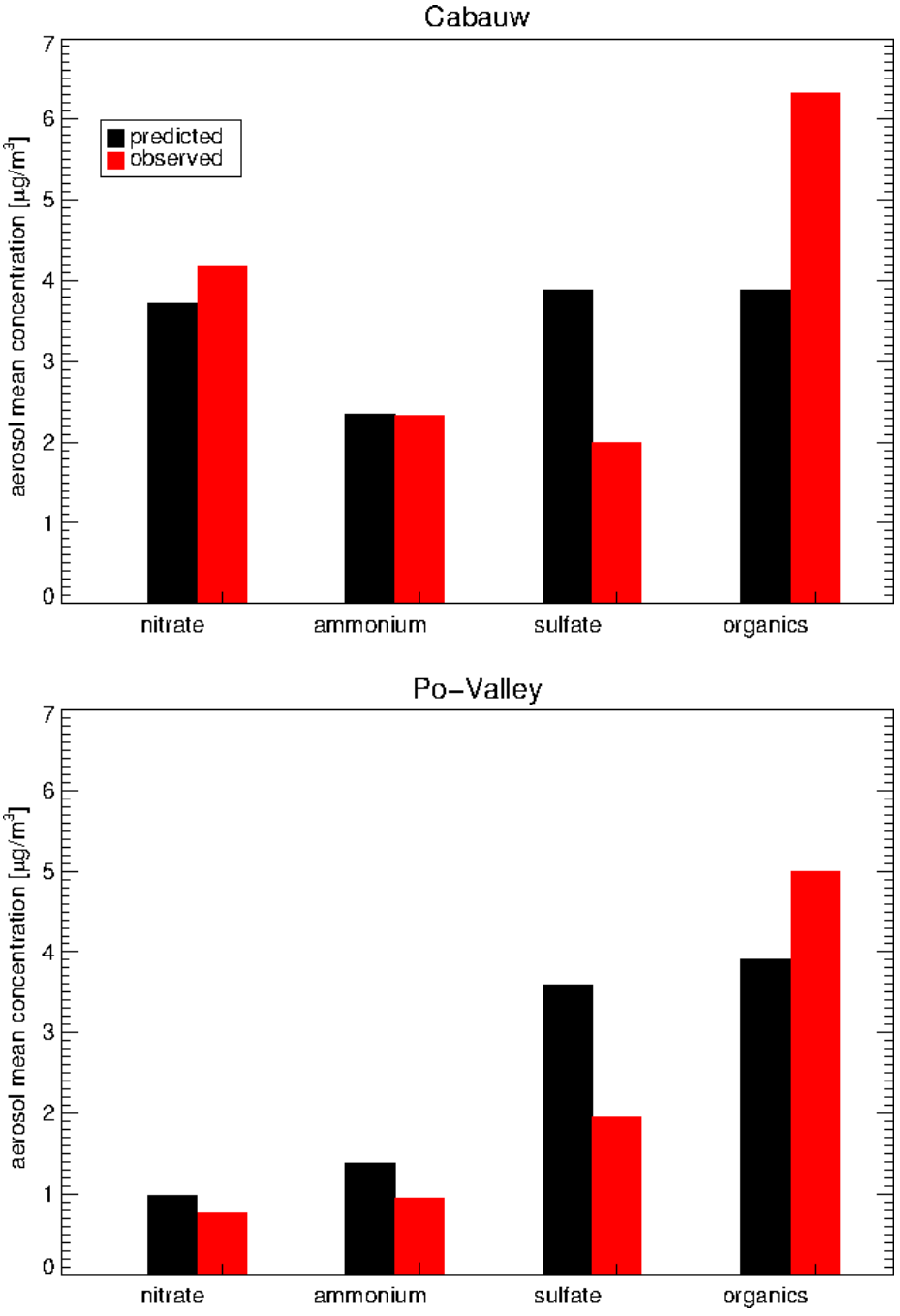

FIGURE 4.15: Mean mass concentrations of predicted and observed aerosols for flights in Cabauw and Po-Valley.

SUMMARY STATISTICS				
May 2012 / Cabauw				
Parameter:	$\bar{M}$	$\bar{O}$	NMBF	r
temperature	18.40	19.06	-0.04	+0.89
rel.humidity	62.77	57.16	+0.10	+0.79
H_2O content	0.09	0.09	+0.06	+0.93
O_3	57.55	56.03	+0.03	+0.55
NO	0.50	1.51	-2.00	+0.42
NO_2	2.19	4.90	-1.24	+0.38
NOx	2.70	6.39	-1.37	+0.41
OH	$6.14*10^6$	$6.09*10^6$	+0.01	+0.39
HO_2	$2.27*10^8$	$1.19*10^8$	+0.91	+0.23
k_{OH}	4.02	5.25	-0.31	+0.60
sulfate	3.89	1.99	+0.95	+0.76
ammonium	2.35	2.33	+0.01	+0.21
nitrate	3.72	4.18	-0.12	+0.29
organics	3.88	6.33	-0.63	+0.02
June-July 2012 / Po-Valley				
Parameter:	$\bar{M}$	$\bar{O}$	NMBF	r
temperature	24.07	24.74	-0.03	+0.90
rel.humidity	54.88	52.02	+0.05	+0.65
H_2O content	0.11	0.11	+0.01	+0.68
O_3	54.11	65.33	-0.21	+0.69
NO	0.21	0.44	-1.09	+0.27
NO_2	1.16	2.04	-0.76	+0.33
NOx	1.36	2.41	-0.78	+0.32
OH	$4.44*10^6$	$7.18*10^6$	-0.62	+0.73
HO_2	$3.99*10^8$	$6.86*10^8$	-0.72	+0.63
k_{OH}	5.34	4.01	+0.33	+0.53
sulfate	3.59	1.95	+0.84	+0.33
ammonium	1.38	0.96	+0.43	+0.42
nitrate	0.99	0.76	+0.31	+0.34
organics	3.91	4.99	-0.28	+0.45

TABLE 4.1: Statistic parameters for the two 2012 PEGASOS campaigns: Cabauw, Netherlands and Po-Valley, Italy. Included days are noted in Table 3.1.

4.2 Comparison over height profiling flights

The model evaluation against the Zeppelin measurements over the two campaign periods provided general information about the model performance over a relatively long time period. However, a more detailed study of selected days can provide insight on specific aspects. The evaluation will continue, by focusing on two campaign days in which height profiles were performed. At the 2012-07-12, the Zeppelin performed 6 hour height profiling measurements, which was also the longest continuous height profiling for this campaign, from 3:20 to 9:19 UTC in the morning, at the San Pietro Capofiume site. This measurement day was characterized as a 'golden day' not only for the long flight duration but also because winds were very low (practically no wind) making the photochemical processes more apparent and distinct from horizontal transport phenomena. For this reason, this flight (F049), can be used as a reference for gas-phase comparisons. There were no aerosol measurements at that day. At the 2012-06-20, the Zeppelin performed two sequential height profiling flights, at the same site, from 4:30 to 12:22 UTC, with a 30 min refueling break in between at about 8:30 UTC. In addition to gas phase measurements, aerosol measurements were operating that day. The first flight (F027) was done when the mixed layer was under development and the second flight (F028) was done during a fully developed mixed layer. Firstly, the model results for both days will be evaluated, as far as selected meteorological variables are concerned. Secondly, specific aspects about the gas-phase of the 2012-07-12 will be discussed. Thirdly the model results as far as the aerosol-phase of the 2012-06-20 is concerned will be evaluated.

4.2.1 Meteorological parameters

As done in Section 4.1.1, we will evaluate temperature, relative humidity and absolute water content for the specific days. In Figures 4.16, the predictions of these variables are plotted against the corresponding observations for the 12/07 and the 20/06. For the 12/07 the mean predicted temperature (22.05°C) slightly underestimates the mean observed temperature (23.39°C) with a NMBF of -0.06 (a factor of 1.06), while for the 20/6 higher temperatures are noted, with the mean predicted temperature (26.65°C) slightly underestimating the mean observed (27.27°C) with a NMBF of -0.02 (a factor of 1.02). The relative humidity is overestimated in both days with NMBF +0.04 and +0.09 (factors 1.04 and 1.09) respectively. The mean values of predicted and observed absolute water content are very close with a slight underestimation on 12/07 (NMBF -0.04) and a slight overestimation on 20/06 (NMBF +0.05).

By comparing the meteorological day statistics for those two days with the summary statistics of the Po-Valley statistics, similar behavior is noted. However, we find that

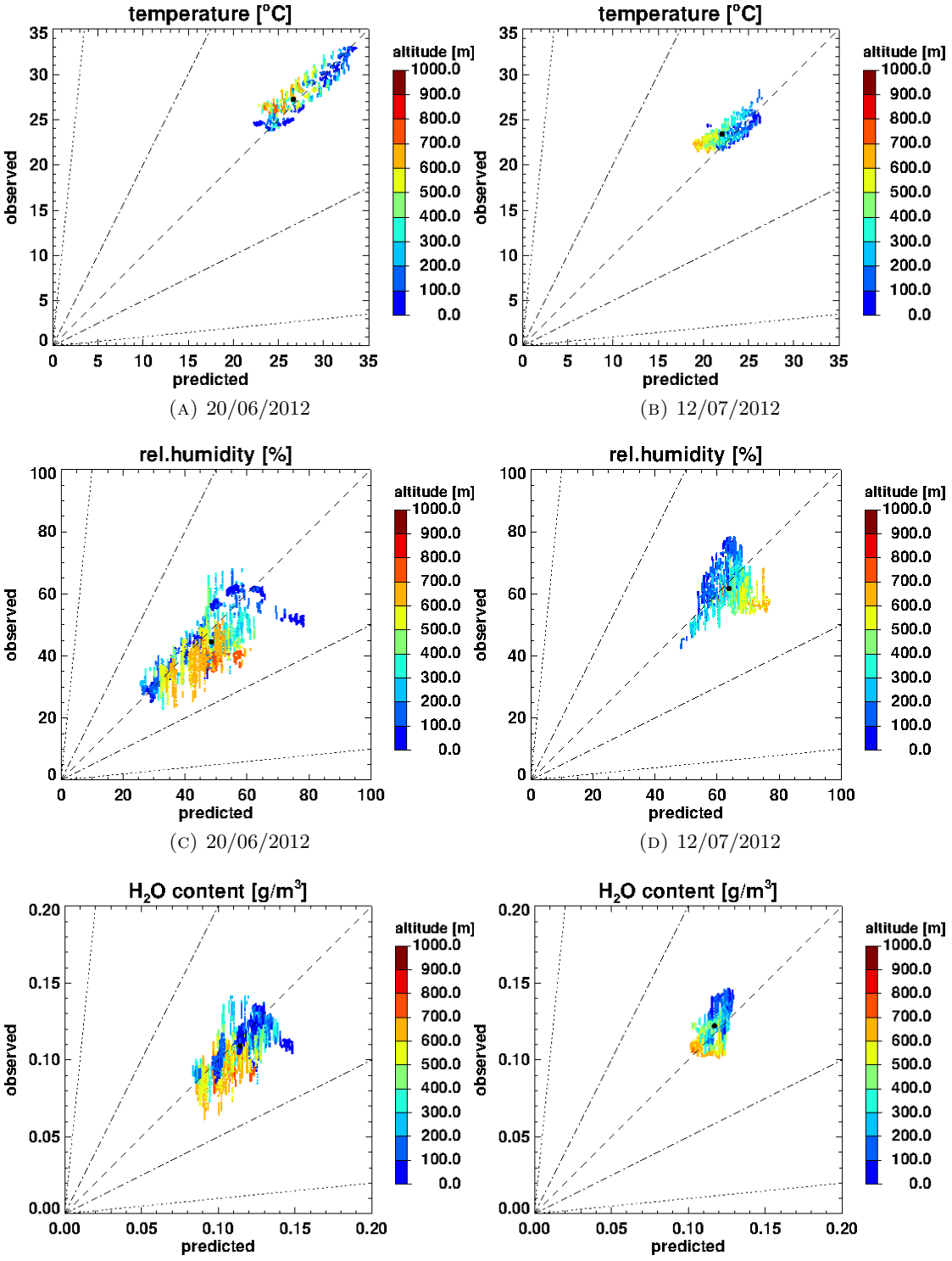

(A) 20/06/2012 (B) 12/07/2012

(C) 20/06/2012 (D) 12/07/2012

(E) 20/06/2012 (F) 12/07/2012

FIGURE 4.16: Scatterplots of temperature, relative humidity and absolute water content, for the 20/06 (left) and the 12/07 (right), colored by altitude.

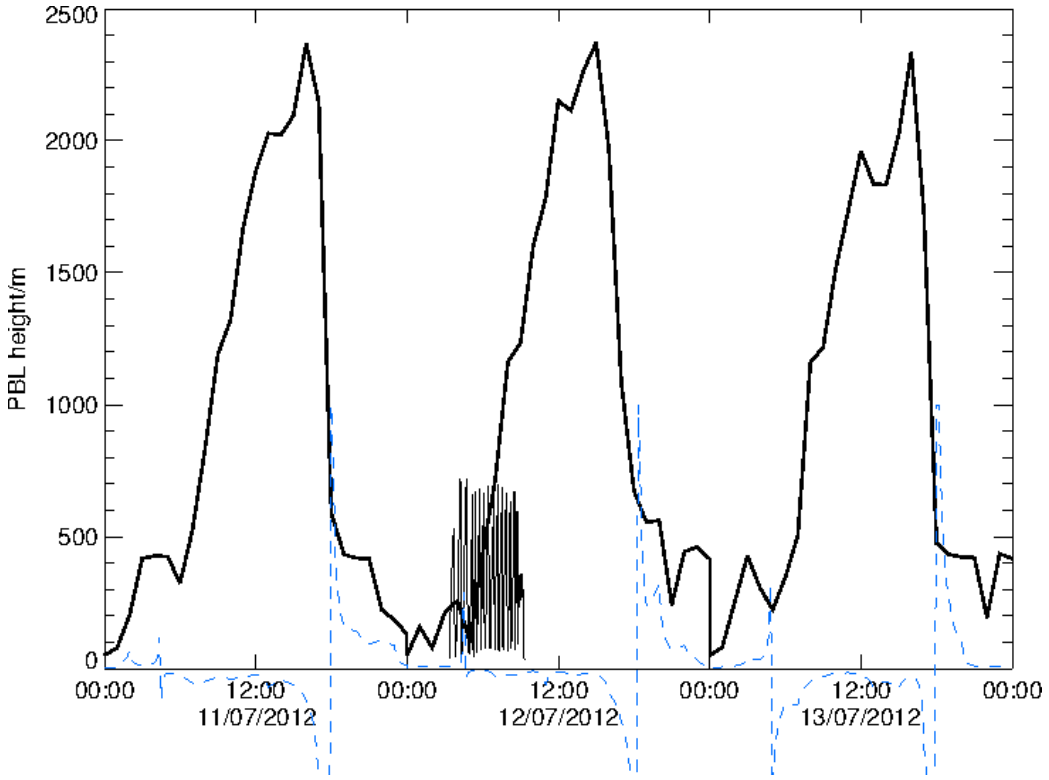

(A)

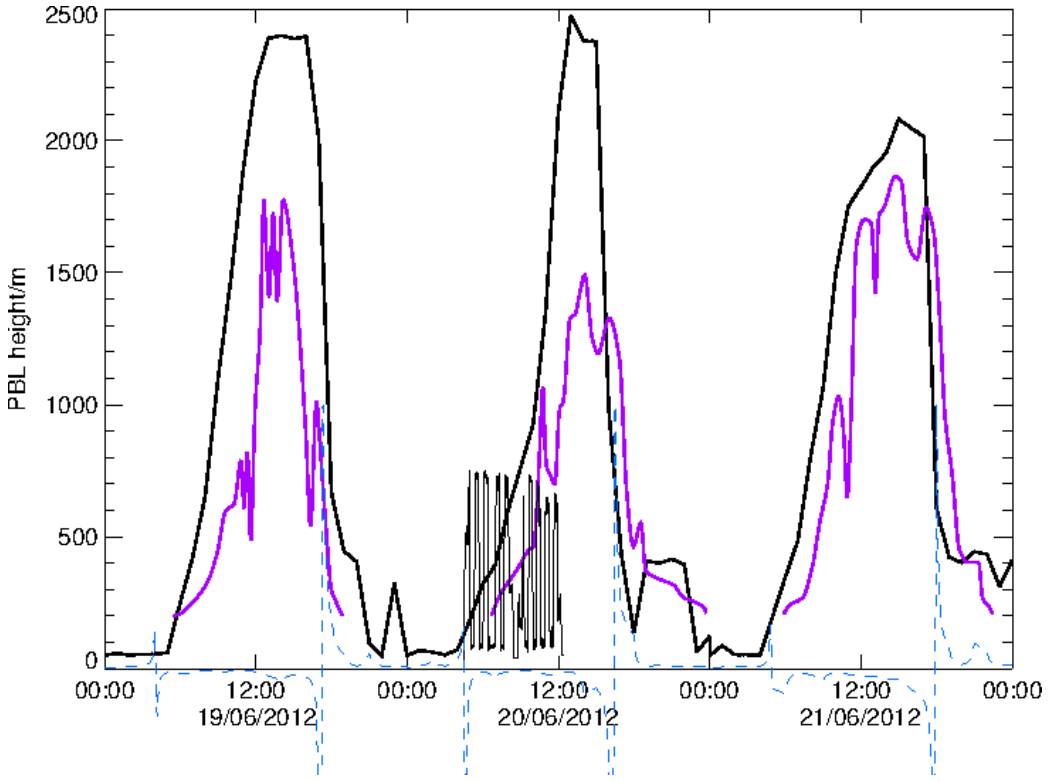

(B)

FIGURE 4.17: Predicted (black) and retrieved only for the 20/06 (violet) PBL height for the 12/07 and the 20/06 with previous and following days. Airship track (thin black), Monin–Obukhov length (dashed blue).

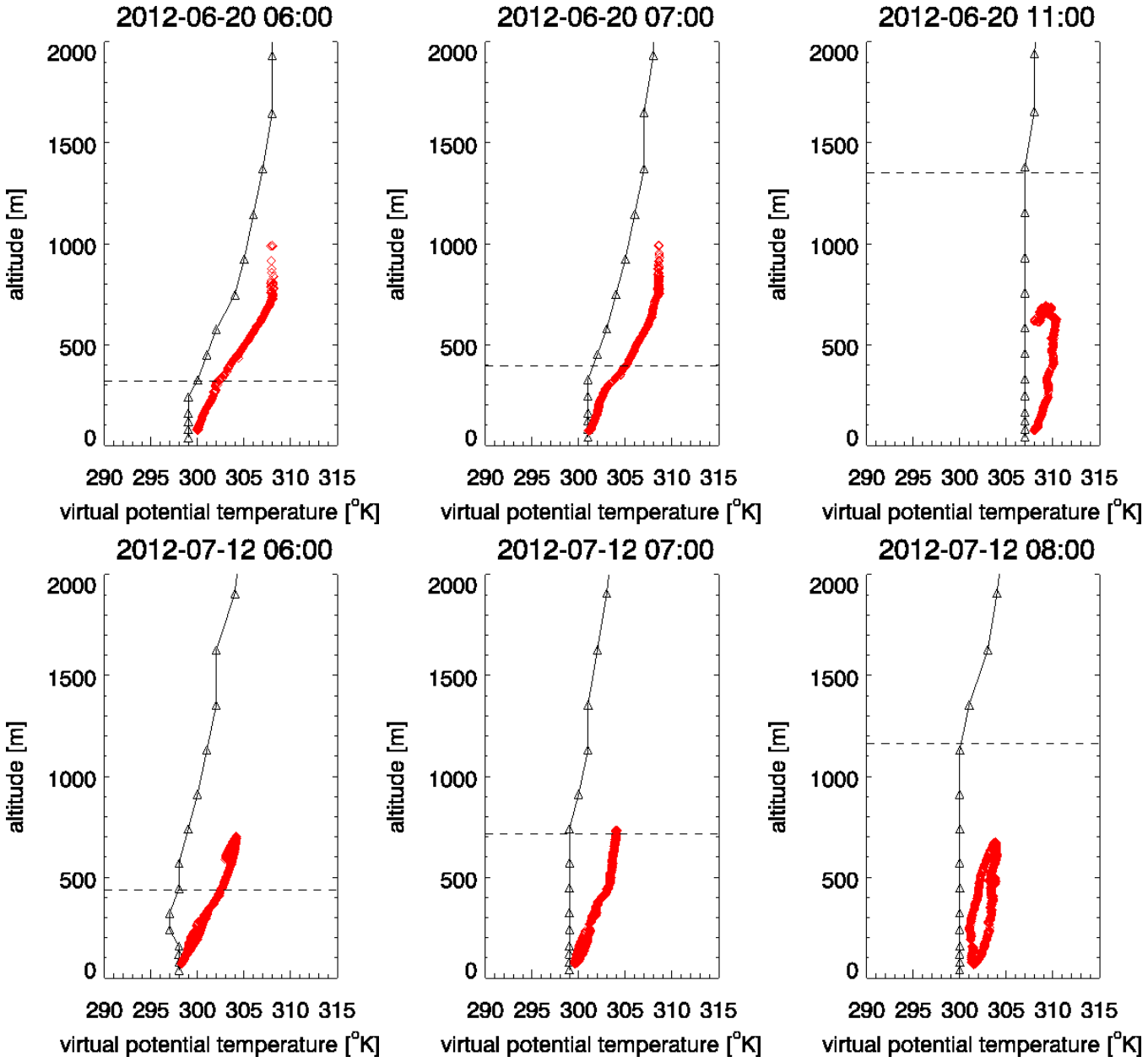

FIGURE 4.18: Virtual potential temperature vertical profiles on 20/06 and 12/07 for selected time instances: model (black) and observations (red), triangles note the model levels, dashed line notes the predicted PBL height.

temperature and relative humidity day statistics are closer to the summary statistics for the 20/06 than for the 12/07. For the later day, the correlation coefficient of predicted with observed values of those two variables is lower, especially for the relative humidity. Such a declining is expected when looking at statistical indices of a short time period against statistical indices of a much longer period.

To characterize stable or unstable layers, with effects of pressure and water content included, the virtual potential temperature (θ_v) is used. The virtual potential temperature is defined as the temperature that an air parcel, at pressure P and absolute temperature T, aquires if it is brought adiabatically to standard pressure P_0 and all water in the parcel is condensed. It is calculated by the formula:

$$\theta_v = T \left(\frac{P_0}{P} \right)^{R/c_p} wv_{corr} \tag{4.3}$$

where wv_{corr} is the water vapor correction term. The height profile of the θ_v through an atmospheric layer, shows if the layer is unstable or stable, thus if vertical mixing occurs or not, respectivelly. If θ_v increases with height, air is stable to vertical motion. If θ_v decreases or is constant with height, air is unstable to vertical motion. A decreasing θ_v with height cannot be maintained and it tends to a constant θ_v with height which counts for adiabatic motion. Another variable that characterizes atmoshperic stability is the Monin-Obukhov Length (L) which is a rough measure of the height at which turbulence is generated more by buoyancy than by wind shear. According to the similarity theory it represents the height (-L) at which the buoyant production of turbulence kinetic energy is equal to that produced by the shearing action of the wind (Obukhov). In the daytime over land, L is typically between 1 to 50 meters.

The PBL height at the location of San Pietro Capofiume, where the height profiling flights were performed, for the above selected days is shown in Figures 4.17. The preceding and following days are also included. In addition, the length L is noted. As expected, L is negative during daytime over land, positive during night, and infinite at dawn and dusk when the virtual potential temperature flux passes through zero. On the 12/07 the modeled PBL ascends and descends between 50 and 300 m, and starts to evolve smoothly at about 05:00 UTC, giving two distinct height maxima in the time inteval 12:00-15:00 UTC, of 2200 and 2300 m. The PBL breaks down at 16:00-18:00 UTC. Both the 11/07 and the 13/07 reveal similar behavior. On the 20/06 the modeled PBL starts low at about 50 m starting a smooth development at 04:00 UTC reaching the maximum height of 2000 m at 14:00 UTC. The following day 21/06 shows similar behavior reaching the same maximum, while the preceding day 19/06 shows not a sharp maximum but a higher maximum 'plateau' at 2400 m between 12:00 and 15:00 UTC and then starts breaking. On the predescribed days of interest the breaking of the PBL

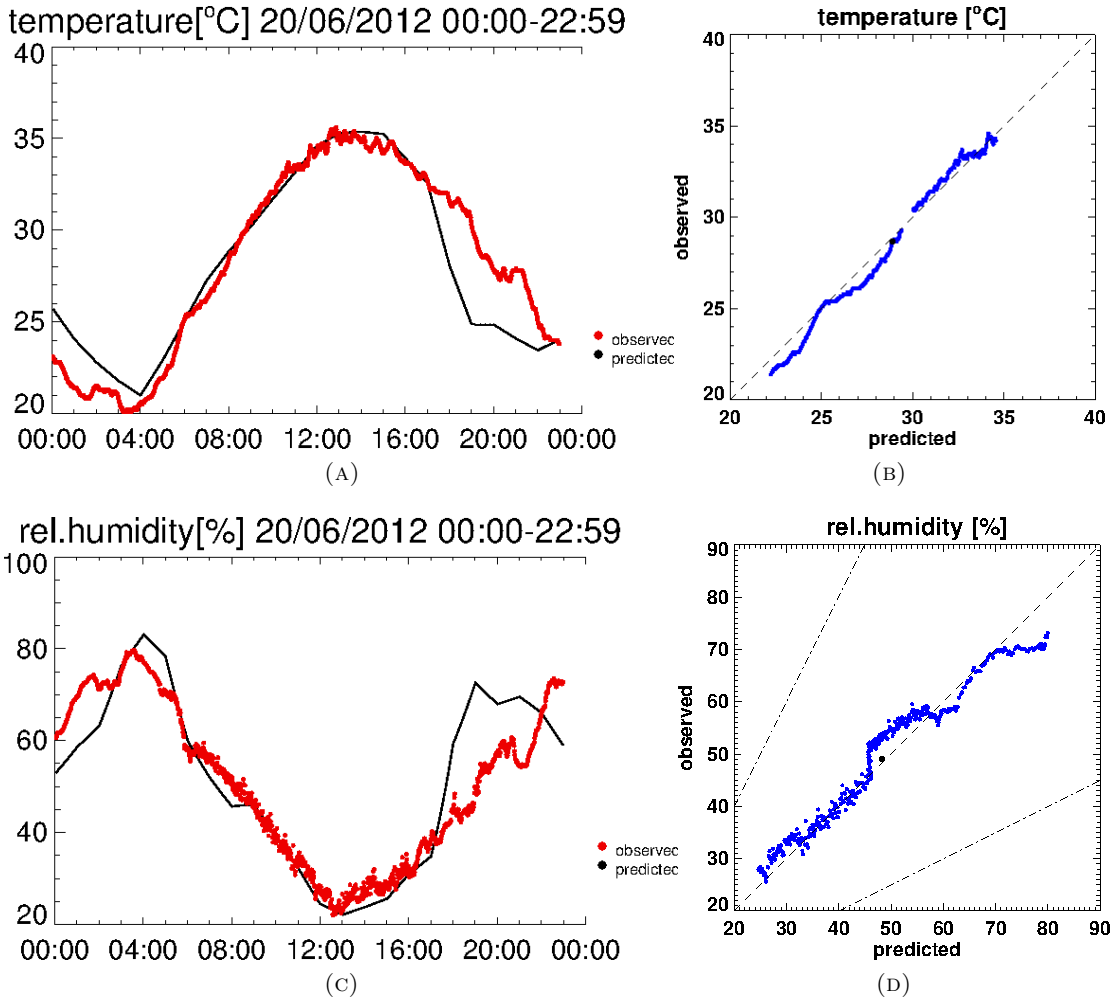

FIGURE 4.19: Ground absolute temperature and relative humidity comparison time-series (left) and scatterplots of the predicted vs observed ground values during the Zeppelin flights F027 (04:36-08:15 UTC) and F028 (08:55-12:04 UTC) (right), at the location of SPC on the 20/06.

comes about as sharp as the evolving, with fluctuations during the last hours of the day. Since the breaking of the PBL is a more complicated procedure, and no observations were done at the daily time frame it happens, it is not discussed in this thesis. For the 20/06 PBL height available PBL retrievals show a significant difference against the calculated PBL height. During the measurement flight, which is noted at the same plot, in early morning the modeled PBL seems to develop faster and earlier than what the retrievals indicate. It will be interesting at a later point, to see what the effect of the PBL height discrepancy is, on the trace species concentrations.

As mentioned, the vertical profile of the virtual potential temperature determines whether vertical mixing occurs. In Figures 4.18, time instances during the morning hours of 20/06 and 12/07 are selected, either during the early morning development of the mixing layer, or under fully mixing conditions. The predicted virtual potential temperature profile is

plotted from the surface to a height up to 2000 m against the observed vertical profile of the closest in time ascending or descending of the Zeppelin. A first inspection of the figures shows an underestimation of the θ_v at all times and heights. But that is not the only difference. Already at 06:00 UTC, both in 20/06 and 12/07, the model gives constant θ_v hence an unstable layer from the surface up to 200 m, while the observations show stability from the surface up to 700 m. At 20/06 07:00 UTC the predicted unstable layer reaches the height of 400 m while the observed profile tends to become steeper from the surface to 250 m indicating a thinner unstable layer. At 20/06 11:00 UTC, in fully unstable conditions, and while the unstable layer in the model reaches clearly the height of 1350 m, the observed profile shows alternating stable unstable layers up to 750 m. The same pattern is noted on the 12/07. One can conclude that even though both predicted and observed θ_v vertical profiles are consistent with what is expected from the θ_v diurnal evolution, there are differences. In the model, instability is manifested earlier, in a steeper way, and in lower values of θ_v. Since the temperature layering in the vertical extend is driven by ground forcing, one should check the ground absolute temperature as well as the ground relative humidity evolution, comparing model and ground field observations.

In Figure 4.19, predicted absolute temperature and relative humidity are evaluated against field measurements at the surface, over a 24 hour time frame. Inspecting the comparison timeseries, one notes temperature and relative humidity to be anti-correlated both in model and observation. This is expected as relative humidity is inversely proportional to temperature under constant water vapour conditions. Predicted and observed values show agreement with larger deviations noted in the early morning (00:00-04:00 UTC) and the evening (17:00-23:00 UTC) hours. In the time frame of the two Zeppelin flights (04:36-12:04) evaluation yields a NMBF of +0.01 (factor 1.01) for temperature and -0.02 (factor 1.02) for relative humidity. The respective scatterplots are shown in the right panels of the same Figure. The prediction-observation agreement at the surface reflects on the lowest altitudes of the virtual potential temperature vertical profiles shown in Figure 4.18 where agreement is also noted.

4.2.2 Gas phase comparison

In order to compare the model results against observations concerning gas-phase, the predicted diurnal evolution of the vertical profiles of ozone and nitric oxides will be investigated. The observations along the flight path will be overlayed correspondingly color-coded. For the location of San Pietro Capofiume the concentration vertical profiles from the surface to a height up to 2500m, from 00:00 to 24:00 UTC are plotted with a

time resolution of 10 min. While examining those plots, it should always kept in mind that ozone is mainly transported while nitrogen oxides are emitted from the surface.

The diurnal evolution of the O_3 vertical profile for the 12/07, as well as for the preceding and following days, is shown in Figure 4.20. The predicted PBL height described in the previous section is overplotted and the observations along the vertical profiling track of 12/07 are overlayed. In the time interval between 8:00 and 18:00 UTC, the effects of mixing in the predicted concentration are apparent in all the three days 11-13/07. O_3 tends to have a uniform vertical profile up to the predicted PBL. In addition, vertical structures of low O_3 concentration are noted in the early morning or late night hours where the PBL is underdeveloped, for example at 11/07 02:00 and 22:00 UTC, at 12/07 03:00 and 20:00 UTC, and at 13/07 03:00 and 20:00 UTC. These sinks can be explained. First, in the absence of light, photochemistry, which generates ozone, is ineffective. Second, there is no vertical mixing. In that case, the dry deposition at the surface creates areas of higher and lower ozone concentration which appear in a model calculation as seen in the figure. Comparing the three days one can notice the mean ozone concentration fluctuating. Although day by day the O_3 level is expected to rise slowly due to seasonal factors, the three day period shown here is much too short for a notable effect.

The O_3 observations on 12/07, done in the time interval 03:30-09:30 UTC, show a somewhat higher concentration, than what predicted by the model, both before and after the mixing layer has developed. The expected features are apparent both in predicted and observed values. The observations reveal a layering, of higher concentration at higher altitudes and lower concentration at lower altitudes of the flight. The observed higher concentration at higher altitudes could be addressed as residual O_3 from the preceding day. After 07:00 UTC, higher ozone concentrations are observed which is an effect of two processes. First, sunlight assists O_3 production, and second as the PBL evolves vertical mixing tends to distribute O_3 uniformly in vertical extend. By comparing observations with the predicted background one can see that the same features appear, although shifted in time with the model underestimating the observations along the flight track.

In Figure 4.21 the diurnal evolution of NOx is shown for the same three day period, 11-13/07, with observations of 12/07 overlayed. The background predicted concentration decreases with altitude, as expected, since NOx are emitted from the surface. The effect of the morning anthropogenic activities (rush hour) which result to surface emissions are noted at about 07:00 UTC on 11/07 and 13/07 but are not so apparent on the 12/07. In the time interval between 00:00 and 06:00 UTC NOx seem to be trapped in lower altitudes below the night-time PBL, with this being more prominent on 12/07, but this is not always the case. In the same time interval, NOx is also noted above the night-time PBL e.g. on 13/07 as the residual of the preceding day. For all the three days and

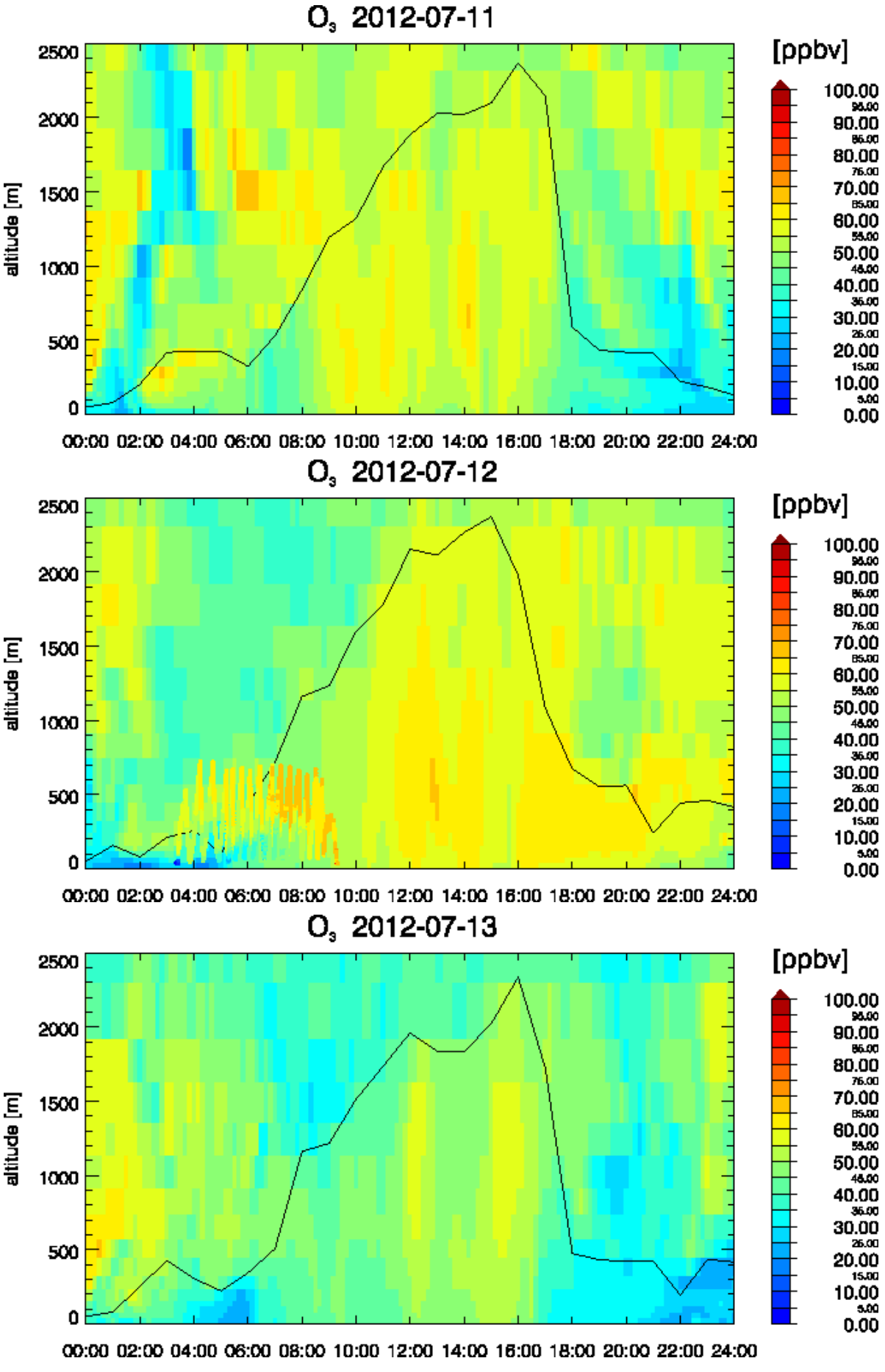

FIGURE 4.20: Time-height plots of O_3, for the San Pietro Capofiume site on: 11/07, 12/07, 13/07, with overlayed observations of 12/07.

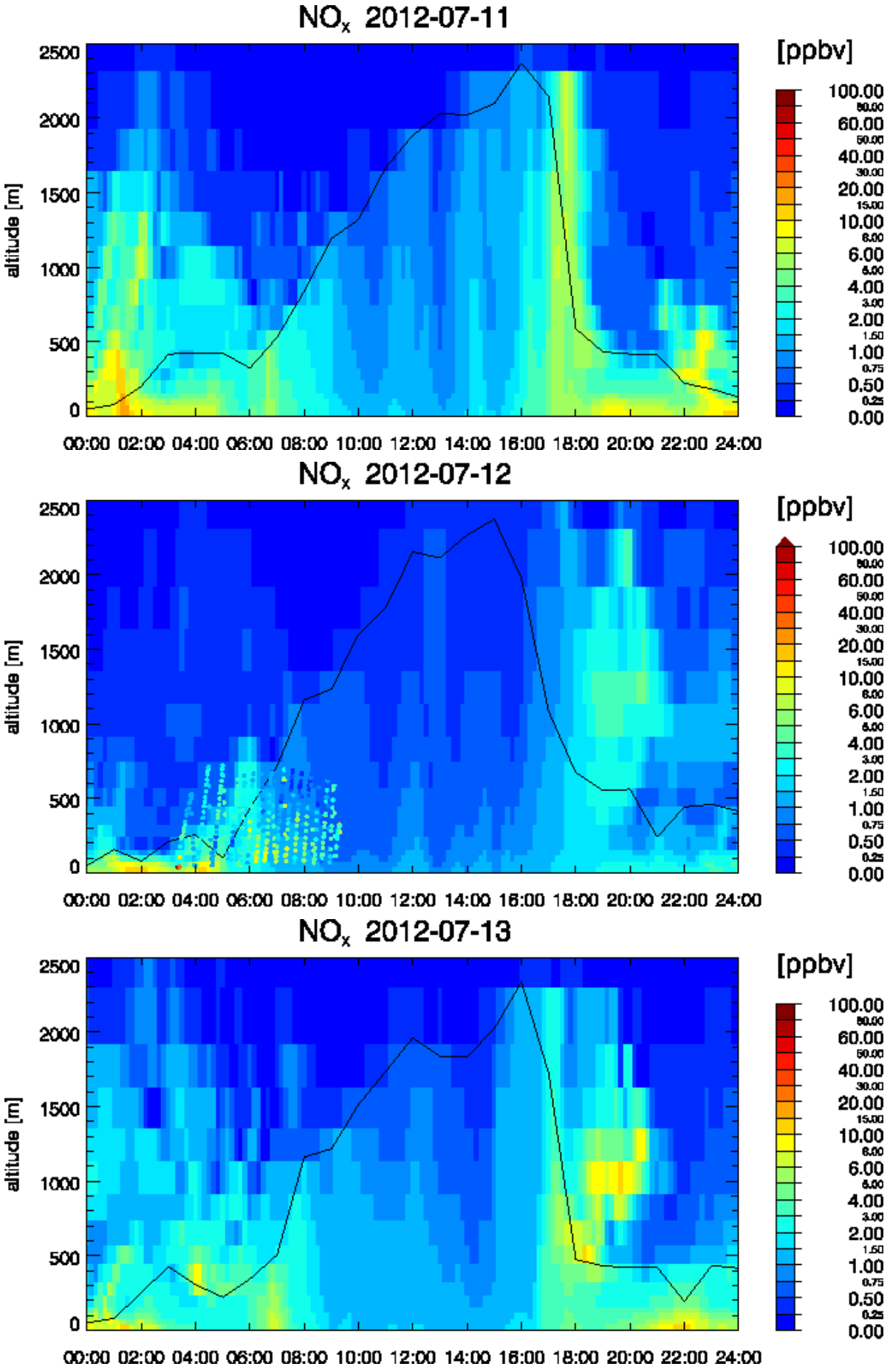

FIGURE 4.21: Time-height plots of NOx, for the San Pietro Capofiume site on: 11/07, 12/07, 13/07, with overlayed observations of 12/07.

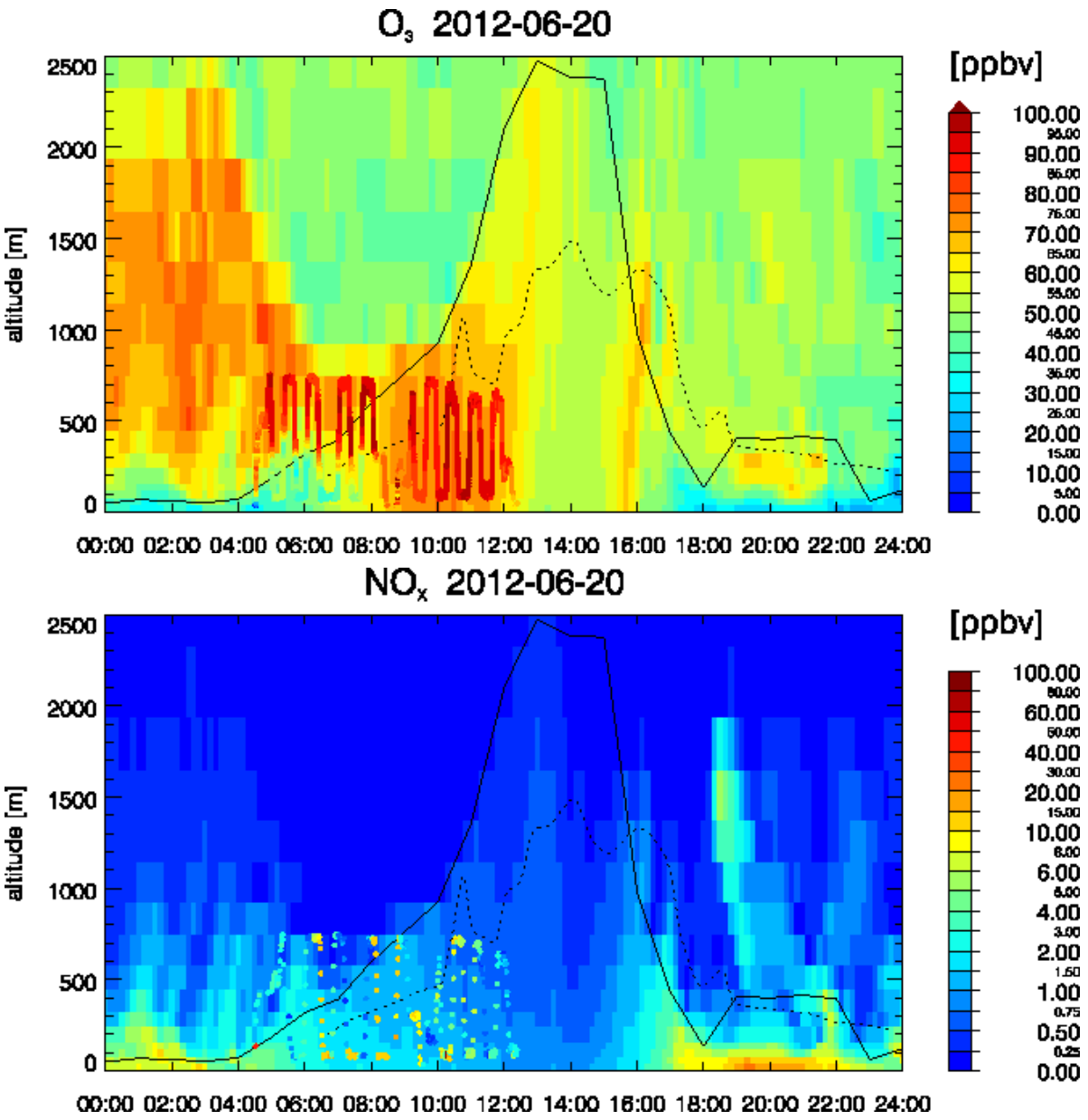

FIGURE 4.22: Time-height plots of O_3 and NOx, for the San Pietro Capofiume site on: 20/06 with overlayed observations.

between 08:00 and 18:00 UTC NOx concentration tends to be vertically uniform from the surface to up to the predicted PBL height, due to vertical mixing, but a gradient still remains since there are ongoing surface NOx emissions throughout the whole day.

The NOx observations on 12/07, done in the time interval 03:30-09:30 UTC show a smoother upward dispersion than what is predicted. A distinct evolving layering is observed. The gradual decreasing with altitude noted from 03:30 to 05:00 UTC becomes steeper after 05:00 UTC. Against the model, NOx are upwards dispersed later, the close to surface concentration is underestimated during the rush hour (07:00 UTC), and maintened for a longer period (06:00-08:00 UTC).

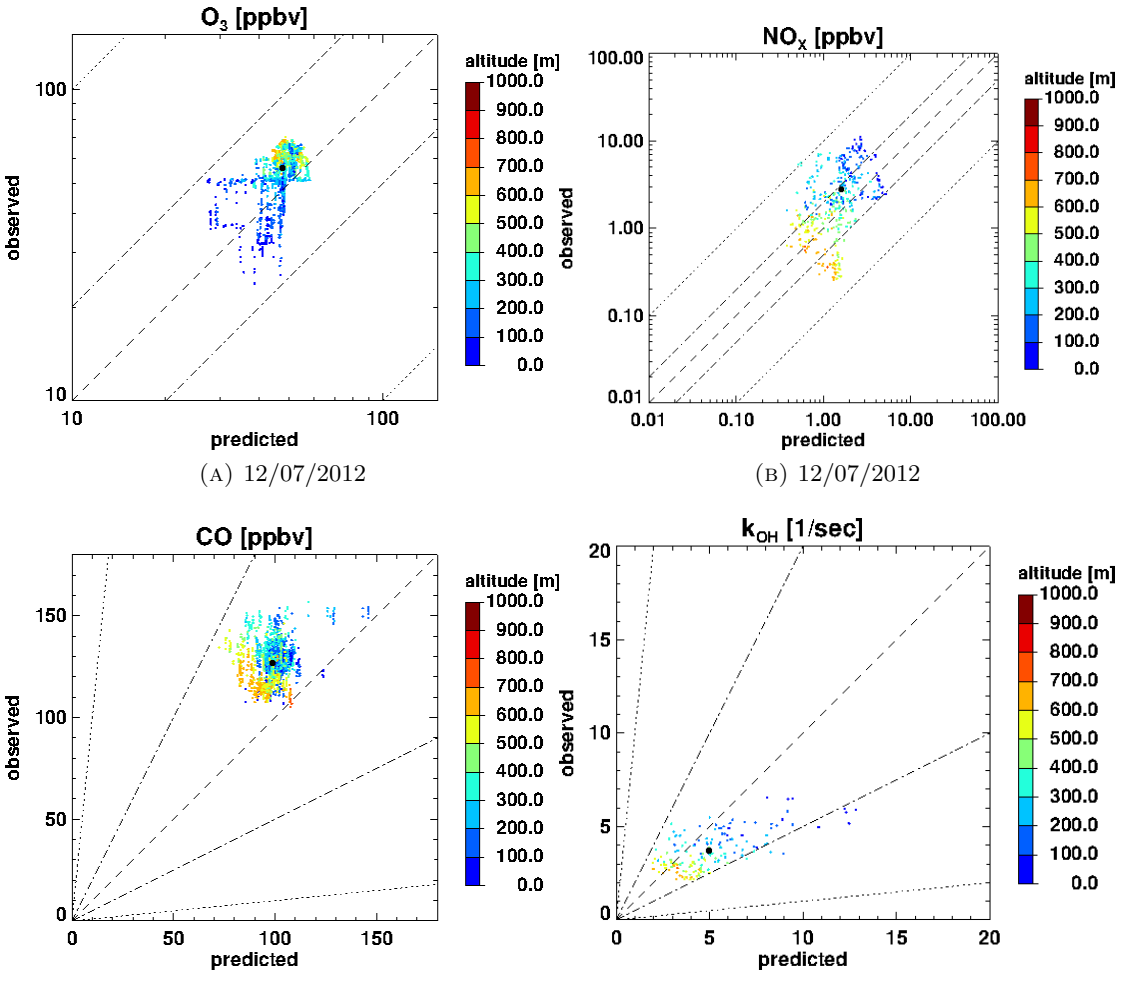

(A) 12/07/2012 (B) 12/07/2012

(C) 12/07/2012 (D) 12/07/2012

FIGURE 4.23: Scatterplots of O_3, NOx, CO, k_{OH}, for the 12/07, color-coded with altitude.

The outcome of the comparisons above can be stated as follows. First, the predicted O_3 and NOx concentrations show qualitive consistancy, as both constituents are dispersed anticipatedly with respect to the PBL evolution. Under mixing conditions, on one hand O_3 formed in an altitude or transported from aloft disperses towards lower and higher altitudes, and on the other NOx as surface emitted disperse towards higher altitudes. The predicted-observed discrepancies can be adressed to the following three reasons. First, the far-transported O_3 contributing to the area of interest level may be biased. Second, the NOx local sources are underestimated. Third, the parameters controlling the PBL development may not be optimal for the area of interest. To support the later, one could take a look at how O_3 and NOx time-height prediction compares to observations for another campaign day, the 20/06, in which retrieved PBL height is available, shown in Figure 4.22.

As done in previous section over the campaign periods, the model results are here evaluated against observations using the same metrics, for the 12/07, based on the altitude

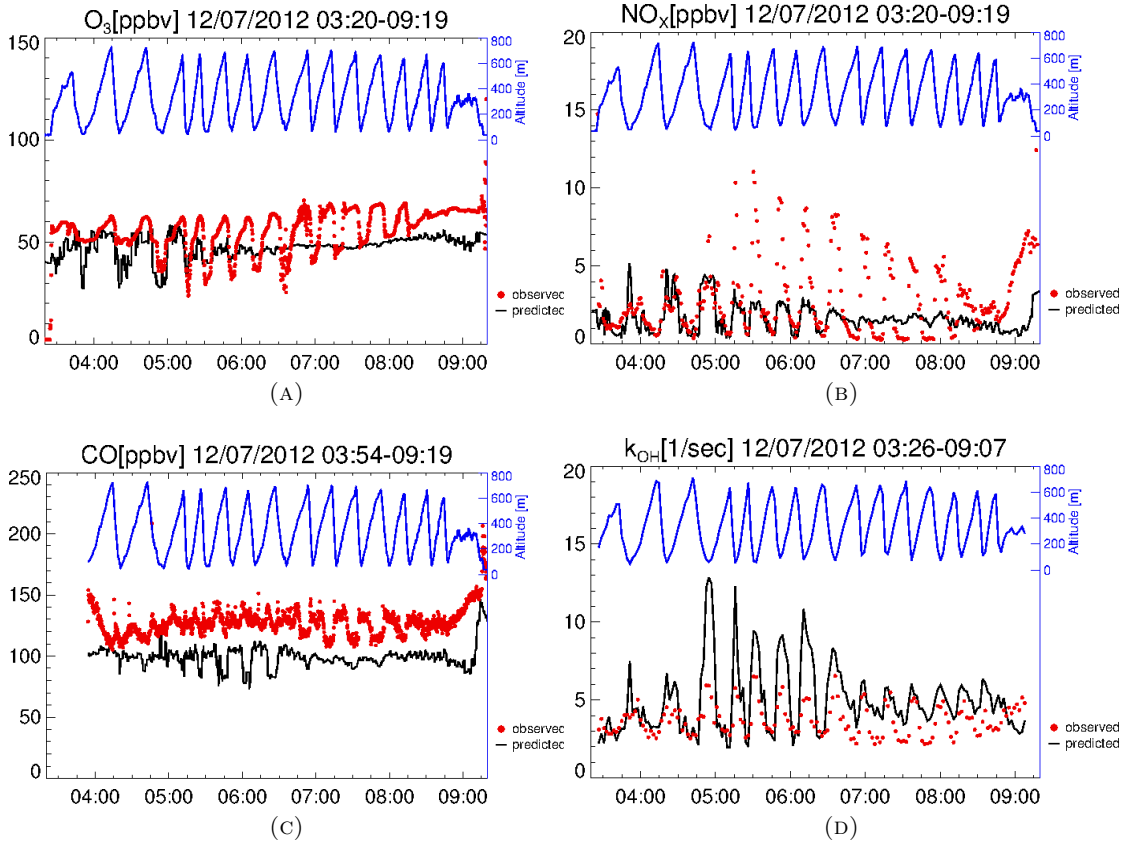

FIGURE 4.24: Comparison time-series of O_3, NOx, CO, k_{OH}, along the flight track, for the 12/07.

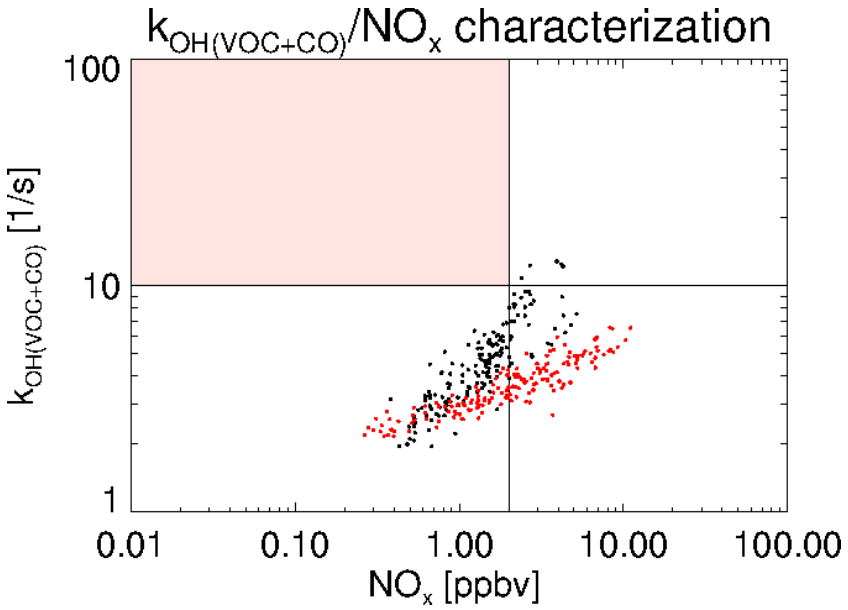

FIGURE 4.25: k_{OH}/NOx characterization plot, for the 12/07 (predicted: black, observed: red). The shaded area notes regimes of low NOx and high VOC concentrations, where the non-classical pathway for the OH regeneration is expected to occur, according to Hofzumahaus et al. [2009].

color-coded scatterplots for O_3, NOx, CO, and k_{OH}, shown in Figure 4.23. The calculated metrics are listed in Table 4.2. The mean observed O_3 (56.09 ppbv) is underestimated by the mean predicted (47.53 ppbv) with a NMBF of -0.18 (factor of 1.18). The mean observed NOx (2.79 ppbv) is underestimated by the mean predicted (1.6 ppbv) with a NMBF of -0.74 (factor of 1.74). The distribution of points on the O_3 and NOx scatterplots reveals the same structures with those for the Po-Valley campaign period (bottom panels of Figures 4.5 and 4.6 respectively). While the majority of O_3 points are distributed around the center of gravity in the factor 2 underestimation area, points corresponding to lower altitudes 0-200 m form elongated structures that show observed variability that was not captured by the model. This is clearly noted for the time period 06:15-08:15 UTC in the O_3 comparison time-series along the flight track, shown in the panel (A) of Figure 4.24. The panel (B) of the Figure 4.24, the NOx comparison time-series along the flight track reveals the underestimation of the observed NOx in the lower altitudes between 05:15-08:00 UTC. The local influence of the NOx emissions near the surface fades with altitude e.g. for the same time period but higher altitudes predicted agrees with observed NOx. From NO and NO_2, the latter is the larger contributor to NOx. It occurs mainly from the oxidation of NO in high temperatures in combustion processes at the surface. As a result, in higher altitudes the model-observation discrepancy in both NO, NO_2 and their sum NOx is less influenced by the discrepancy in the surface emission distribution.

The mean observed k_{OH} with VOCs and CO (3.69 sec^{-1}) is overestimated by the mean predicted (4.96 sec^{-1}) with a NMBF of +0.34 (factor of 1.34). The mean observed CO (126.95 ppbv) is underestimated by the mean predicted (98.77 ppbv) with a NMBF of -0.29 (factor of 1.29). Since the CO is underestimated it cannot be responsible for the k_{OH} overestimation. This means that predicted VOC components that are overestimated in the model react with OH, causing the k_{OH} overestimation. A high overestimation of isoprene can be responsible for the k_{OH} overestimation. It can be seen in the comparison time-series of CO and k_{OH}, panels (C) and (D) of Figure 4.24 respectively, that k_{OH} is mostly overestimated between 04:45 and 06:30 UTC and close to surface. In this time period, which includes the sunrise, plants emit VOC compounds with the most important being isoprene but also other hydrocarbons (terpenes). However, different VOC components can have not only biogenic but an anthropogenic origin also and their production is difficult to measure. In fact, the amount of emitted anthropogenic VOCs, being uncertain could be used as a tuning parameter in model calculations. Here, we can conclude that the k_{OH} overestimation is a result of the uncertainties of estimated both biogenic and anthropogenic VOCs.

As far as tropospheric OH recycling is concerned, both VOCs and CO react with OH, forming organic peroxy radicals (RO_2) and HO_2. As it is widely understandood, the later

two products in the presence of NO regenerate OH, maintaining a balanced cycle, but also produce NO_2, which is photolysed by daylight to give O_3 as a side product. However, in regimes of low NOx and high VOC concentrations, the existence of a non-classical pathway for the OH regeneration is proposed in Hofzumahaus et al. [2009], which is independent of NO, amplifying the removal of pollutants without the O_3 production. Here, a characterization diagram is used to note under which conditions (NOx, k_{OH} with VOCs and CO) the observations of 12/07 were done and compare it with the corresponding model predictions. In Figure 4.25, the k_{OH} is plotted against the NOx concentration, with the shaded area indicating the range in which the proposed pathway could be verified. All points are distributed into elongated structures, which are classified in the 'continental'/'urban' land use environment according to Rohrer et al. [2014]. The predictions reveal a steeper slope than the observations. This declining occurs from the k_{OH} overestimation and NOx underestimation in lower altitudes. For the 12/07, it is noted that both predicted and observed values lie outside of the proposed range.

4.2.3 Aerosol phase comparison

Following the same procedure as in the previous section, the model results will be evaluated against observations for aerosols. The predicted diurnal evolution of the vertical profiles of nitrate, ammonium and sulfate, from the surface to a height up to 2500m will be investigated, overlaying correspondingly color-coded observations, for the location of San Pietro Capofiume. The time resolution of the predicted vertical profiles is 10min.

The diurnal evolution of the vertical profiles for the 20/06, as well as for the preceding and following days, for sulfate, ammonium and nitrate is shown in Figures 4.26, 4.27, 4.28. The predicted PBL height is overplotted and the observations along the vertical profiling track of 20/06 are overlayed. Inspecting the predicted background, similarities as well as differences are noted between the three inorganic aerosol species. First, commenting on the three day evolution, a typical diurnal profile seems difficult to be addressed. On one hand it looks there is a dependance on the reserved aerosol from the preceding day, e.g. the ammonium from 20:00 to 24:00 UTC on 19/06 between 300 and 1500m is noted also from 00:00 to 03:00 UTC on 20/06, or the absence of nitrate from 18:00 to 24:00 UTC between 500 and 2000m continues until 03:00 UTC of 21/06. On the other hand, local high concentration of aerosols is distinct close to surface, e.g. from 01:00 to 05:00 UTC on 19/06 and from 03:00 to 06:00 UTC on 20/06 in both nitrate and ammonium. High aerosol concentration, is also noted in higher altitudes, e.g. for nitrate at 10:00 UTC on 21/06 at 1000m dispersing upwards in the following hours. Such a high concentration in the last example could be a combination of local nitrate formation, horizontal transport or entrainment from the residual layer into the mixing

layer. The latter becomes more apparent in the nitrate vertical profiles evolution on 19/06, where structures of high concentration following the mixing layer evolution, from 08:00 to 12:00 UTC, are vertically dispersed. At the same time period on 21/06 the same applies, only here the entrainment from the residual layer can be excluded since there is not significant amount of nitrate noted in the residual layer. Comparison with overlayed observations gives an irregular pattern that cannot be easily explained here.

Before trying to explain the discrepancies between predicted and observed values we will quantify them, based on the altitude color-coded scatterplots for nitrate, ammonium, sulfate, and organics, shown in Figure 4.29. The calculated metrics are listed in Table 4.2. The mean observed sulfate (3.25 $\mu g/m^3$) is overestimated by the mean predicted (3.93 $\mu g/m^3$) with a NMBF of +0.21 (factor of 1.21). The mean observed ammonium (1.74 $\mu g/m^3$) is slightly underestimated by the mean predicted (1.60 $\mu g/m^3$) with a NMBF of -0.09 (factor of 1.09). The mean observed nitrate (1.75 $\mu g/m^3$) is underestimated by the mean predicted (1.24 $\mu g/m^3$) with a NMBF of -0.41 (factor of 1.41). Organic particles are also underestimated, (mean observed value 9.74 $\mu g/m^3$, mean predicted 6.66 $\mu g/m^3$) with the largest NMBF from the previous species -0.46 (factor of 1.46). The largest correlation coefficients are those for ammonium and nitrate yielding +0.49 and +0.42 respectively. The distribution of points on the scatterplots reveals again the same structures with those for the Po-Valley campaign period (bottom panels of Figures 4.11, 4.12, 4.13, 4.14). Sulfate shows homogeneity in predictions and observations, while ammonium and nitrate show variability with altitude. The largest variability is shown in nitrate which, as it was also explained for the whole Po-Valley campaign, because of its volatility, is in lower concentration than sulfate.

The effect of temperature and relative humidity on nitrate is apparent in the comparison time-series shown in Figure 4.30. First, commenting on absolute temperature, both predicted and observed values show a variability with altitude of the same magnitude. It is interesting to note short time periods of about 30min, during which the temperature variability comes to a still. Although this can be seen in both prediction (06:00 UTC) and observation (07:30 UTC), it is noted 90min later in the observation. This is an indication of what was mentioned earlier, that the predicted mixed layer develops too early in the model. In the time period 04:30-08:30 UTC, during the first part of the flight in an underdeveloped mixed layer, discrepancies up to 3°C are noted. However, after 09:00 UTC, during the second part of the flight under fully mixing conditions an almost perfect agreement is noted. Similar kind of discrepancies as in temperature for the two flight parts are noted in the relative humidity time-series.

The first part of the flight reveals an irregular pattern of discrepancies in the nitrate comparison time-series. Several of these discrepancies can be explained as follows. In

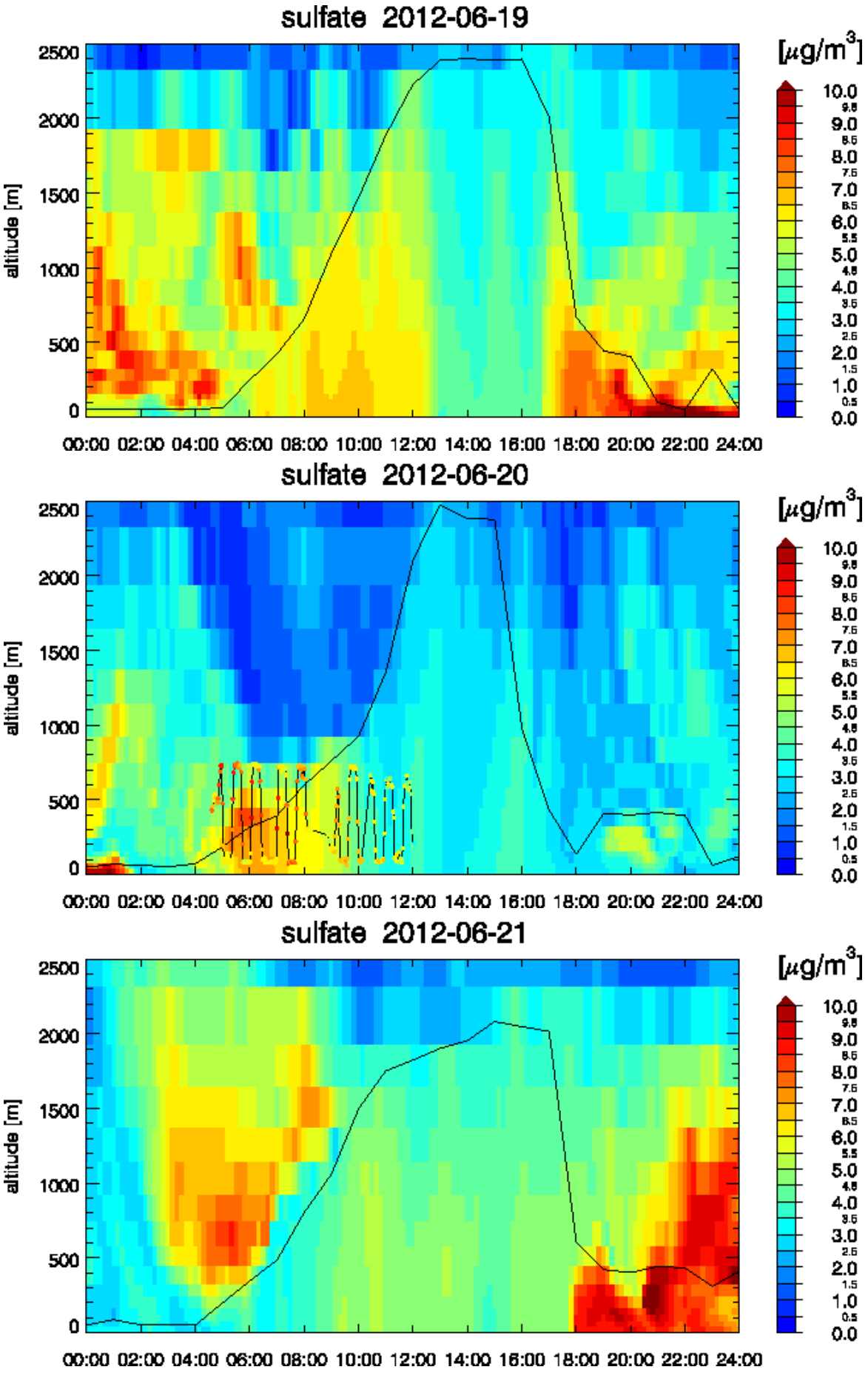

FIGURE 4.26: Time-height plots of sulfate, for the San Pietro Capofiume site on: 19/06, 20/06, 21/06, with overlayed observations of 20/06.

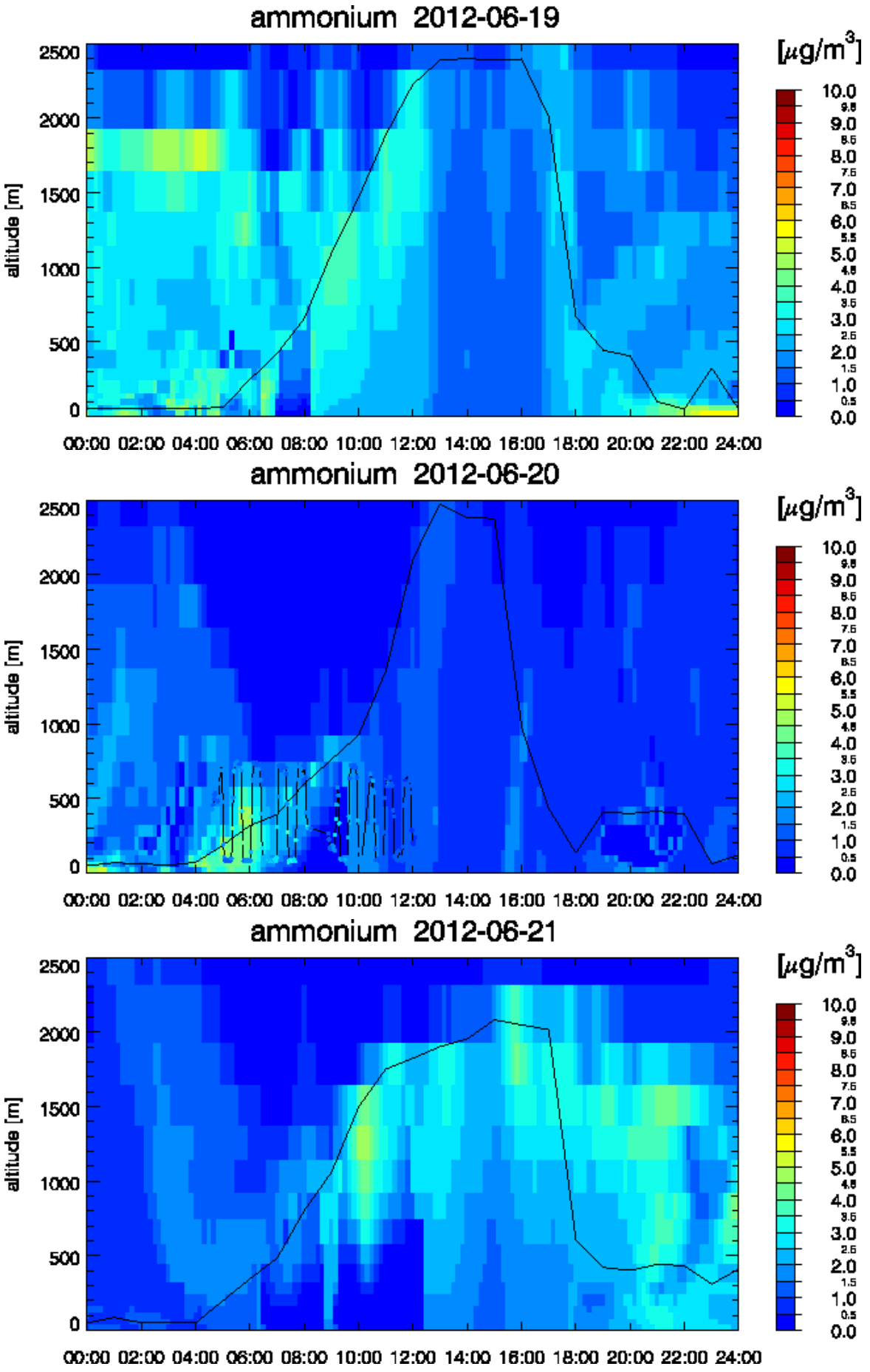

FIGURE 4.27: Time-height plots of ammonium, for the San Pietro Capofiume site on: 19/06, 20/06, 21/06, with overlayed observations of 20/06.

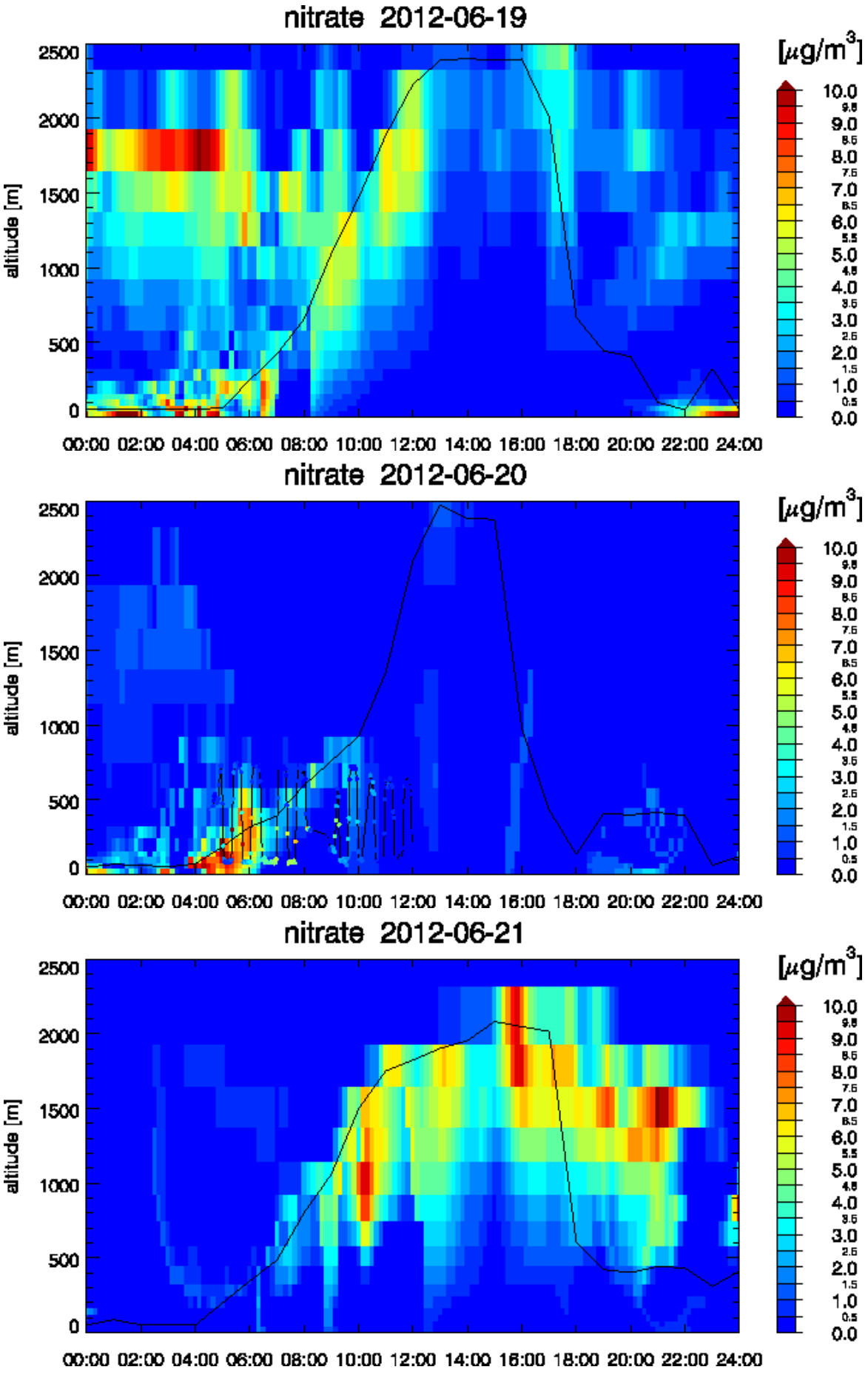

FIGURE 4.28: Time-height plots of nitrate, for the San Pietro Capofiume site on: 19/06, 20/06, 21/06, with overlayed observations of 20/06.

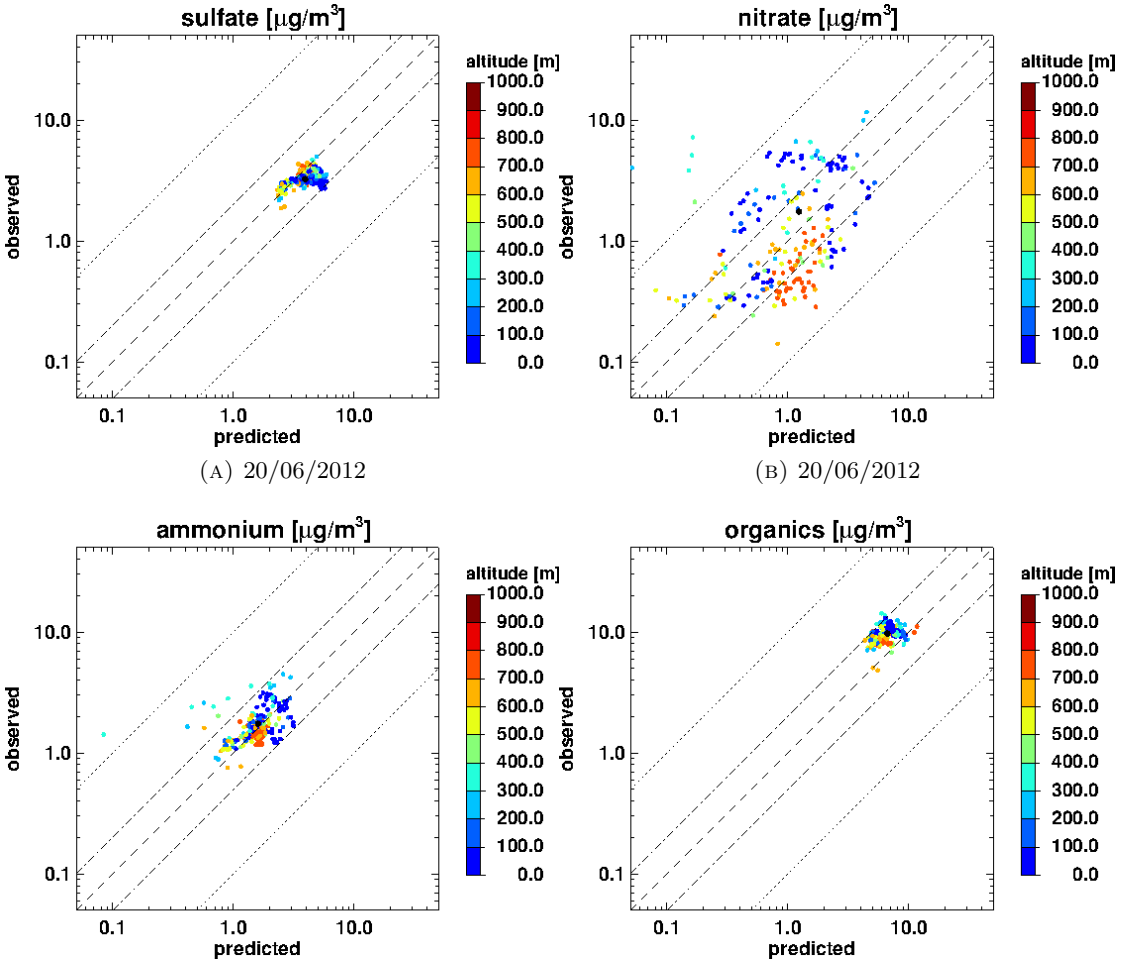

(A) 20/06/2012 (B) 20/06/2012

(C) 20/06/2012 (D) 20/06/2012

FIGURE 4.29: Scatterplots of sulfate, ammonium, nitrate, organics, for the 20/06, color-coded with altitude.

the first low altitude track period, the temperature underestimation and the relative humidity overestimation act both in favor of the nitrate overestimation. On the contrary, in the third low altitude track period, the temperature overestimation and the relative humidity underestimation act both in favor of the nitrate underestimation. The same discrepancy pattern is noted for ammonium although in a smaller amplitude. In the second part of the flight there are still discrepancies noted in nitrate which tend to be smaller with time. Ammonium behaves in the same way. Since in the second part of the flight, predicted temperature and relative humidity agree with observations, the latter cannot be responsible for discrepancies in aerosols.

The nitrate dependance on temperature and relative humidity is illustrated in another way, using the scatterplots shown in Figure 4.31. In panel (A), the color-coding corresponds to the temperature discrepancy defined as T(predicted)-T(observed). As expected, the majority of yellow- to red-ish colored points tend to distribute above the

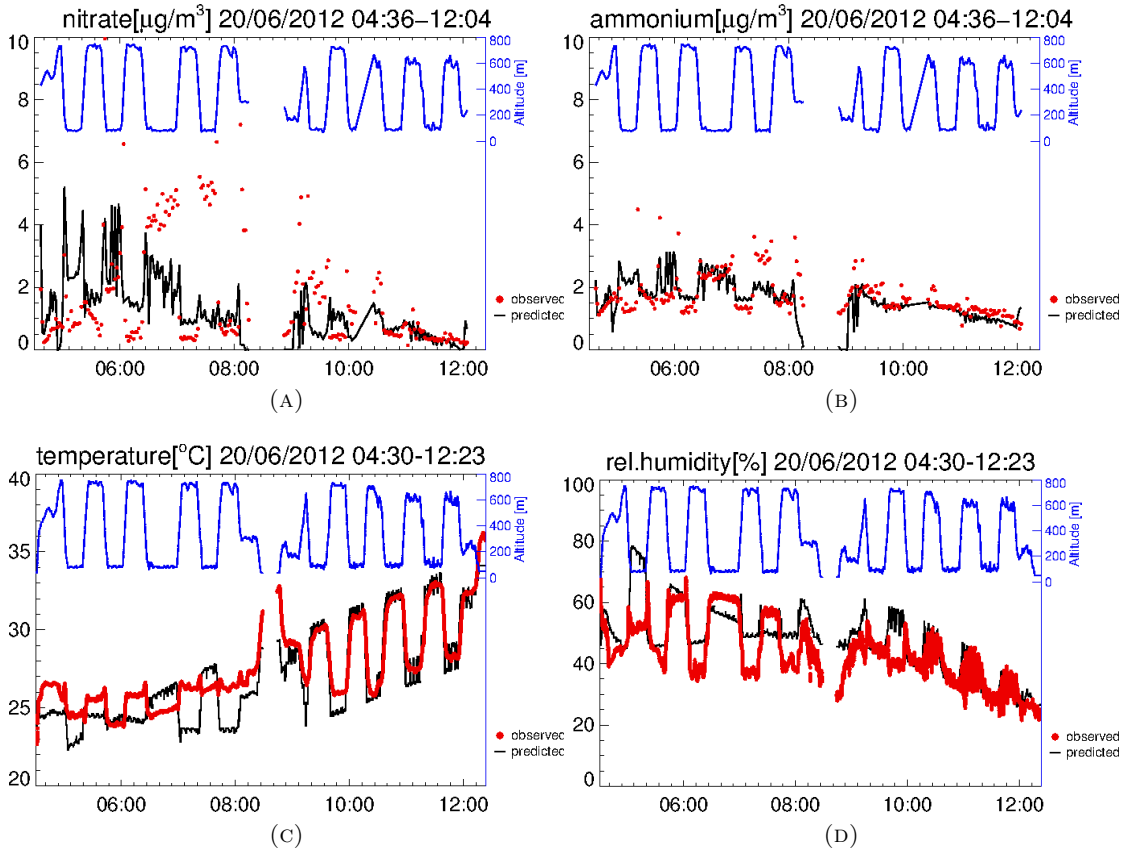

FIGURE 4.30: Comparison time-series of nitrate, ammonium, temperature, relative humidity, along the flight track, for the 20/06.

1:1 ratio line indicating the tendency of the model to underestimate nitrate concentration when temperature is overestimated, while green- to blue-ish points are distributed mostly below the 1:1 ratio line indicating the counter effect. In panel (B), the color-coding notes the relative humidity discrepancy defined as RH(predicted)-RH(observed). Similarly, here in the overestimation area, below the 1:1 diagonal, the majority of points correspond to overestimated relative humidity, and vice-versa. However, relative humidity and absolute temperature discrepancies are not the only variables that control nitrate concentration. Discrepancies in NO2 and NH_3 emissions which are precursors of nitrate and ammonium respectively play a significant role.

4.2.4 Summary

In this chapter, focus was given on two campaign days, in which vertical profiles were performed. Comparing the predicted with the observed vertical mixing conditions, by deriving the virtual potential temperature vertical profiles, revealed significant discrepancies. Although predicted ground temperature, relative humidity and consequently ground virtual potential temperature were found to agree with the observed values at

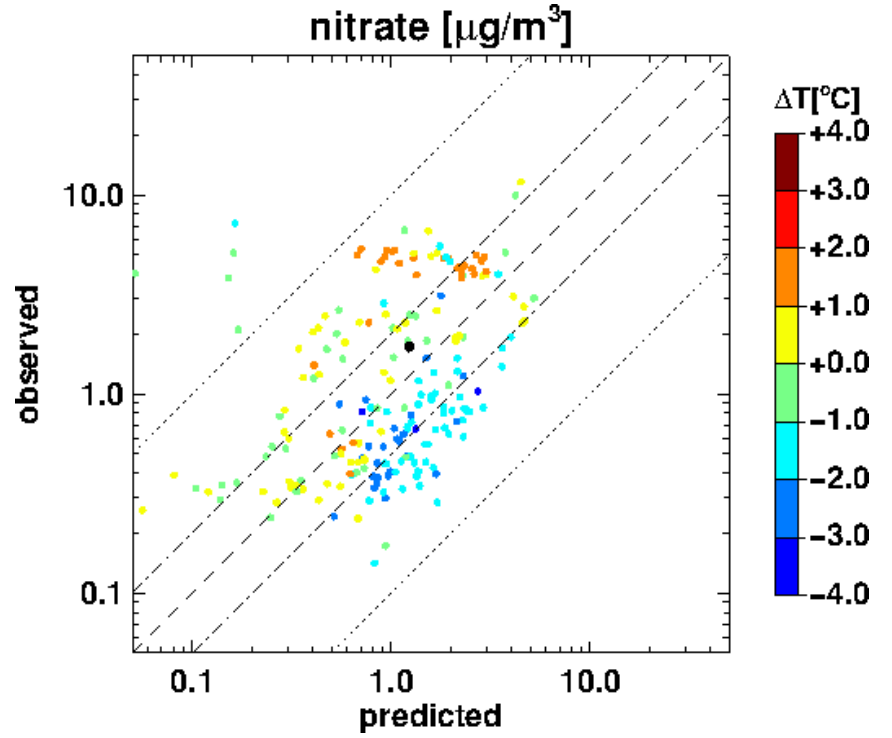

(A)

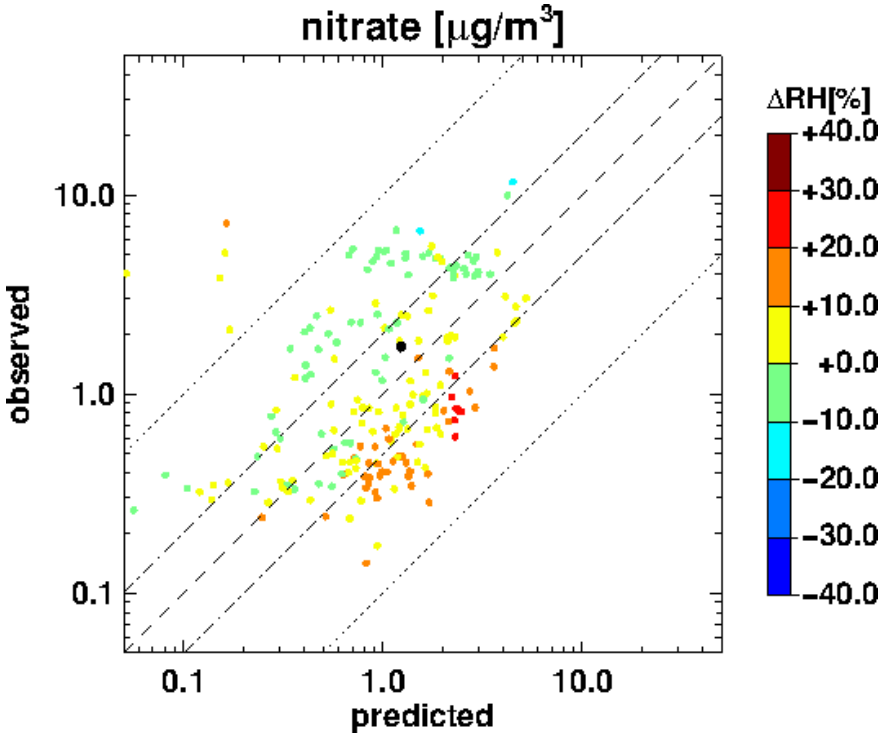

(B)

FIGURE 4.31: Scatterplot of predicted versus observed nitrate (SPC on 20/06/2012), colored with: (A) temperature discrepancy ΔT, (B) relative humidity discrepancy ΔRH, where ΔX= $X_{predicted}$-$X_{observed}$, 1:1(dashed), 2:1(dashed-dotted),10:1 (dotted).

the ground, in higher altitudes, virtual potential temperature was underestimated. After all, it could be the case that a finer vertical resolution may be more appropriate for the representation of such high vertically resolved transport phenomena. The campaign day of the 12/07 was evaluated with respect to O_3, NOx, CO, and the OH reactivity. Firstly, the overestimation of the k_{OH} was attributed to the overestimation in VOC components and mostly in isoprene. Secondly, the conditions under which a non-classical pathway for the OH regeneration were inpected. Such conditions were not met, neither in observations or in predictions. The campaign day of the 20/06 was evaluated with respect to aerosol phase components, that is, sulfate, ammonium, nitrate, and organics. With respect to the NMBF, the best prediction was noted for ammonium. The discrepancies between predicted and observed nitrate were associated with the discrepancies in temperature and relative humidity.

DAY STATISTICS				
12 July 2012				
Parameter:	$\bar{M}$	$\bar{O}$	NMBF	r
temperature	22.05	23.39	-0.06	+0.75
rel.humidity	63.87	61.67	+0.04	+0.19
H_2O content	0.12	0.12	-0.04	+0.58
O_3	47.53	56.09	-0.18	+0.50
NOx	1.60	2.79	-0.74	+0.39
CO	98.77	126.95	-0.29	+0.14
k_{OH}	4.96	3.69	+0.34	+0.66
20 June 2012				
Parameter:	$\bar{M}$	$\bar{O}$	NMBF	r
temperature	26.65	27.27	-0.02	+0.90
rel.humidity	48.51	44.56	+0.09	+0.69
H_2O content	0.11	0.11	+0.05	+0.73
O_3	66.56	77.58	-0.17	+0.74
NOx	1.48	4.47	-2.02	+0.72
sulfate	3.93	3.25	+0.21	+0.36
ammonium	1.60	1.74	-0.09	+0.49
nitrate	1.24	1.75	-0.41	+0.42
organics	6.66	9.74	-0.46	+0.26

TABLE 4.2: Statistic parameters calculated for two measurement days in Po-Valley: 12 July 2012 (top), 20 June 2012 (bottom).

4.3 Regionality of ammonium-nitrate

In the previous sections, the predicted concentration of the aerosol components along the Zeppelin track, as calculated from the regional model, was compared against the observations on board, in terms of accuracy. The prediction accuracy was found to be different for all of the three inorganic aerosol components, as concluded by the calculated statistical indices. Overall, in Po-Valley, sulfate, ammonium, and nitrate mass concentrations were overpredicted with a NMBF of +0.84, +0.43, and +0.31 respectively. A systematic overprediction was apparent in sulfate as displayed in the bottom panel of Figure 4.11. A similar systematic overprediction was noted in ammonium although in a smaller degree as displayed in the bottom panel of Figure 4.12. The latter two results could point to an overall systematic gas precursor source overestimation, that is SO_2 for sulfate and NH_3 for ammonium. As far as nitrate is concerned, the error appears far less systematic, placing the points in the scatterplot (bottom panel of 4.13) more symmetrically distributed with respect to the 1:1 axis. A contribution to this symmetry in nitrate can be found in the fact that the predicted range of values agrees with the range of the observed values, meaning that the variability is well captured. This reveals that the processes in the model describing nitrate formation have the same dynamic range as the real processes. In terms of variability for sulfate and ammonium, the predicted values did not capture the range of the observed values. Instead, the later two were predicted more uniformly distributed than observed.

The above statements concern a time span that covers the whole campaign, including different areas. Sulfate and ammonium show a systematic bias in all flights within the different areas of Po-Valley, and being secondary aerosols, they are not emitted as particles by surface sources, but they are formed from their gas precursors. SO_2 enters the atmosphere as a product of the continual fossil fuel combustion in industry. In addition, sulfuric acid, the respective oxidation product, condenses under all atmospheric conditions into sulfate particles. Consequently, there is enough time for sulfate, while in particle-phase, to extend horizontally establishing a background concentration aquiring, thus, a regional character. A part of ammonium is connected with sulfate, but in this case, it could be also the spatially smooth and homogeneous sources of NH_3 that contribute to the ammonium concentration background. The overestimated predicted values of sulfate and ammonium reflect the need to revise the predicted constant sources of SO_2 and NH_3. On the contrary, over the Po-Valley, both observed and predicted nitrate mass concentration spans over high and very low values, yielding no background concentration. It is therefore likely that ammonium-nitrate has more of a local origin, i.e. it is formed near its observation in time and space, than ammonium-sulfate which seems to have more of a regional nature.

Rubach [2013] suggests the same argument from a horizontal transect on the 21/06/2012, in the Po-Valley area. The observed mass concentration along the Zeppelin track, of the aforementioned aerosol components, was found to have a linear relation with the residence time of the sampled air in Po-Valley. As noted in the adopted Figure 4.32, the latter allowed the calculation of the aerosol production rates along the sampled air mass tracks in Po-Valley, yielding 0.15 $(\mu g/m^3)/h$ on a background of 4 $(\mu g/m^3)$ for sulfate, and 0.88 $(\mu g/m^3)/h$ on a background of -0.37 μ/m^3 for nitrate. This means on one hand that the observed nitrate along the transect was locally formed along the air mass streamlines in the Po-Valley, and with a larger production rate than sulfate.

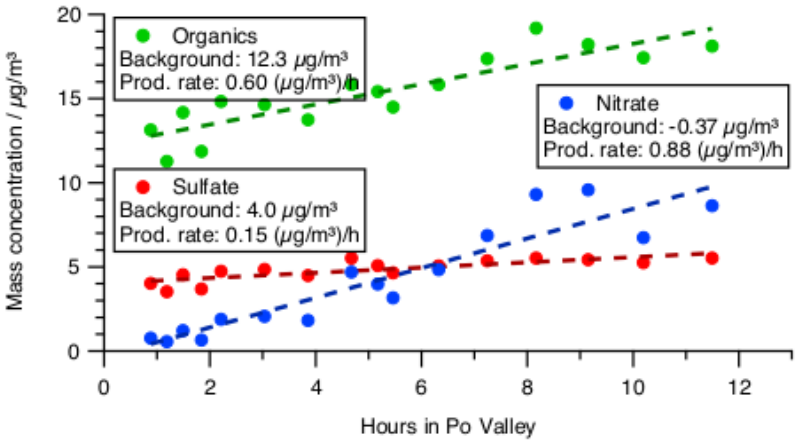

FIGURE 4.32: Display of observed aerosol mass concentrations of sulfate (red), nitrate (blue), and organics (green), versus the time the sampled air (coming from the Apennines) had spend in the Po-Valley according to 24h backward trajectories for the 21/06/2012. Figure adopted from Rubach [2013].

Here, instead of the horizontal transect, the more localized vertical profiling flight of the previous day, the 20/06/2012 will be discussed. In terms of accuracy, sulfate, ammonium, and nitrate mass concentrations were predicted with a NMBF of +0.21, -0.09, -0.41 respectively, ammonium and nitrate being predicted with the highest and the lowest accuracy respectively. Considering the surface emitted gas precursors, the influence of the local sources on the aerosol mass concentration is expected to be more apparent in the lower than in the higher altitudes. In order to study this influence in more detail, the Zeppelin track of that day is separated in altitude bins. As illustrated in Figure 4.33, the track is separated in the following three bins: low altitudes from 0 to 200 m, middle altitudes from 200 to 600 m, and high altitudes from 600 to 800 m. The predicted values are then evaluated against the observed values, by calculating the statistical indices separately for every altitude bin, as noted in Table 4.4. The corresponding scatterplots are displayed in Figure 4.34.

In the aforementioned Figure 4.34, the predicted mass concentration for sulfate, ammonium, and nitrate, is plotted against the corresponding observed values for the full

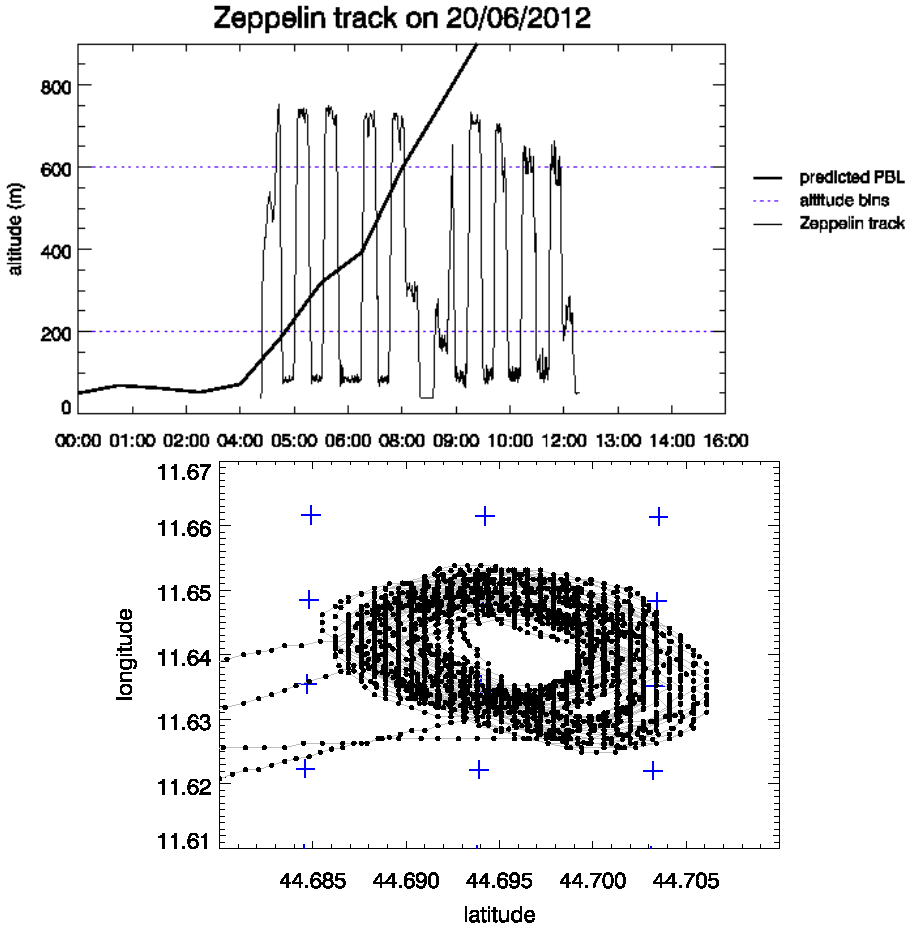

FIGURE 4.33: Zeppelin track on 20/06 (near SPC at Po-Valley): (top) Zeppelin altitude versus time, bined by altitude (bins:0-200 m, 200-600 m, 600-800 m). The solid thick line represents the predicted PBL height, (bottom) Zeppelin track on latitude/longitude projection with grid cell centers as blue crosses.

dataset and separately for the three altitude bins. By inspecting the plots the following is noted. Sulfate is observed with a clear background mass concentration that is independent of altitude. The predictions also manifest a background. Although a very good agreement between observed and predicted values in the higher altitudes, a tendency for overestimation is noted as moving to the middle and lower altitudes. The observed variability is constant with altitude, but the predicted variability grows larger when moving to the middle and lower altitudes. Nitrate on the other hand is observed with no background mass concentration in all altitudes, that is, very low values are observed. The predictions do not manifest a background either. The predictions overestimate the observations in the higher altitudes and underestimate them in the middle and lower altitudes. The predicted variability is only slighly larger from the observed variability in the higher altitudes, significantly smaller in the middle altitudes, and only slightly smaller in the lower altitudes. Ammonium shows some similar tendencies with sulfate and others with nitrate, while manifesting a background in both observations and predictions. The predictions of ammonium have the best agreement with the observations

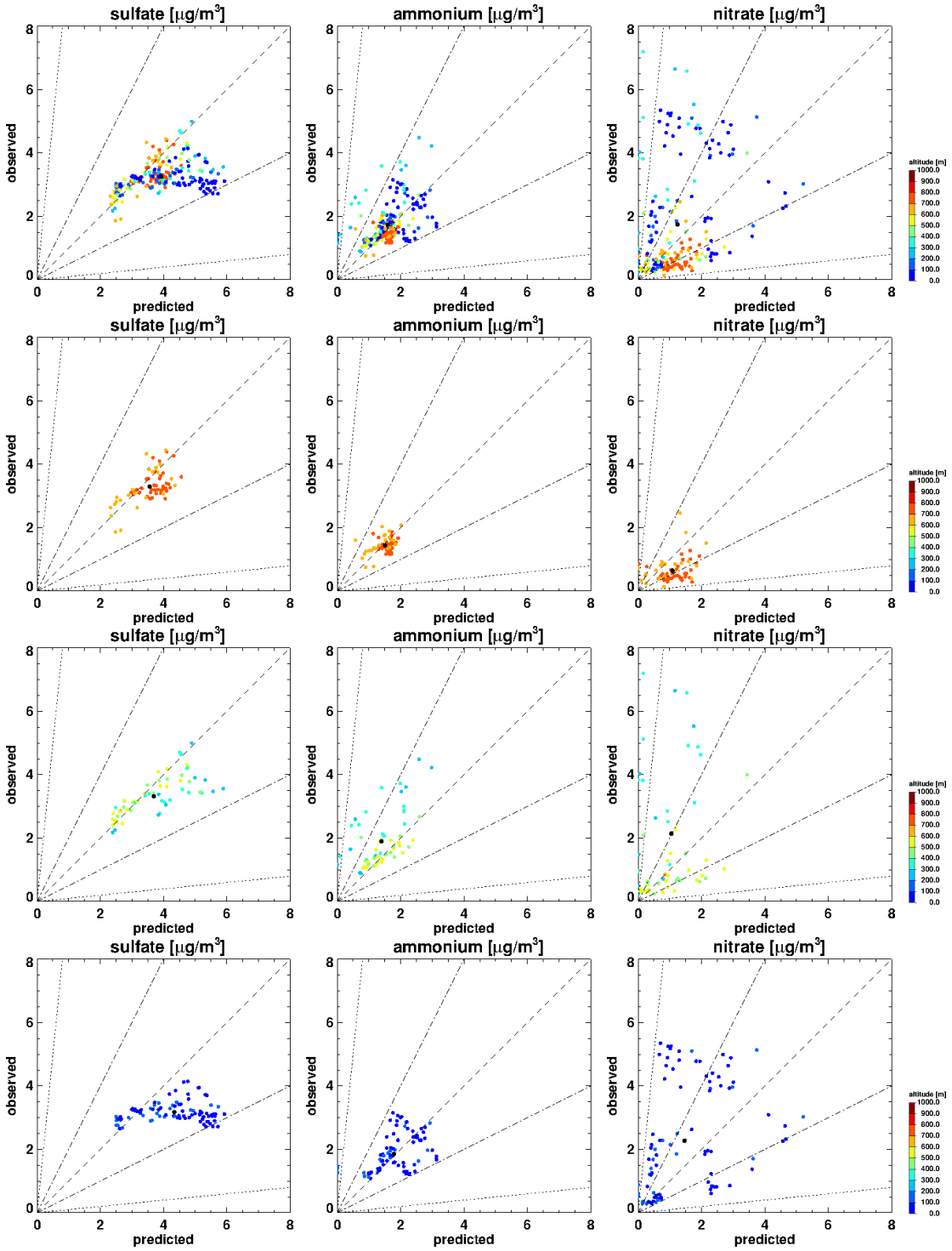

FIGURE 4.34: Scatterplots of sulfate, ammonium, nitrate, on 20/06, bined by flight altitude as illustrated in Figure 4.33. The top row panels dispay the full dataset for that day. The following three row panels display the subsets for the same day for the altitude spans 0-200 m, 200-600 m, and 600-800 m, from bottom to top, respectively. Statistics are noted in Table 4.4.

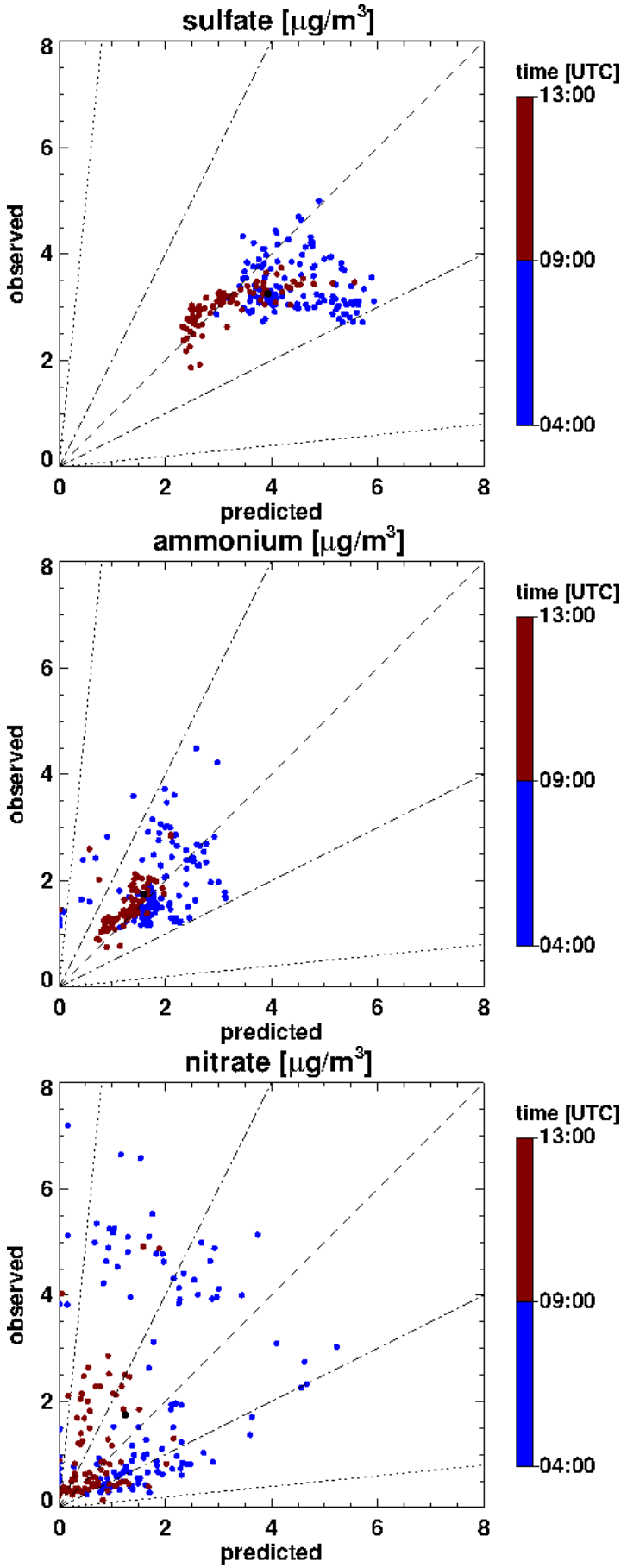

FIGURE 4.35: Scatterplots of sulfate, ammonium, nitrate, on 20/06, color-coded with time, separating the flight by mixing conditions: from 04:00 to 09:00 the PBL is under development, from 09:00 to 13:00 the PBL is fully developed. Statistics are noted in Table 4.4.

in the higher altitudes, like in the case of sulfate. Its variability, however, especially in the middle and lower altitudes, resembles more to the variability of nitrate. The predictions overestimate slightly the observations in the higher altitudes and underestimate them in the middle and slightly in lower altitudes like in the case of nitrate. The predicted variability is only slighly larger from the observed variability in the higher altitudes, significantly smaller in the middle altitudes and only slightly smaller in the lower altitudes, like in the case of nitrate.

The predicted NH_3 emissions in the area of SPC, are relatively homogeneously distributed, as seen in Figure 3.2. Assuming that the sufficient amount of NH_3 is available, we expect that the fraction of NH_3 which bounds as ammonium to sulfate on regional scale shows the same variability as sulfate itself. On the other hand the fraction of NH_3 which accopanies ammonium nitrate which is locally formed, shows the same variability as nitrate itself. In turn, this "mixed" variability confirms that there seems to be sufficient NH_3, and that it is indeed homogeneously distributed, since ammonium features signatures of sulfate as well as nitrate.

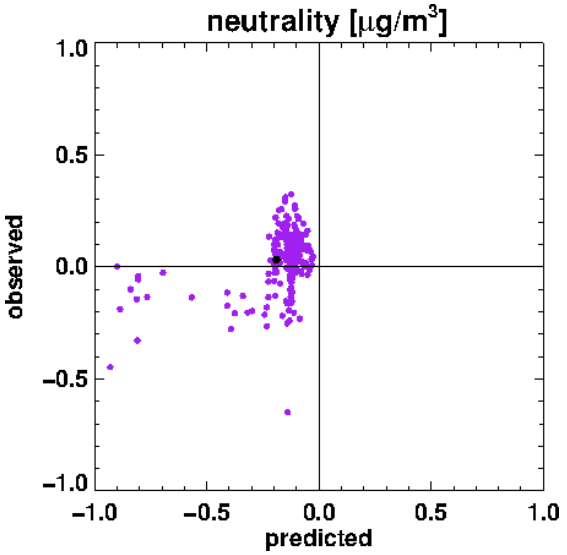

FIGURE 4.36: Predicted versus observed neutrality, as mass concentration of ammonium in excess to anionic components sulfate and nitrate, on 20/06.

Our considerations are confirmed by the inspection of the molar ratios of the three aerosol components. For a neutral aerosol, the concentration of ammonium, which is a cation, should be the ammount required to neutralize the given anions, sulfate, nitrate, and cloride, forming ammonium-sulfate, ammonium-nitrate, and ammonium-cloride. Higher concentrations would indicate an excess ammonium, while lower concentrations would indicate an acidic aerosol, when, in the latter case, the charge is neutralized by the hydrogen cation. The molar mass ratios of ammonium with sulfate and nitrate yield 18/96 and 18/62 respectively. The following equation calculates the excess ammonium

as:

$$excess_{[NH_4^+]} = [NH_4^+] - \frac{18}{62} * [NO_3^-] - 2 * \frac{18}{96} * [SO_4^{2-}] \quad (4.4)$$

where [] stands for mass concentration of the respective aerosol component. The concentration of cloride was found to be negligible as compared to the other aerosol components. For the 20/06 the observed excess ammonium (neutrality) is plotted against the predicted in Figure 4.36. Observations show clearly values around zero, with a mean value of +0.03 $\mu g/m^3$, thus a neutral aerosol. Predictions are also very close to zero, with a mean value of -0.19 $\mu g/m^3$, noting only a slight tendency towards acidic aerosol. The neutrality within the accuracy of the observations indicates the presence of sufficient ammonia in the formation process. This supports the assumptions about regional and local character of the aerosol components.

Commenting on the evaluation by altitude above, for the location of SPC, the observations reveal a regional nature for sulfate since they are homogeneous by altitude and the deviation from the predictions is noticed in the lower altitudes, where the local surface influence is expected to be larger. On the other hand, the local surface influence seems to be larger for nitrate, since it is observed as inhomogeneous by altitude and with larger deviation from predictions in the lower altitudes. This local surface influence, can be partly attributed to the emissions of the gas-phase precursors.

Before analyzing the effect of the gas-phase precursors, it should be noted that the PBL dynamics all along the flight was not the same. The latter was addressed in section 4.2.3, where the prediction performance of temperature and relative humidity was found to have an effect on the prediction performance of nitrate. The Zeppelin flight of the 20/06 is well divided into two parts, each of those corresponding to different vertical mixing conditions. As it was noted in the aforementioned section, the temperature and relative humidity conditions were better captured by the predictions in a fully mixed PBL than in a PBL under development. As illustrated in the top panel of the Figure 4.33, in the time interval 04:00-09:00 UTC the Zeppelin is crossing a PBL that is under development multiple times, while, in the time interval 09:00-12:00 UTC the Zeppelin measures only in a fully developed mixed layer. In Figure 4.35, the observed concentrations are plotted against the predicted concentrations, color coded with time, separating the two parts of the flight. The calculated metrics separately for the two flight parts are noted in Table 4.4. On first sight, the distribution of data points reveals larger concentrations in the first part than in the second part of the flight, in both observed and predicted values, and in all three aerosol components. In the second part of the flight, the values are smaller and more homogeneously distributed as it is expected in a fully developed mixed layer. But there are differences in the variability as well. In a fully developed PBL the predicted concentrations of sulfate show a larger dynamical range than the

observed concentrations yielding a NMBF of +0.06. In a PBL under development, although the same dynamical range is noted the predicted concentrations of sulfate are systematically shifted to larger values yielding a larger overestimation with a NMBF of +0.31. Nitrate and ammonium manifest similar behavior with each other. Both, show a larger variability in a PBL under development than in a fully developed PBL. However, in a fully developed PBL, both shift to be more underpredicted yielding an NMBF of -0.24 and -0.65, and ammonium is more similar to sulfate than nitrate.

Commenting on the evaluation by mixing conditions above, the following can be noted. The precursor H_2SO_4 condenses in the particle phase under all atmospheric conditions forming sulfate. This means that the prediction quality of the partitioning, that is the prediction quality of temperature and relative humidity, does not have a noticeable effect on the prediction quality of the sulfate concentration. This means that the overprediction noted in the first part of the flight, can be adressed both to horizontal transport, that is, more sulfate is predicted to be horizontally transported, and to an overestimation of the SO_2 emissions, that is the emission rates of SO_2 from the surface sources are overpredicted. At the first part of the flight, in a PBL under development, surface emitted constituents are constrained in low altitudes. In that case, overpredicted SO_2 surface sources could explain the overpredicted sulfate concentration in low altitudes, noted also in the evaluation by altitude above. After all, by comparing the top panel of 4.35 with the bottom-left panel of 4.34 one can note that the points showing large overprediction in low altitudes belong to the first part of the flight. As for the prediction quality of both ammonium and nitrate is concerned, it is affected by the prediction quality of the partitioning. The effect of the partitioning however, can be addressed only in the first part of the flight, as the bottom panels of Figure 4.30 indicate. In all cases, the discrepancies in both ammonium and nitrate are also attributed to both horizontal transport and the surface emissions. In the later case, for the 20/06, since the predicted NH_3 sources result to the most accurate prediction for ammonium, among all aerosol components (Table 4.2), supporting a neutral aerosol as shown above, the discrepancies could be addressed to the gas-phase precursor of nitrate, HNO_3, along the flight track.

Unfortunately, there were no observations of the gas precursors H_2SO_4, NH_3, and HNO_3 to be compared with the respective predicted concentrations. Similarly there were no observations of SO_2. However, the predicted aerosol concentrations, can be examined, firstly with respect to the predicted gas-phase precursor concentrations and secondly with respect to the predicted production rates of these precursors, along the flight track.

The time series of the predicted gas precursor concentrations along the flight track, are displayed in the left column of Figure 4.37. The predicted emissions of SO_2, NH_3,

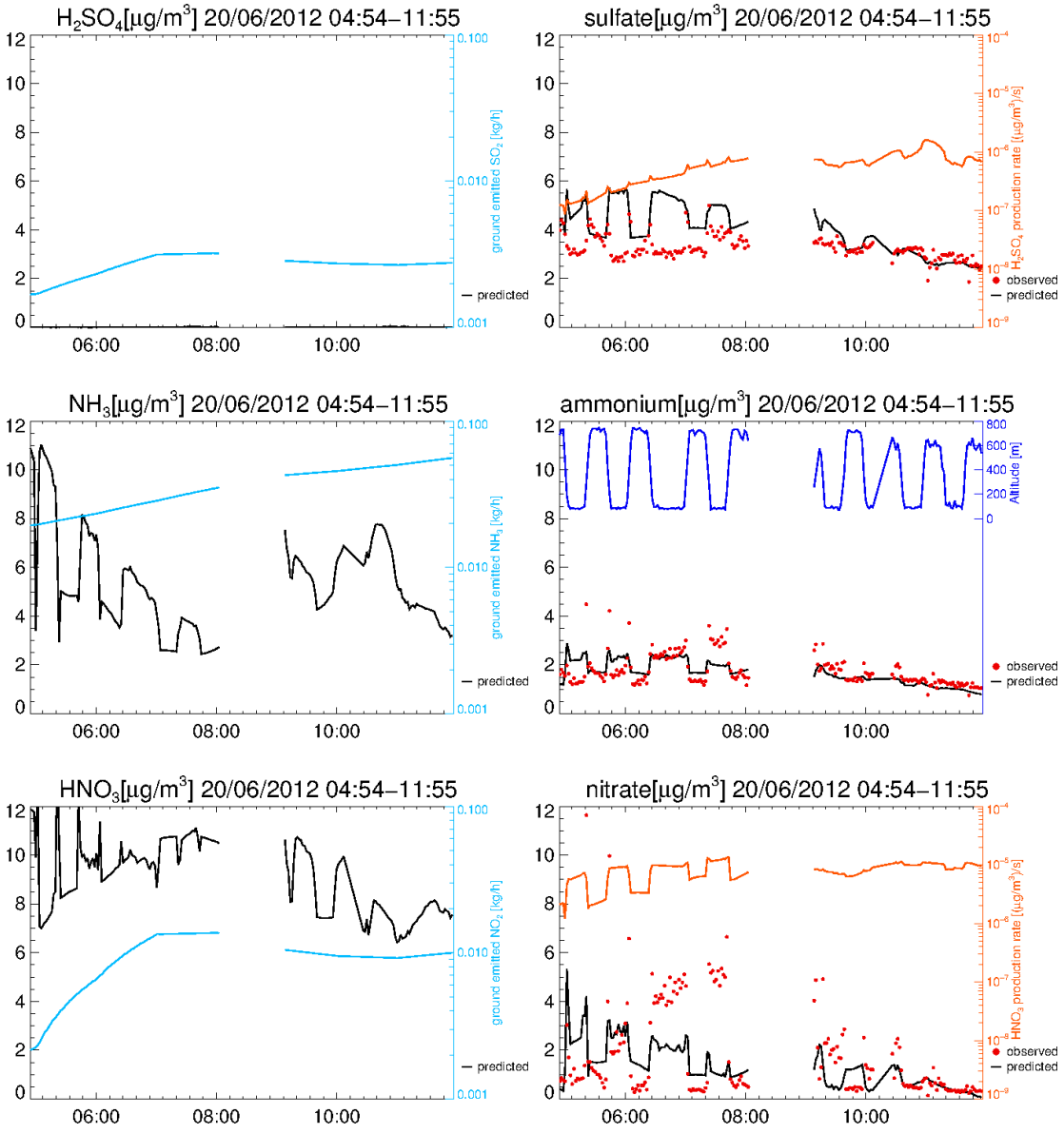

FIGURE 4.37: Left column: Time-series of predicted gas-phase H_2SO_4, NH_3, HNO_3 concentrations along the flight track (left axis), with overplotted the SO_2, NH_3, NO_2 surface emissions directly below (right axis). Right column: Predicted and observed concentrations of the corresponding aerosol components sulfate, ammonium, nitrate (left axis), with overplotted the predicted production rates of H_2SO_4, HNO_3, and the altitude, along the flight track (right axis). The production rates correspond to the reactions $OH + SO_2 \longrightarrow HSO_3$ (rate limiting for the production of H_2SO_4) and $OH + NO_2 \longrightarrow HNO_3$.

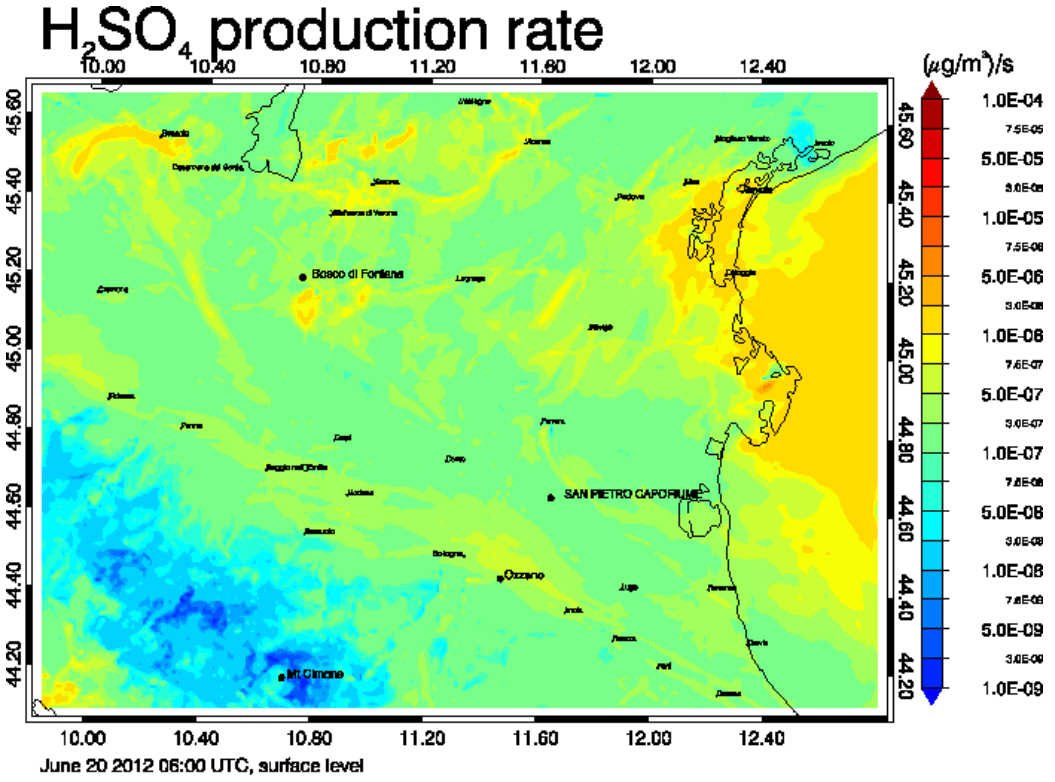

(A)

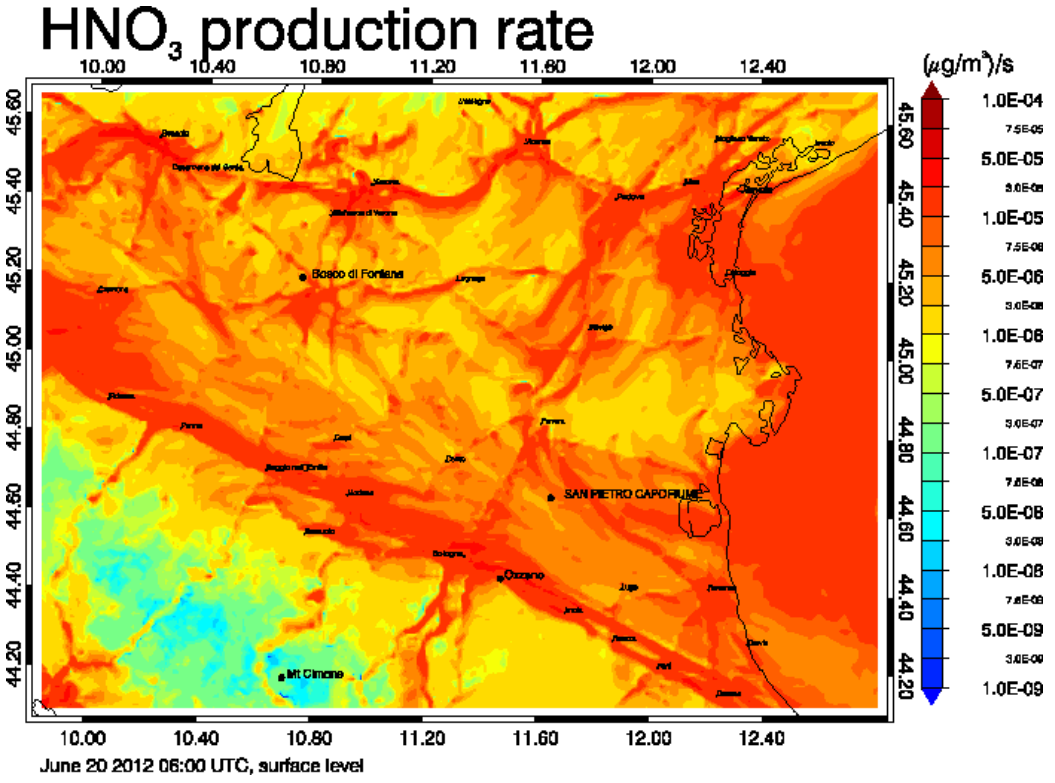

(B)

FIGURE 4.38: Predicted production rates of H_2SO_4 and HNO_3 corresponding to the oxidation reactions of SO_2 and NO_2, at the ground level, at 06:00 UTC, over the Po-Valley.

NO_2, directly below the Zeppelin during the flight, are overplotted. The right column of Figure 4.37 displays the respective to the gas precursors, along the flight track, aerosol components that is sulfate, ammonium, and nitrate. The predicted production rates of H_2SO_4 and HNO_3 are overplotted. As the bottom panel of Figure 4.33 illustrates, the Zeppelin is spiraling with respect to a constant location, projecting on 9 cells of the horizontal model grid. Here, the horizontal movement of the Zeppeling is ignored and a mean value of these 9 cells is assigned as the predicted value.

A glance at the left column of Figure 4.37 reveals the following. The predicted concentrations of NH_3 and HNO_3 are variable both with altitude and time, between the values 2-11 $\mu g/m^3$ and 6-14 $\mu g/m^3$ respectively. The predicted concentration of H_2SO_4, however, varies on a practically negligible scale, between the values 0.005-0.3 $\mu g/m^3$, reflecting the fact that H_2SO_4 is found in the particle phase, under all conditions, unlike NH_3 and HNO_3. The emissions directly below indicate the following. The predicted rate of emitted NH_3 increases linearly during the complete time frame of the flight. In contrast, the predicted rates of emitted SO2 and NO2, appear more variable. An increase in both rates is noted until about 08:30 UTC with a more rapid increase for NO2. During the second part of the flight after 09:00 UTC, both emission rates tend to be constant. The relation of the gas emission rate with the concentration of the relevant gas precursor along the flight track is examined next only in terms of predicted values. The calculated correlation coefficients for the pairs emitted SO_2 with predicted H_2SO_4, emitted NH_3 with predicted NH_3, and emitted NO_2 with predicted HNO_3, yield +0.54, -0.19, and +0.21 respectively. The same correlation coefficients calculated for the initial data-set without the 9-cell averaging yielded similar although lower values (+0.15,-0.12,+0.16). After all, no simple connection can be made regarding the relation of emission rates and concentrations for such a short time frame. It could also be the case that the area of the predicted emissions cannot be related to the altitudes of the measurements because of the horizontal wind. That is, the emitted gas-precursors of a nearby area, other than the 9 square km directly below considered here, could be related with the measurements of the Zeppelin. Since, at the studied time frame of the 20/06, the emission rates are increasing with time, it is the predicted dynamics that result to the given concentrations in the studied altitude. After all, if there would be no horizontal wind at all, only then a direct connection of the surface sources below the Zeppelin with the concentrations along the flight track would be possible. For a direct comparison of the gas-phase precursors along the flight track with the respective aerosol concentrations plotted in the right column of Figure 4.37, aerosol mass concentration units are used. As for the comparison of the amounts of gas-phase NH_3 and HNO_3 against the amounts of particle-phase ammonium and nitrate, in contrast to the case

of H_2SO_4, here the particle-phase is comparable with the gas-phase, but the gas-phase seems to dominate.

Our hypothesis is examined with respect to the predicted gas-phase production rates. A regional aerosol constituent is expected to have a weak correlation with the local production rate of the respective gas-phase precursor. One the other hand, the concentration of a locally formed aerosol constituent is expected to be positively correlated with the production rate of its precursor. The predicted production rates of the two gas-phase precursors H_2SO_4 and HNO_3, that are not directly emitted like NH_3, but they are formed in the atmosphere from the oxidation of SO_2 and NO_2 by OH, are calculated by:

$$r_{H_2SO_4} = k_1[OH][SO_2] \tag{4.5}$$

$$r_{HNO_3} = k_2[OH][NO_2] \tag{4.6}$$

in units of $(\mu g/m^3)/s$, where $k_1 = k_{[OH+SO2->HSO3]}$ and $k_2 = k_{[OH+NO2->HNO3]}$ the reaction coefficients accounting for all the factors that influence the reaction rate except concentration, which is explicitly taken into account. Since the flight was during daytime, the production of HNO_3 from the hydrolysis of N_2O_5 is not illustrated here. The two production rates plotted in the right column of Figure 4.37 are examined. The predicted production rate of HNO_3 notes higher values ($\sim 10^{-5}$ $\mu g/m^3 s$) as compared to the predicted production rate of H_2SO_4 ($\sim 10^{-6}$ $\mu g/m^3 s$). This is expected since under equal concentrations of reactants the oxidation of NO_2 is about 10 times faster than the oxidation of SO_2. The predicted values of the two production rates are in addition inspected in the horizontal plane of the Po-Valley area, as displayed in figure 4.38. The r_{HNO_3} rate notes sharp gradients that reveal clearly the road network over which, together with the area covering the east sea, the maximum rates are noted. Although several structures that can be associated with the road network are also noticeable in the $r_{H_2SO_4}$ rate, the gradients are noted to be smoother. Maximum rates are also noted over the east sea. The aforementioned r_{HNO_3}:$r_{H_2SO_4}$ ratio of 10 is also noted here. The fine structures in r_{HNO_3} alone, already prepare for nitrate formation closely related to the road network.

In more detail, as far as the flight in SPC is concerned, the correlation between gas-precursor production rate and the corresponding aerosol concentration is investigated. The correlation coefficients between the H_2SO_4 production rate and the sulfate concentration and between the HNO_3 production rate and the nitrate concentration are noted in the Table 4.3, where the correlation coefficients are calculated first for the entire flight and then separately for the two parts of the flight (04:00-09:00,09:00-12:00 UTC). The correlation coefficients gave a significant negative value (-0.63) for the pair

sulfate-$r_{H_2SO_4}$, and a small negative value (-0.13) for the pair nitrate-r_{HNO_3}. The same coefficients have been calculated considering separately the two parts of the flight. Since, considering the second part of the flight, yields similar correlations (-0.43 and -0.24), the above result cannot be entirely attributted to the representation of the rising PBL dynamics. The daytime increasing OH concentration, as a common factor for both rates $r_{H_2SO_4}$ and r_{HNO_3}, is responsible for the overall increase of the rates, during the flight time interval. However, the variability of the SO_2 and NO_2 concentrations are to be addressed for the short term variability of the rates. Considering the first part of the flight, the small positive correlation calculated for the pair nitrate-r_{HNO_3} (+0.21), could be explained as follows. The early morning PBL confines the NO_2 emissions in low altitudes, creating a steep gradient in the NO_2 concentration near the PBL. This has an effect at the calculated r_{HNO_3}, which varies together with the nitrate concentration. In the pair sulfate-$r_{H_2SO_4}$ this effect is not noted, because of the absence of such a gradient for SO_2.

			04:00-12:00	04:00-09:00	09:00-12:00
sulfate	-	$r_{H_2SO_4}$	-0.63	-0.05	-0.43
nitrate	-	r_{HNO_3}	-0.13	+0.21	-0.24

TABLE 4.3: Correlation coefficients for the pairs sulfate-$r_{H_2SO_4}$ and nitrate-r_{HNO_3} calculated for the flight of 20/06 and separately for the two parts of the flight.

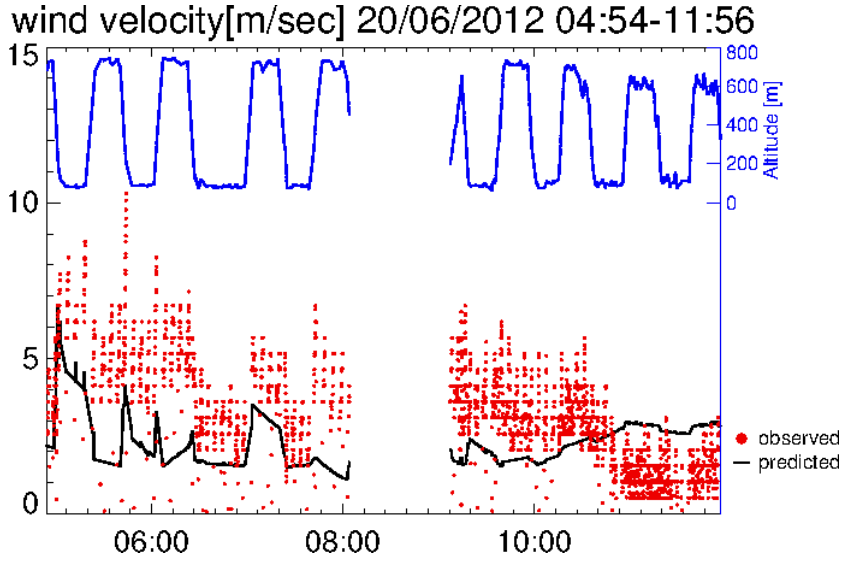

FIGURE 4.39: Predicted and observed wind velocity, along the flight track on the 20/06.

Commenting on the above, the correlations between predicted aerosol concentrations and predicted precursor formation rates, do not cancel the premise either of a regional sulfate, or of a locally formed nitrate. The fact that this precursor concentration variability does

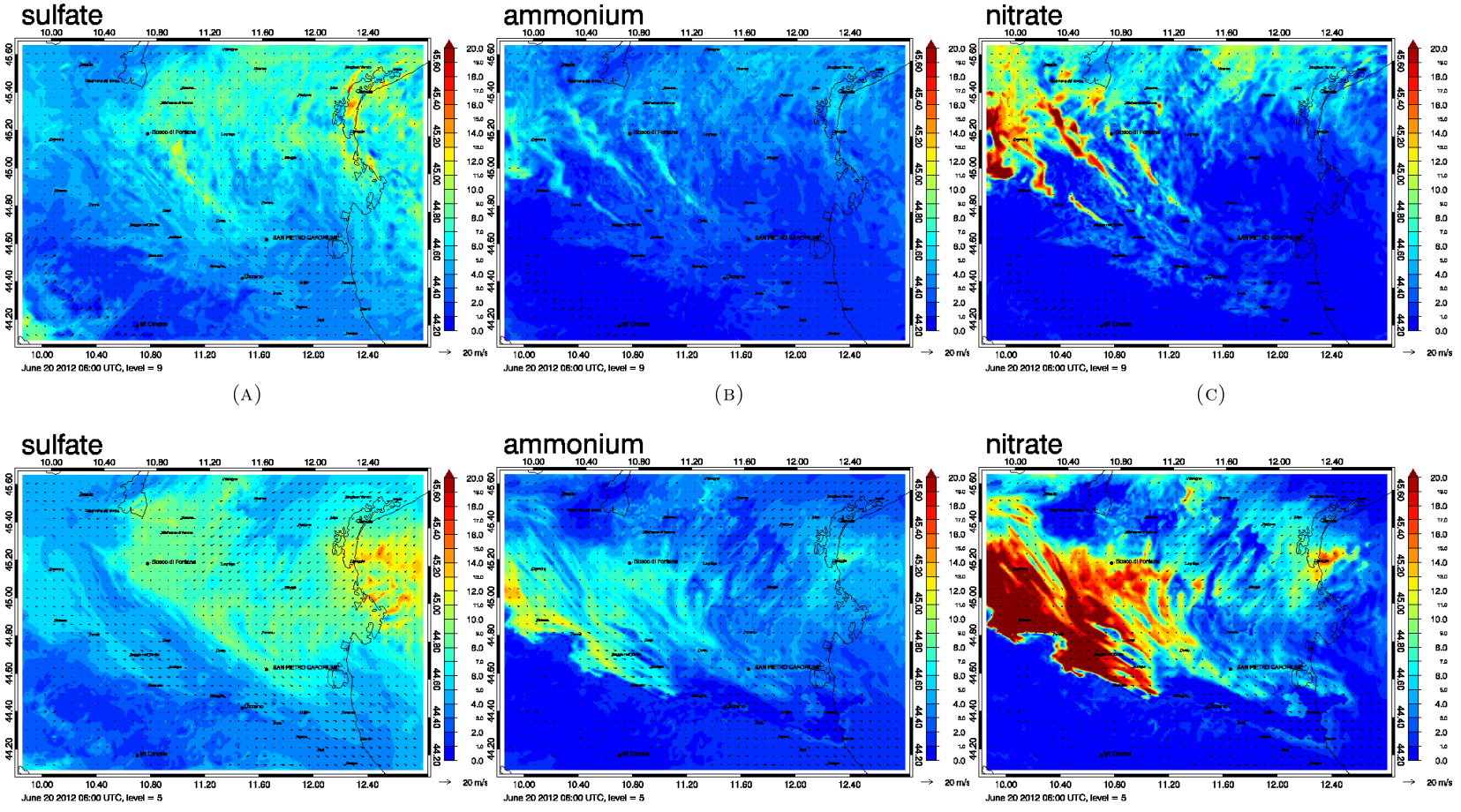

FIGURE 4.40: Distribution of predicted sulfate (left), ammonium (middle), and nitrate (right) concentration at 06:00 UTC 06/2012, at the 5th (bottom) and 9th (top) model layers with altitude extensions (at the location of SPC) 161-243m and 578-749m respectively.

not result in aerosol concentrations and precursor formation rates that vary together, suggests the importance of transport as the major cause of this deviation. Only if there would be no horizontal transport, would the precursor production rates be highly correlated with the aerosol concentrations.

The effect of transport concerning a fixed location, is either to add, or to remove, amounts of both gas phase and particle phase. The predicted horizontal transport of aerosols can be inspected by the horizontal distribution of the respective aerosol components. Figure 4.40 displays the distribution of predicted sulfate, ammonium, and nitrate concentration at 06:00 UTC on 06/2012, at the 5th and 9th model layers which correspond, for the location of SPC, to the altitude extends of 161-243 m and 578-749 m respectively, included in the Zeppelin profiles. In the computational domain displayed, although sulfate and nitrate components follow the same wind field, differences are noted in the two distributions. Over the entire domain sulfate manifests a smooth background and maximum concentrations above the area of the east sea and coast-line. Nitrate, on the other hand, manifests practically no background and maximum concentrations above the north-west Po-Valley area and along the traffic line connecting Ozzano, Bologna, and the other cities in the Po-Valley boundary with the Apennines. The signatures of sulfate and nitrate on ammonium are apparent also in the horizontal extent. According to the model results, the sulfate and nitrate, have not topologically the same sources. In addition, comparing the two model layers, we note the same structures, but on a different horizontal extend. This points to different evolution in time, which is partly because the wind speed is different at the two altitude extends. The predicted wind velocity, along the flight track, is plotted against the observed wind velocity in Figure 4.39. The observed mean value (3.18 m/s) is only slightly underestimated by the predicted mean value (2.32 m/s). Even though the wind speed is relatively low, by ignoring the wind direction, an approximate estimation yields a distance of ∼42 km that can be covered by a transported constituent, in a time interval of 5 h. Considering the fact that aerosols have a lifetime of several days before being deposited, it is then predicted that aerosol material from both the two aforementioned relatively high concentration areas can be transported in the site of SPC, on a daily basis.

The above are combined as follows. The previously calculated production rates $r_{H_2SO_4}$ and r_{HNO_3}, can be translated into amounts of H_2SO_4 and HNO_3 formed 'on site' from the relevant oxidation processes. The integration $r_{H_2SO_4} * dt$ and $r_{HNO_3} * dt$, is performed considering a time step of dt equal to 107 sec, which is the mean time interval between two observations. The estimated amounts of H_2SO_4 and HNO_3 formed are overlaid in the top panel of Figure 4.41. The mean values of formed H_2SO_4 and HNO_3, $6.2{*}10^{-5}$ $\mu g/m^3$ and $8.4{*}10^{-4}$ $\mu g/m^3$ make a negligible fraction of the mean predicted gas phase concentrations, of the orders of 10^{-3} and 10^{-5} respectively. The change in precursor

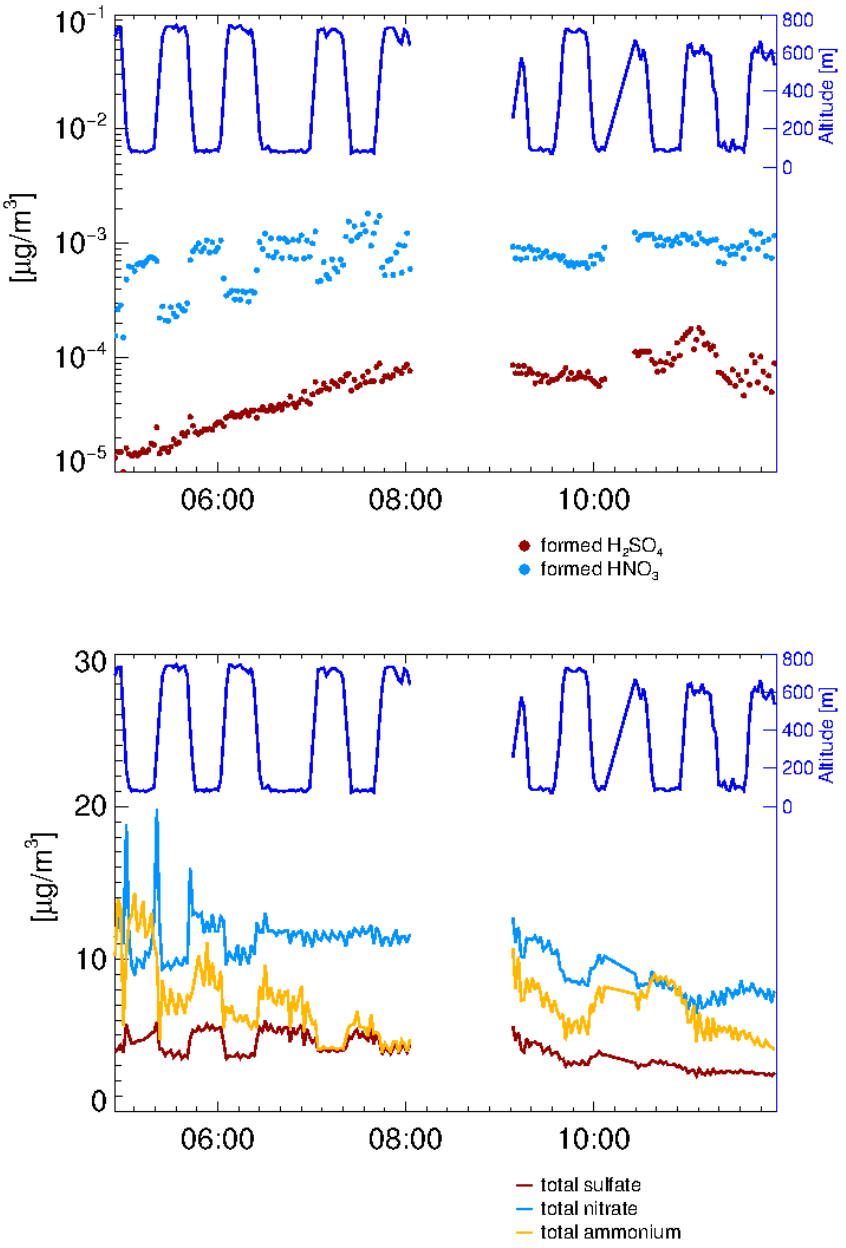

FIGURE 4.41: Top: Concentration of the 'on site' formed precursors H_2SO_4 and HNO_3, estimated from the predicted production rates $r_{H_2SO_4}$ and r_{HNO_3}. Bottom: Sum of gas precursor concentration and respective particle concentration (H_2SO_4(g)+sulfate, NH_3(g)+ammonium, HNO_3(g)+nitrate), along the flight track on the 20/06.

concentration due to oxidation shows an amount of formed HNO_3 about 10 times larger than the amount of formed H_2SO_4. We would then roughly estimate, that the total HNO_3, that is the sum of HNO_3 and nitrate, would be 10 times larger from the total H_2SO_4, that is the sum of H_2SO_4 and sulfate. However, as displayed in the bottom panel of Figure 4.41, that is not the case. Considering mean values in the flight time interval, the total HNO_3, is only about 2.5 times the total H_2SO_4, instead. This deviation from the roughly estimated ratio could be explained considering transport. On one hand, one

can consider transported total H_2SO_4 as the reason for this deviation, that is transported air masses could result in an overall increase of the total H_2SO_4 concentration, in this case mostly sulfate. This would mean that the total H_2SO_4 concentration deviates from the expected concentration increasingly as a result of transport. This could describe a constituent of a regional nature. On the other hand, one can consider transported total HNO_3 as the reason for this deviation, that is, transported air masses could result in an overall decrease of the total HNO_3 concentration, in this case partly gas-phase HNO_3 and nitrate. This would mean that the total HNO_3 concentration deviates from the expected concentration decreasingly as a result of transport. Of course, since the total HNO_3 is partitioned between gas and particle phase, unlike H_2SO_4, one cannot claim that transport removes nitrate from the site.

Summarizing all the above, in this section, the regional character of each of the three inorganic aerosol components that were observed at the Po-Valley area was discussed. This was done by using the observations and the corresponding model predictions of the vertical profiling flight on the 20/06/2012. The property that a constituent has of being regional, termed informally as regionality, is inspected by its background concentration and its concentration variability. A small concentration variability on a uniformly distributed bakground indicates a constituent with a regional nature, while a large concentration variability on a negligible background indicates a locally formed constituent. Based on the latter, already by a first inspection of the observed values, sulfate notes the largest background concentration while nitrate notes the largest variability. The respective predicted values supported the same argument with slight deviations. An evaluation by altitude showed predicted sulfate concentration of larger variability in lower altitudes and nitrate concentration of smaller variability in lower and middle altitudes, than the observations. An evaluation by mixing conditions separated the deviations related to the failure in representation of the dynamical conditions in the model. It was found that, for the second part of the flight, when the predictions of temperature and relative humidity capture the observations, the predicted variability of sulfate and the overestimation of nitrate could be caused by the failure in gas-phase sources representation. Although there were no observations of the gas-phase precursors, the predicted concentrations of H_2SO_4, NH_3, HNO_3, are compared with the respective aerosol components to find all of H_2SO_4 in the particle phase, while in contrast the gas phase NH_3 and HNO_3 dominating over the particle phase. The predicted horizontal distributions estimate that sulfate and nitrate, are two constituents with different topological sources, that, for the location of SPC, operate on a relatively homogeneous and abundant ammonium field. The production rates of H_2SO_4 and HNO_3 indicate a rough ratio of 10, of the total HNO_3 (sum of gas plus particle phase) over the total H_2SO_4. It is found, for the location of the SPC site, that the local production rates cannot be accounted for such a high sulfate

concentration over nitrate concentration. The transport is addressed for the deviation, that is, sulfate has a larger transported component in comparison to nitrate, the predictions , thus, support the consideration of a sulfate more of a regional nature than ammonium-nitrate.

STATISTICS BY ALTITUDE				
Parameter:	$\bar{M}$	$\bar{O}$	NMBF	r
600m < altitude < 800m				
sulfate	3.56	3.29	+0.08	+0.60
ammonium	1.51	1.44	+0.05	+0.38
nitrate	1.08	0.64	+0.68	+0.33
200m < altitude < 600m				
sulfate	3.69	3.32	+0.11	+0.75
ammonium	1.40	1.90	-0.36	+0.59
nitrate	1.04	2.15	-1.05	+0.53
050m < altitude < 200m				
sulfate	4.34	3.17	+0.37	+0.12
ammonium	1.79	1.86	-0.04	+0.51
nitrate	1.47	2.28	-0.55	+0.37

STATISTICS BY MIXING CONDITIONS				
Parameter:	$\bar{M}$	$\bar{O}$	NMBF	r
PBL under development				
sulfate	4.48	3.42	+0.31	-0.19
ammonium	1.91	1.95	-0.02	+0.31
nitrate	1.71	2.31	-0.35	+0.29
PBL fully developed				
sulfate	3.23	3.03	+0.06	+0.71
ammonium	1.20	1.49	-0.24	+0.57
nitrate	0.63	1.04	-0.65	+0.36

TABLE 4.4: Statistic parameters calculated for the 20 June 2012, by altitude, and by mixing conditions.

Chapter 5

Conclusions

This work enabled the comparison of spatially highly resolved gas and aerosol phase measurements in all layers of the PBL with a regional model of a 1km horizontal resolution. The latter was done by extending the EURAD-IM meteorological and chemical forecast system especially to support measurement missions. The tool was developed to account for daily changes of the computational domain that follow areas of interest during an airborne campaign.

The developed model based planning system was used for the online support of the three PEGASOS airborne campaigns. In the framework of these campaigns a Zeppelin NT equipped with measurement instruments of gas, aerosol and meteorological parameters performed flights in the areas of Cabauw in the Netherlands, Po-Valley in northern Italy, and Hyytiälä in Finland. The forecast system was operated in the time-periods 17/05/2012-29/05/2012, 16/06/2012-15/07/2012, 15/04/2013-29/06/2013 which covered the measurement flights in the three aforementioned areas respectively, as well as the transfer flights from/to Friedrichshafen in Germany. The obtained data has been presented online.

With the obtained datasets of the two 2012 campaigns, including the Zeppelin NT time-location series, the model mapping routine of airborne measurements on the computational domain was extended to account for the observed concentrations, photolysis frequencies, reactivities, and meteorological parameters of the instruments on board. This enabled a "one to one" observed versus predicted comparison.

The comparison of the relevant observed meteorological parameters with the respective predicted, for the time periods of the two 2012 campaigns showed a good performance of the model as concerns temperature but larger discrepancies in relative humidity and absolute water content.

Comparing predicted and observed gas-phase concentrations, gave both similarities and differences in model performance between the two 2012 campaigns. Ozone was more underestimated in Po-Valley, indicating underpredicted photochemical ozone production. Nitrogen oxides were underestimated in both areas, but more pronouncely in Cabauw, indicating a better model performance in an urban than in an industrial area. Both, hydroxyl and hydroperoxyl radicals were slighly overestimated in Cabauw and underestimated in Po-Valley. This, as far as hydroxyl radical is concerned, comes as a result of the fact that hydroxyl reactivity was accordingly underestimated in Cabauw and overestimated in Po-Valley.

The model performance, as far as the mean aerosol concentrations are concerned, was similar for the two 2012 campaigns. The mean sulfate concentration was overestimated and the mean organics concentration was underestimated. The predicted mean ammonium-nitrate concentrations were very close to the observed mean although with higher values noted in Cabauw than in Po-Valley. The latter has been adressed to the high source strength regime in Cabauw. In addition, refering to aerosol components separately, comparing to the homogeneously distributed sulfate, larger value variability was noted for nitrate than for ammonium in predictions, as in observations.

Specific aspects of two measurement days of vertical profiling at the San Pietro Capofiume site in Po-Valley, were analysed. First, the model performance at the 12/07/2012 was inspected, when an extended vertical profiling of gas-phase was performed. Discrepancies between predictions and observations were addressed to biases in the predicted far-transported and long-lived ozone, to local nitrogen oxides source underestimation, as well as to a non-optimized mixing parametrization. The possibility of 'non-classical' hydroxyl radical recycling was examined, which was not predicted during the 12/07/2012 flight, as it was not observed accordingly. Second, the model performance at the 20/06/2012 was inspected, for two sequential vertical profiling flights that included aerosol composition measurements. The model for that specific day performed similarly as it performed for the whole campaign in the Po-Valley area. The effect of temperature and relative humidity discrepancies on aerosol discrepancies was examined. Discrepancies in relative humidity prediction were found to have a larger effect on the quality of aerosol concentration prediction than temperature discrepancies.

Finally, the regional character of the three inorganic aerosol components was investigated for the area of SPC in the Po-Valley area on the 20/06. The observations reveal a sulfate with a background with a homogeneous altitude profile suggesting a constituent of a regional nature. On the other hand, nitrate is observed with higher variability at the ground which suggests a local influence. The signatures of both appear in a uniformly distributed ammonium with an abudancy to neutralize the two anions, in

both observed and predicted values. An evaluation of the predicted values by altitude supported the observed regionality considerations with deviations partly attributed to local sources. The local production rates of the gas precursors, for the location of the SPC site, indicated a large fraction of sulfate as transported. Local sources along the traffic network were found to have a larger effect on the formation of ammonium-nitrate, than the formation of sulfate.

As far as mitigation strategies are concerned, considering the above, the limitation of ammonium-sulfate concentrations would require a reducing of sources in a much larger area, than what the limitation of ammonium-nitrate would.

A future outlook could include the use of a 'back-plume' approach to the measurement days of interest, as described and applied cautiously on the 20/06/2012 and 21/06/2012 measurements in Kazanas et al. [2014]. The latter could complement a detailed study on the origin of the measured ammonium-nitrate along the Zeppelin NT track. The performance of regional models, as the chemistry transport component of the EURAD-IM, depend strongly on the quality of surface sources for the area of interest. In addition, for simulations of long time periods as it was done here, as well as for satisfying back-plume calculations, the mixing conditions should be extensively validated. Although the horizontal model resolution of 1 km was high relatively to what had been used so far, a more satisfying model performance and a comparison with observations of a high time resolution as those of the PEGASOS project, would require also a better vertical resolution than the one used here. Finally, meteorological parameters that control the mixing conditions, like soil humidity and heat capacity should be tailored and validated for the area of interest.

Appendix A

Comparison time-series

For illustration purposes, in this appendix, the comparison time-series of predicted against observed values are displayed, over the 2012 PEGASOS campaigns. The displayed variables include: temperature, relative humidity, ozone, nitrogen oxides, hydroxyl, hydroperoxyl, hydroxyl reactivity, sulfate, ammonium, and nitrate. Observed values are plotted in red and predicted values are plotted in black. A common time range for all days has been selected.

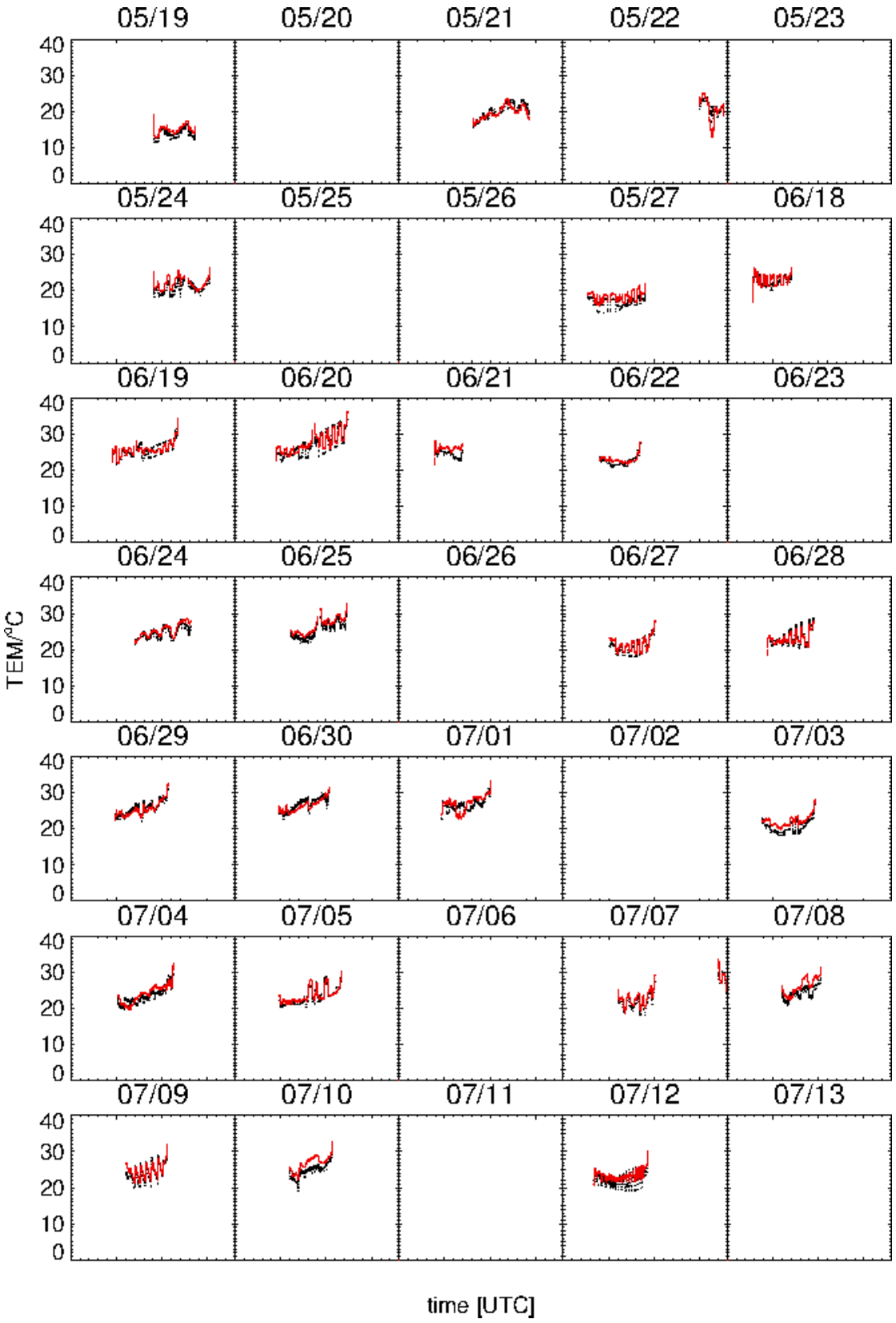

FIGURE A.1: Comparison timeseries - observed(red), predicted(black): temperature.

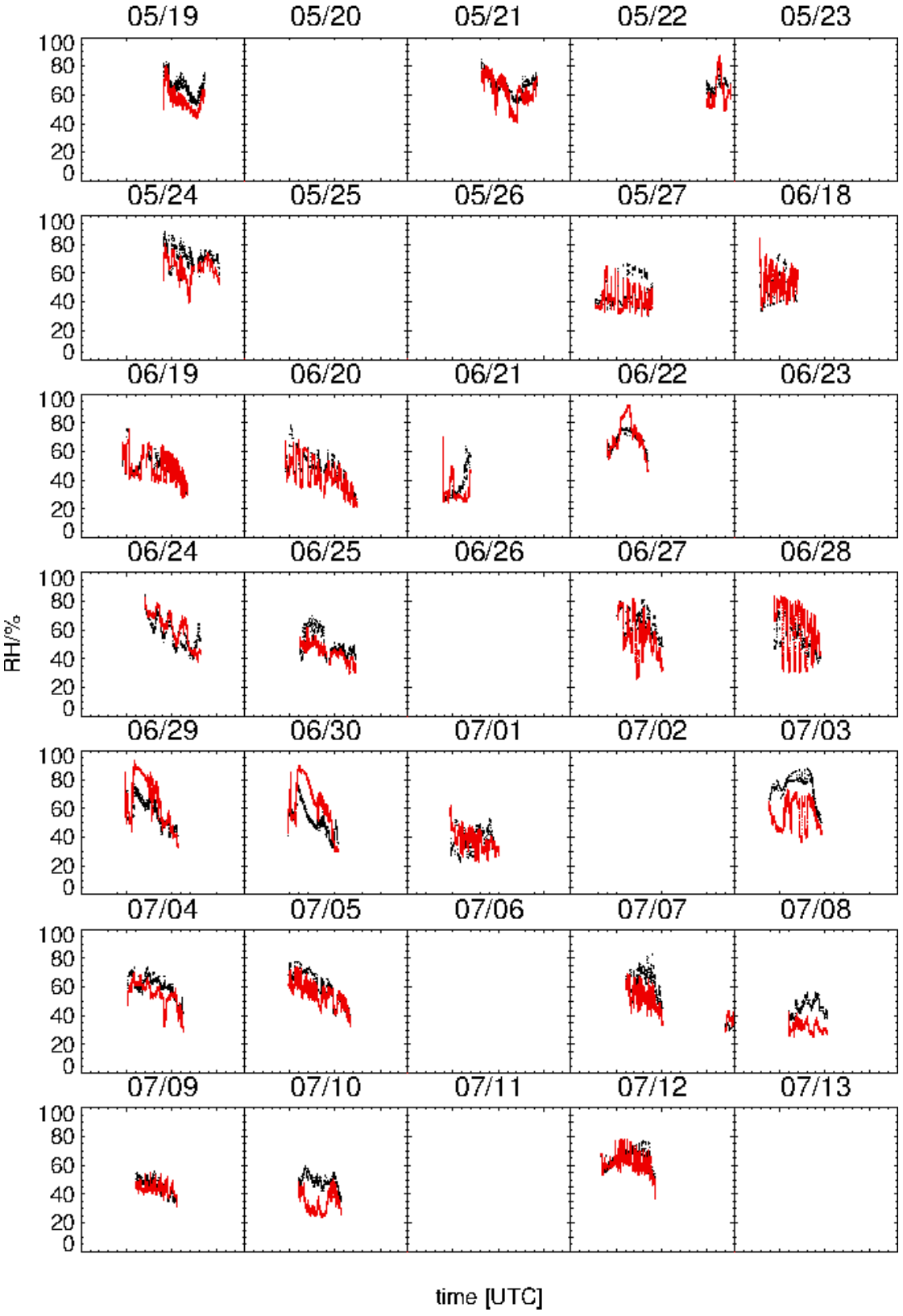

FIGURE A.2: Comparison timeseries - observed(red), predicted(black): rel.humidity.

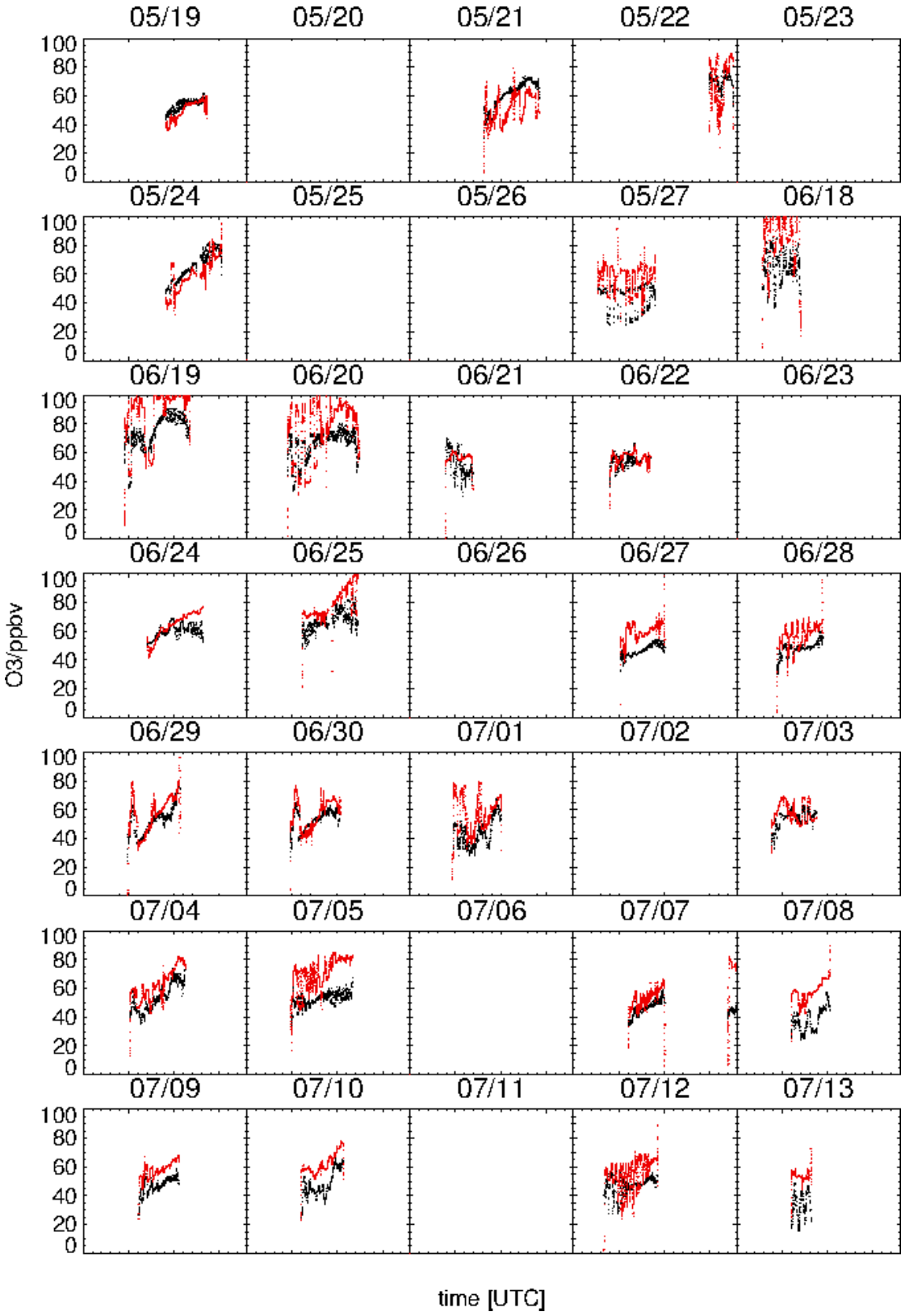

FIGURE A.3: Comparison timeseries - observed(red), predicted(black): O_3.

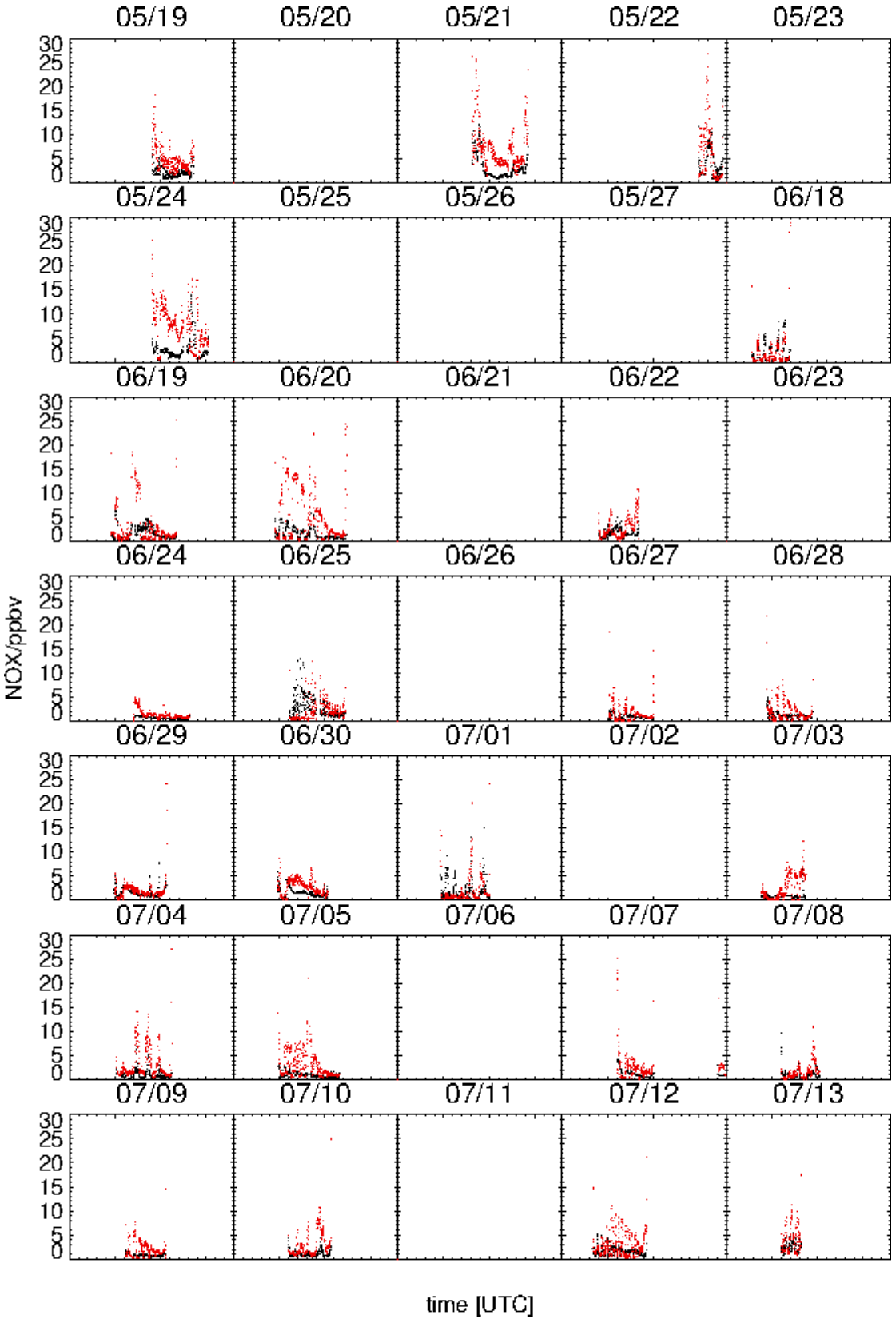

FIGURE A.4: Comparison timeseries - observed(red), predicted(black): NO_x.

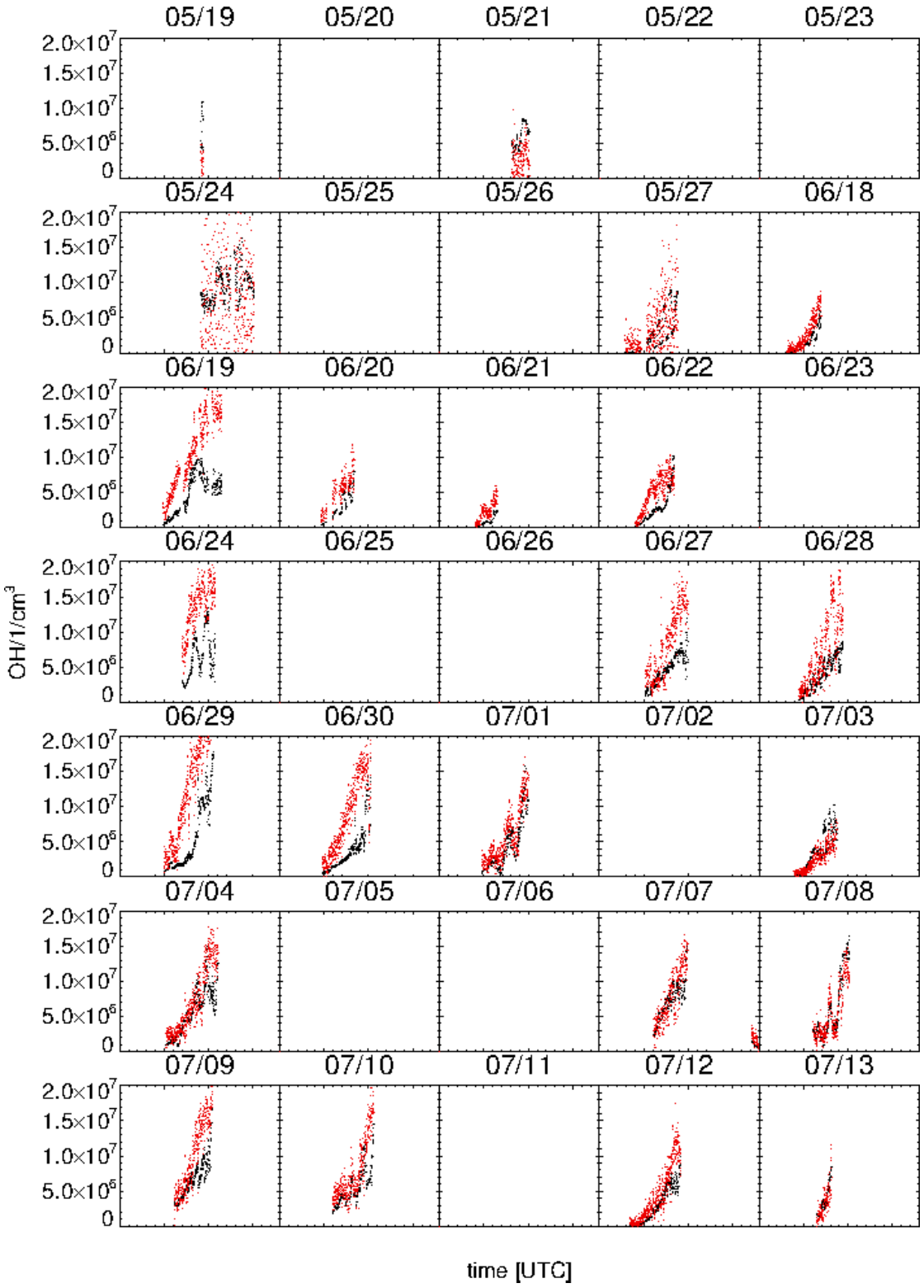

FIGURE A.5: Comparison timeseries - observed(red), predicted(black): OH.

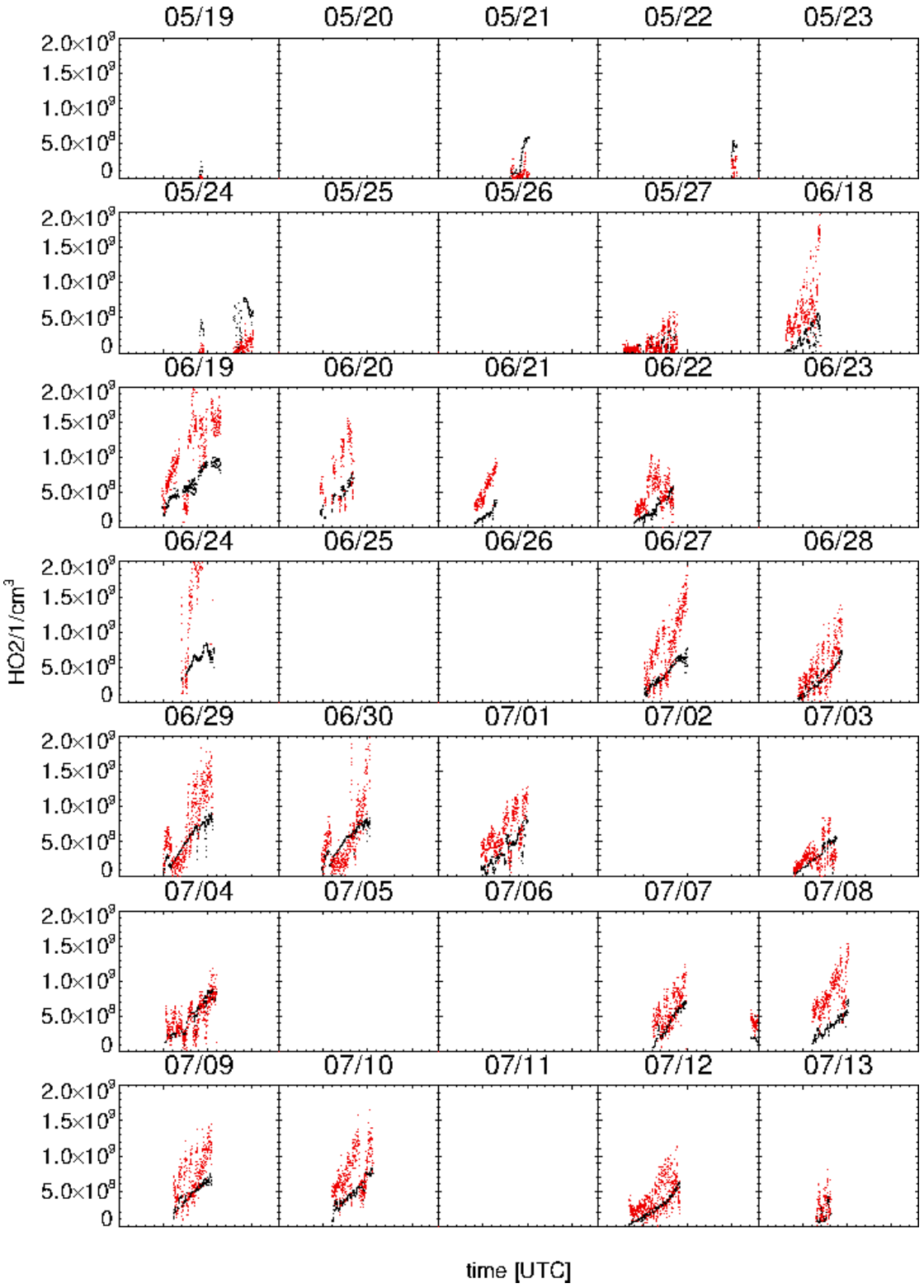

FIGURE A.6: Comparison timeseries - observed(red), predicted(black): HO_2.

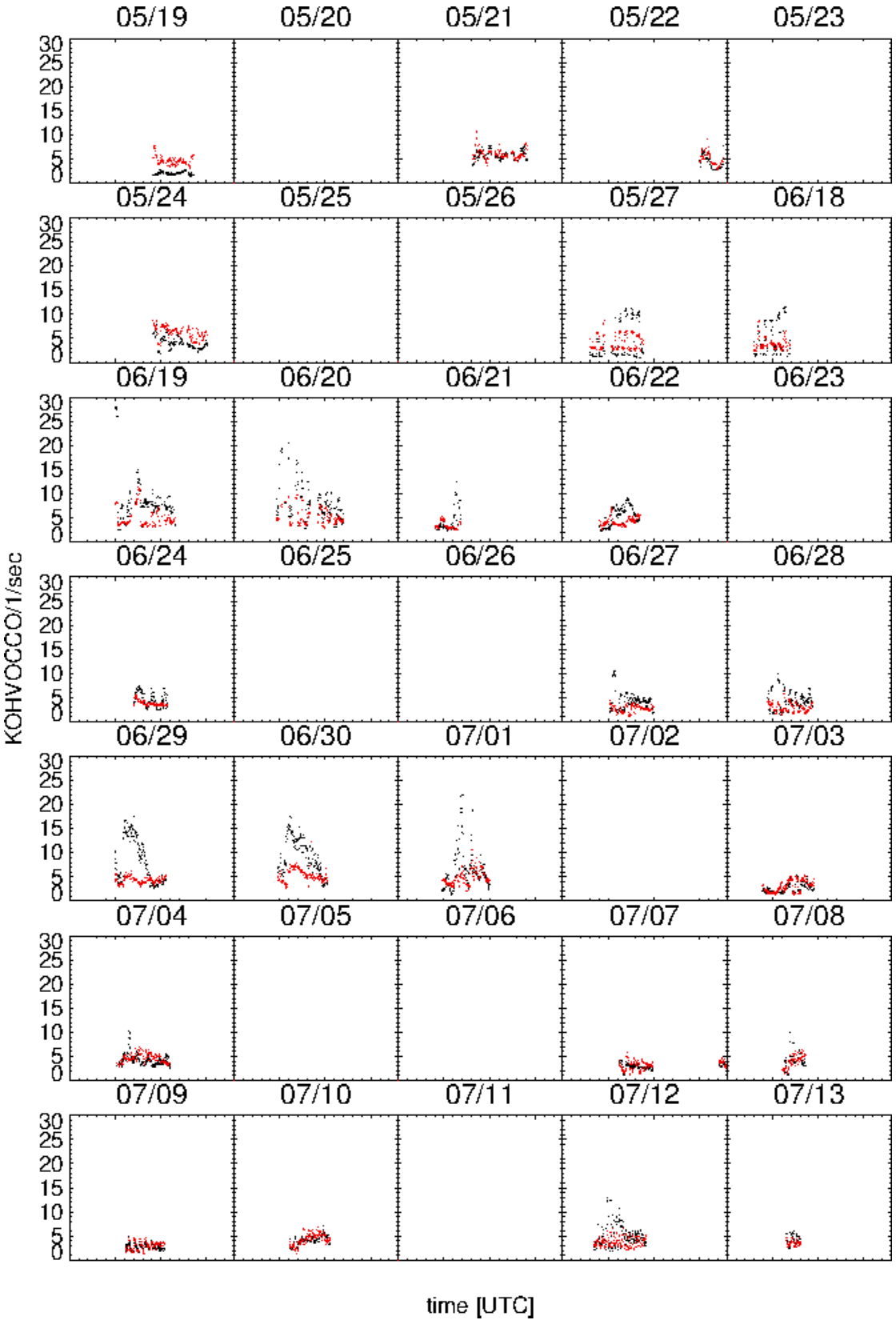

FIGURE A.7: Comparison timeseries - observed(red), predicted(black): k_{OH}.

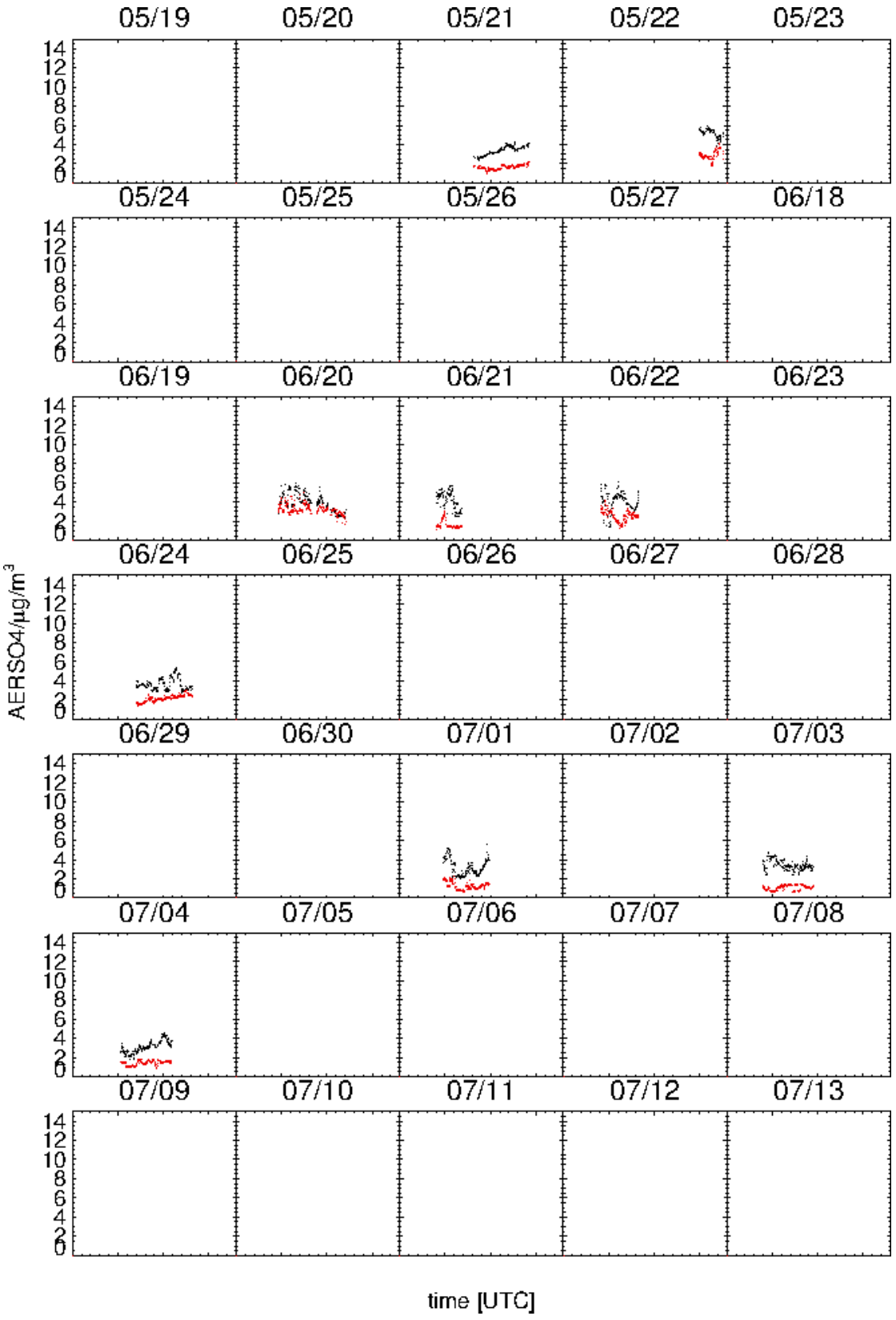

FIGURE A.8: Comparison timeseries - observed(red), predicted(black): sulfate.

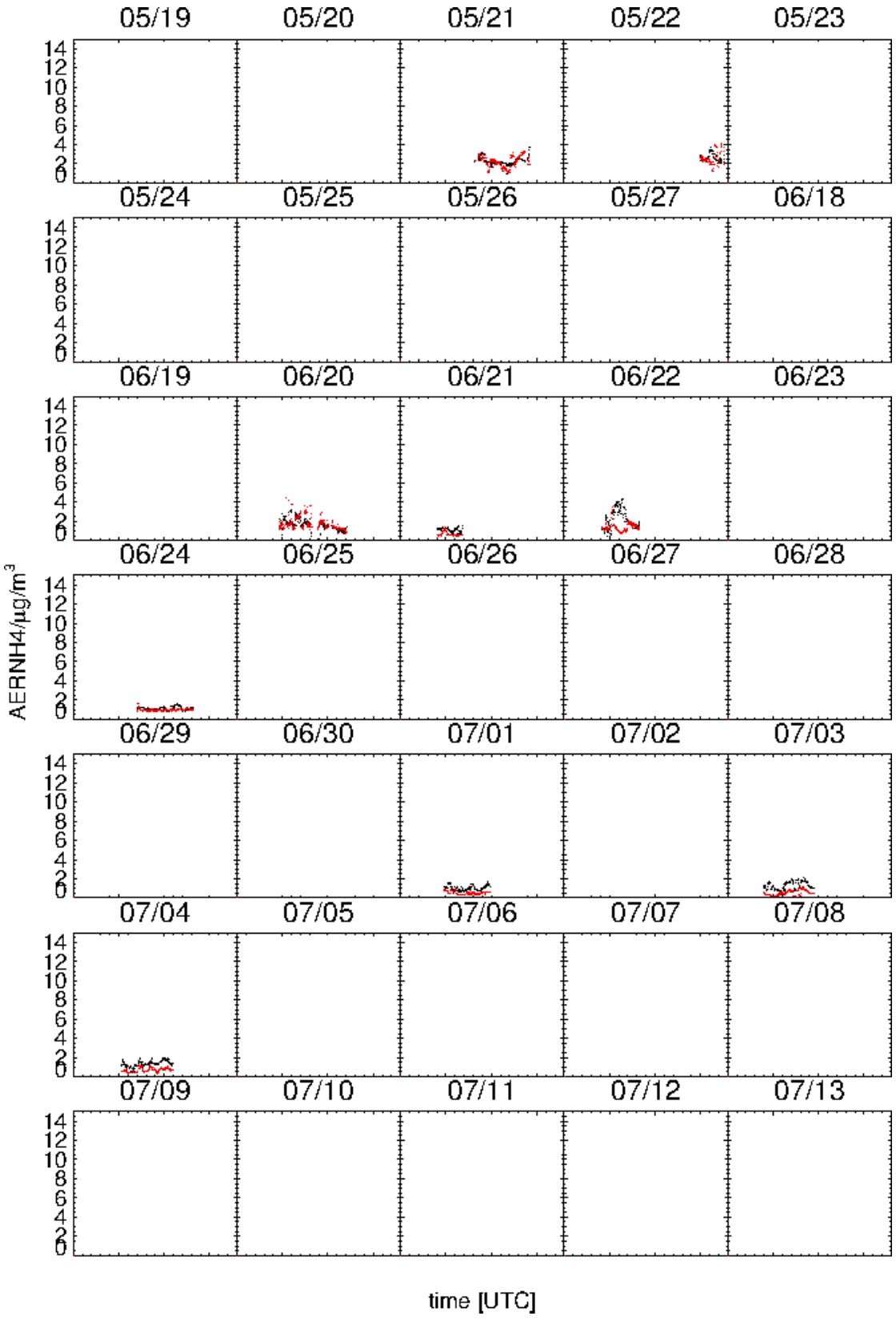

FIGURE A.9: Comparison timeseries - observed(red), predicted(black): ammonium.

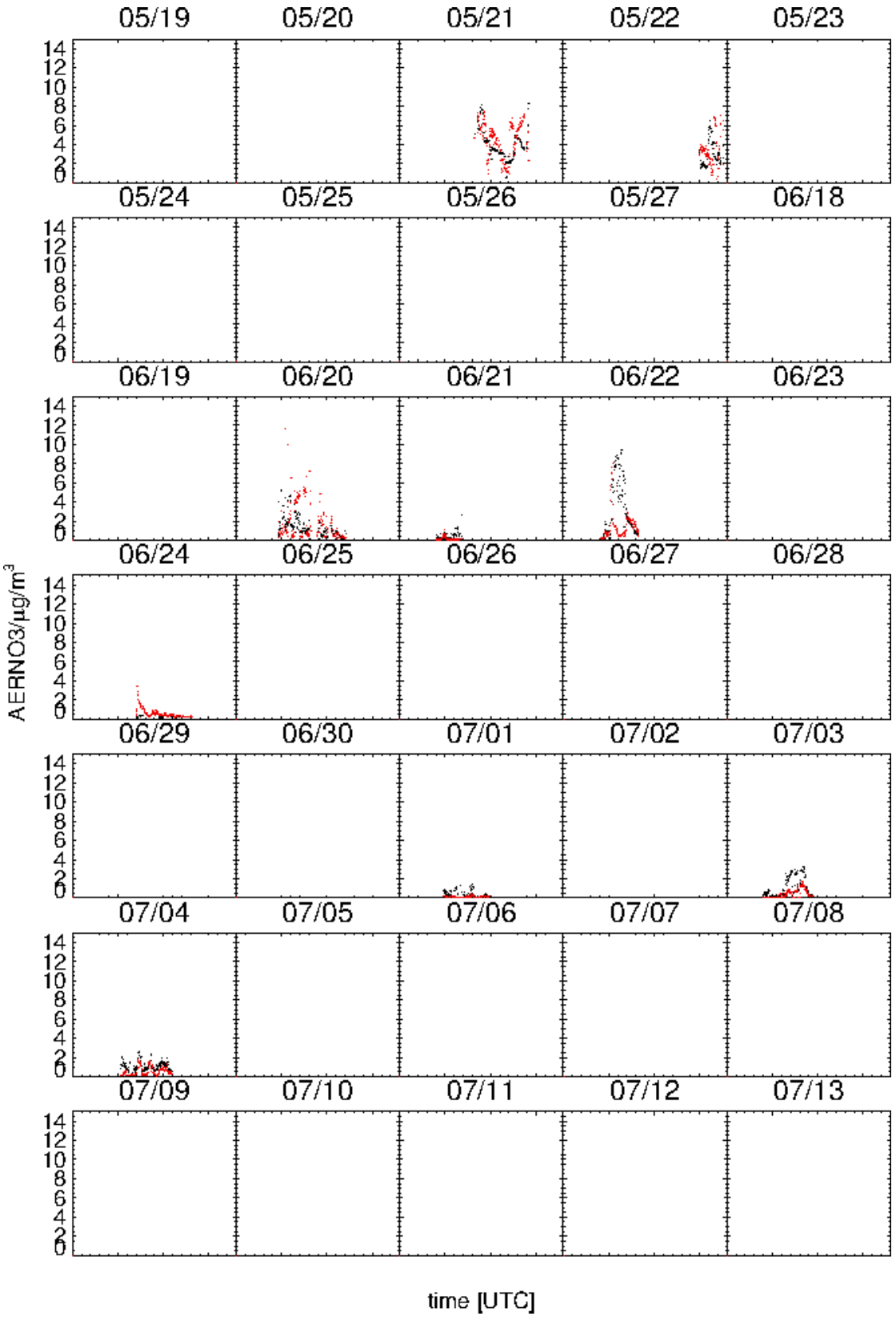

FIGURE A.10: Comparison timeseries - observed(red), predicted(black): nitrate.

Appendix B

Extended metrics table

In this section, an extended table of the commonly used evluation metrics is displayed, that have been calculated over the two 2012 PEGASOS campaign periods.

The normalized mean bias is defined as:

$$B_{NMB} = (\frac{\bar{M}}{\bar{O}} - 1) \times 100\% \tag{B.1}$$

The normalized mean error is defined as:

$$E_{NME} = \frac{\sum_{i=1}^{N} |M_i - O_i|}{\sum_{i=1}^{N} O_i} \times 100\% \tag{B.2}$$

The root mean square error is defined as:

$$E_{RMSE} = \sqrt{\frac{1}{N} \sum_{i=1}^{N} (M_i - O_i)^2} \tag{B.3}$$

The normalized mean error factor is defined as:

$$NMEF = \begin{cases} (\frac{\sum |M_i - O_i|}{\sum O_i}) & \text{if } \bar{M} \geq \bar{O} \quad \text{(overprediction)} \\ (\frac{\sum |M_i - O_i|}{\sum M_i}) & \text{if } \bar{M} < \bar{O} \quad \text{(underprediction)} \end{cases} \tag{B.4}$$

The NMBF and r, that are used in this thesis, have been defined in section 2.5.

SUMMARY STATISTICS								
May 2012 / Cabauw								
Parameter:	$\bar{M}$	$\bar{O}$	NMBF	NMEF	NMB	NME	RMSE	r
temperature	18.40	19.06	-0.04	0.06	-3.46	6.18	1.53	+0.89
rel.humidity	62.77	57.16	+0.10	0.14	+9.82	13.90	9.50	+0.79
H_2O content	0.09	0.09	+0.06	0.10	+6.41	10.10	0.01	+0.93
O_3	57.55	56.03	+0.03	0.17	+2.73	16.75	11.30	+0.55
NO	0.50	1.51	-2.00	2.19	-66.70	72.93	1.63	+0.42
NO_2	2.19	4.90	-1.24	1.44	-55.36	64.50	4.13	+0.38
NOx	2.70	6.39	-1.37	1.54	-57.78	65.07	5.47	+0.41
OH	$6.14*10^6$	$6.09*10^6$	+0.01	0.65	+0.85	65.16	$6.26*10^6$	+0.39
HO_2	$2.27*10^8$	$1.19*10^8$	+0.91	1.41	+90.88	141.46	$2.46*10^8$	+0.23
k_{OH}	4.02	5.25	-0.31	0.45	-23.45	34.76	2.18	+0.60
sulfate	3.89	1.99	+0.95	0.95	+95.24	95.24	2.00	+0.76
ammonium	2.35	2.33	+0.01	0.23	+0.94	23.45	0.70	+0.21
nitrate	3.72	4.18	-0.12	0.46	-11.03	40.70	2.05	+0.29
organics	3.88	6.33	-0.63	0.64	-38.74	39.00	2.69	+0.02
PM0.75	14.49	14.95	-0.03	0.21	-3.09	20.06	3.81	+0.08
June-July 2012 / Po-Valley								
Parameter:	$\bar{M}$	$\bar{O}$	NMBF	NMEF	NMB	NME	RMSE	r
temperature	24.07	24.74	-0.03	0.05	-2.70	4.41	1.35	+0.90
rel.humidity	54.88	52.02	+0.05	0.18	+5.49	17.83	11.85	+0.65
H_2O content	0.11	0.11	+0.01	0.14	+1.25	13.83	0.02	+0.68
O_3	54.11	65.33	-0.21	0.23	-17.17	19.20	16.42	+0.69
NO	0.21	0.44	-1.09	1.58	-52.15	75.59	0.61	+0.27
NO_2	1.16	2.04	-0.76	1.15	-43.33	65.28	2.25	+0.33
NOx	1.36	2.41	-0.78	1.18	-43.72	66.48	2.72	+0.32
OH	$4.44*10^6$	$7.18*10^6$	-0.62	0.73	-38.20	45.25	$4.58*10^6$	+0.73
HO_2	$3.99*10^8$	$6.86*10^8$	-0.72	0.87	-41.87	50.30	$4.95*10^8$	+0.63
k_{OH}	5.34	4.01	+0.33	0.50	+33.10	49.77	3.48	+0.53
sulfate	3.59	1.95	+0.84	0.86	+83.78	86.28	1.91	+0.33
ammonium	1.38	0.96	+0.43	0.59	+42.78	59.22	0.76	+0.42
nitrate	0.99	0.76	+0.31	1.08	+31.02	107.91	1.52	+0.34
organics	3.91	4.99	-0.28	0.59	-21.66	46.17	2.99	+0.45
PM0.75	10.33	8.70	+0.19	0.48	+18.78	48.27	5.18	+0.43

TABLE B.1: Extended statistic parameter table, for the two 2012 PEGASOS campaigns. Included days are noted in Table 3.1.

Bibliography

Aan de Brugh, J., Henzing, J., Schaap, M., Morgan, W., van Heerwaarden, C., Weijers, E., Coe, H., and Krol, M. (2012). Modelling the partitioning of ammonium nitrate in the convective boundary layer. *Atmospheric Chemistry and Physics*, 12(6):3005–3023.

Ball, R. and Robinson, G. (1982). The origin of haze in the central united states and its effect on solar irradiation. *Journal of Applied Meteorology*, 21(2):171–188.

Bohren, C. and Albrecht, B. (1998). Atmospheric thermodynamicsoxford university press. *New York*.

Clegg, S. L., Pitzer, K. S., and Brimblecombe, P. (1992). Thermodynamics of multicomponent, miscible, ionic solutions. mixtures including unsymmetrical electrolytes. *The Journal of Physical Chemistry*, 96(23):9470–9479.

Crippa, M., Canonaco, F., Lanz, V., Äijälä, M., Allan, J., Carbone, S., Capes, G., Ceburnis, D., Dall'Osto, M., Day, D., et al. (2014). Organic aerosol components derived from 25 ams data sets across europe using a consistent me-2 based source apportionment approach. *Atmospheric chemistry and physics*, 14(12):6159–6176.

Elbern, H., Strunk, A., Schmidt, H., and Talagrand, O. (2007). Emission rate and chemical state estimation by 4-dimensional variational inversion. *Atmospheric Chemistry and Physics*, 7(14):3749–3769.

Fountoukis, C., Megaritis, A., Skyllakou, K., Charalampidis, P., Pilinis, C., Denier Van Der Gon, H., Crippa, M., Canonaco, F., Mohr, C., Prévôt, A., et al. (2014). Organic aerosol concentration and composition over europe: insights from comparison of regional model predictions with aerosol mass spectrometer factor analysis. *Atmospheric chemistry and physics*, 14(17):9061–9076.

Friese, E. and Ebel, A. (2010). Temperature dependent thermodynamic model of the system h+- nh4+- na+- so42– no3– cl– h2o. *The Journal of Physical Chemistry A*, 114(43):11595–11631.

Griffin, R. J., Cocker, D. R., Flagan, R. C., and Seinfeld, J. H. (1999). Organic aerosol formation from the oxidation of biogenic hydrocarbons. *Journal of Geophysical Research*, 104(D3):3555–3567.

Guenther, A., Jiang, X., Heald, C., Sakulyanontvittaya, T., Duhl, T., Emmons, L., and Wang, X. (2012). The model of emissions of gases and aerosols from nature version 2.1 (megan2. 1): an extended and updated framework for modeling biogenic emissions.

Haklay, M. and Weber, P. (2008). Openstreetmap: User-generated street maps. *Pervasive Computing, IEEE*, 7(4):12–18.

Han, S., Bian, H., Feng, Y., Liu, A., Li, X., Zeng, F., and Zhang, X. (2011). Analysis of the relationship between o3, no and no2 in tianjin, china. *Aerosol Air Qual. Res*, 11:128–139.

Hofzumahaus, A., Rohrer, F., Lu, K., Bohn, B., Brauers, T., Chang, C.-C., Fuchs, H., Holland, F., Kita, K., Kondo, Y., et al. (2009). Amplified trace gas removal in the troposphere. *science*, 324(5935):1702–1704.

Jacobson, M. Z. (1997). Numerical techniques to solve condensational and dissolutional growth equations when growth is coupled to reversible reactions. *Aerosol Science and Technology*, 27(4):491–498.

Jacobson, M. Z. (2012). Effects of meteorology on air pollution. In *Air Pollution and Global Warming*, pages 127–152. Cambridge University Press, second edition. Cambridge Books Online.

Jakobs, H. J., Feldmann, H., Hass, H., and Memmesheimer, M. (1995). The use of nested models for air pollution studies: an application of the eurad model to a sana episode. *Journal of Applied Meteorology*, 34(6):1301–1319.

Kazanas, K., Rubach, F., Tillmann, R., Mentel, T., Elbern, H., Wahner, A., and Zeppelin Pegasos-Team 2012 (2014). Secondary aerosol formation in the planetary boundary layer: observations on board on a Zeppelin and analysis by back plume approach. In *EGU General Assembly Conference Abstracts*, volume 16 of *EGU General Assembly Conference Abstracts*, page 9403.

Kraus, A. and Hofzumahaus, A. Field measurements of atmospheric photolysis frequencies for o3, no2, hcho, ch3cho, h2o2, and hono by uv spectroradiometry. *Journal of Atmospheric Chemistry*, 31(1):161–180.

Kuenen, J., Visschedijk, A., Jozwicka, M., and Denier van der Gon, H. (2014). Tnomacc_ii emission inventory; a multi-year (2003–2009) consistent high-resolution european emission inventory for air quality modelling. *Atmospheric Chemistry and Physics*, 14(20):10963–10976.

Lee, C.-G., Yuan, C.-S., Chang, J.-C., and Yuan, C. (2005). Effects of aerosol species on atmospheric visibility in kaohsiung city, taiwan. *Journal of the Air & Waste Management Association*, 55(7):1031–1041.

Lohse, I. M. (2015). *Spektrale aktinische Flussdichten und Photolysefrequenzen-Untersuchungen in der atmosphärischen Grenzschicht und der freien Troposphäre*, volume 285. Forschungszentrum Jülich.

Memmesheimer, M., Friese, E., Ebel, A., Jakobs, H., Feldmann, H., Kessler, C., and Piekorz, G. (2004). Long-term simulations of particulate matter in europe on different scales using sequential nesting of a regional model. *International Journal of Environment and Pollution*, 22(1-2):108–132.

Menut, L., Vautard, R., Flamant, C., Abonnel, C., Beekmann, M., Chazette, P., Flamant, P., Gombert, D., Guédalia, D., Kley, D., et al. (2000). Measurements and modelling of atmospheric pollution over the paris area: an overview of the esquif project. In *Annales Geophysicae*, volume 18, pages 1467–1481. Springer.

Nieradzik, L. (2005). Application of a high dimensional model representation on the atmospheric aerosol module made of the eurad-ctm. *Institut fur Geophysik und Meteorologie der Universitat zu Koln*.

Nieradzik, L. and Elbern, H. (2006). Variational assimilation of combined satellite retrieved and in situ aerosol data in an advanced chemistry transport model. In *Proceedings of the ESA Atmospheric Science Conference*, volume 8, page 12.

Obukhov, A. M. Turbulence in an atmosphere with a non-uniform temperature. *Boundary-Layer Meteorology*, 2(1):7–29.

Persson, A. (2001). User guide to ecmwf forecast products.

Pye, H., Chan, A., Barkley, M., and Seinfeld, J. (2010). Global modeling of organic aerosol: the importance of reactive nitrogen (no x and no 3). *Atmospheric Chemistry and Physics*, 10(22):11261–11276.

Reddington, C. L., Carslaw, K., Spracklen, D., Frontoso, M., Collins, L., Merikanto, J., Minikin, A., Hamburger, T., Coe, H., Kulmala, M., et al. (2011). Primary versus secondary contributions to particle number concentrations in the european boundary layer. *Atmospheric Chemistry and Physics*, 11(23):12007–12036.

Rohrer, F., Brüning, D., Grobler, E., Weber, M., Ehhalt, D., Neubert, R., Schüßler, W., and Levin, I. (1998). Mixing ratios and photostationary state of no and no2 observed during the popcorn field campaign at a rural site in germany. *Journal of atmospheric chemistry*, 31(1-2):119–137.

Rohrer, F., Lu, K., Hofzumahaus, A., Bohn, B., Brauers, T., Chang, C.-C., Fuchs, H., Häseler, R., Holland, F., Hu, M., et al. (2014). Maximum efficiency in the hydroxyl-radical-based self-cleansing of the troposphere. *Nature Geoscience*, 7(8):559–563.

Rubach, F. (2013). *Aerosol processes in the Planetary Boundary Layer: High resolution Aerosol Mass Spectrometry on a Zeppelin NT Airship*. PhD thesis, University of Wuppertal.

Schmidt, G. A., Shindell, D. T., and Tsigaridis, K. (2014). Reconciling warming trends. *Nature Geoscience*, 7(3):158–160.

Seinfeld, J. and Pandis, S. (1998). Atmospheric chemistry and physics, 1326 pp.

Shon, Z.-H., Madronich, S., Song, S.-K., Flocke, F., Knapp, D., Anderson, R., Shetter, R., Cantrell, C., Hall, S., and Tie, X. (2008). Characteristics of the no-no 2-o 3 system in different chemical regimes during the mirage-mex field campaign. *Atmospheric Chemistry and Physics*, 8(23):7153–7164.

Spracklen, D., Jimenez, J., Carslaw, K., Worsnop, D., Evans, M., Mann, G., Zhang, Q., Canagaratna, M., Allan, J., Coe, H., et al. (2011). Aerosol mass spectrometer constraint on the global secondary organic aerosol budget. *Atmospheric Chemistry and Physics*, 11(23):12109–12136.

Stjernholm, M. (2009). Corine land cover 2006. *Final report on interpreta*.

Stull, R. B. (2012). *An introduction to boundary layer meteorology*, volume 13. Springer Science & Business Media.

Trenberth, K. E. and Guillemot, C. J. (1994). The total mass of the atmosphere. *Journal of Geophysical Research: Atmospheres*, 99(D11):23079–23088.

Viterbo, P., Beljaars, A., Mahfouf, J.-F., and Teixeira, J. (1999). The representation of soil moisture freezing and its impact on the stable boundary layer. *Quarterly Journal of the Royal Meteorological Society*, 125(559):2401–2426.

Walker, J., Philip, S., Martin, R., and Seinfeld, J. (2012). Simulation of nitrate, sulfate, and ammonium aerosols over the united states. *Atmospheric Chemistry and Physics*, 12(22):11213–11227.

Wegener, R., Jäger, J., Hofzumahaus, A., Rohrer, F., Bohn, B., Brauers, T., Broch, S., Gomm, S., Häseler, R., Holland, F., et al. (2014). Total oh reactivity measurements aboard the zeppelin nt during the pegasos campaign 2012: Contributions of substance classes to the total oh reactivity. In *EGU General Assembly Conference Abstracts*, volume 16, page 3429.

Wexler, A. and Hyland, R. W. (1980). Formulations for the thermodynamic properties of dry air from 173.15 k to 473.15 k, and of saturated moist air from 173.15 k to 372.15 k, at pressures to 5 mpa. *Final Report ASHRAE Project RP216*.

Yu et al., S. (2006). New unbiased symmetric metrics for the evaluation of air quality models. *Atmospheric Science Letters*.

Acknowledgements

Undertaking this PhD has been a truly life-changing experience for me and it would not have been possible to do without the support that I received from several people. First, I would like to say a big thank you to PD Dr. Thomas F. Mentel for his expert, sincere guidance and his continuous encouragement. I appreciate Prof. Dr. Andreas Wahner for his approval and for giving me the chance to work in Forschungszentrum Jülich (IEK-8). I place on record, my gratitude to PD Dr. Hendrik Elbern for providing the resources of the Rhenish Institute for Environmental Research, needed for the completion of this thesis. The technical support and advice I received from Dr. Elmar Friese is greatly acknowledged. Finally, I want to sincerely thank my parents Spyros and Zoi, my sisters Vivi and Giota, and my friends Panagiotis and especially Iliana, for being patient with me. Thank you very much! :-)

Erklärung

Ich versichere, daß ich die von mir vorgelegte Dissertation selbständig angefertigt, die benutzten Quellen und Hilfsmittel vollständig angegeben und die Stellen der Arbeit – einschließlich Tabellen, Karten und Abbildungen –, die anderen Werken im Wortlaut oder dem Sinn nach entnommen sind, in jedem Einzelfall als Entlehnung kenntlich gemacht habe; daß diese Dissertation noch keiner anderen Fakultät oder Universität zur Prüfung vorgelegen hat; daß sie – abgesehen von unten angegebenen Teilpublikationen – noch nicht veröffentlicht worden ist sowie, daß ich eine solche Veröffentlichung vor Abschluß des Promotionsverfahrens nicht vornehmen werde. Die Bestimmungen dieser Promotionsordnung sind mir bekannt. Die von mir vorgelegte Dissertation ist von Prof. Dr. Andreas Wahner betreut worden.

Köln, 06/06/2018